International
Progress Report

IPR-03-41

Äspö Hard Rock Laboratory

True Block Scale continuation project

Assessment of the feasibility of tracer tests with injection in "background fractures" using a model based on a power law fracture length distribution

Caroline Darcel

Itasca Consultants SA

November 2003

Svensk Kärnbränslehantering AB
Swedish Nuclear Fuel
and Waste Management Co
Box 5864
SE-102 40 Stockholm Sweden
Tel +46 8 459 84 00
Fax +46 8 661 57 19

Äspö Hard Rock
Laboratory

Report no.
IPR-03-41
No.
F56K
Author
Caroline Carcel
Date
November 2003
Checked by
Anders Winberg
Date
December 2003
Approved
Christer Svemar
Date
2003-12-16

Äspö Hard Rock Laboratory

True Block Scale continuation project

Assessment of the feasibility of tracer tests with injection in "background fractures" using a model based on a power law fracture length distribution

Caroline Darcel

Itasca Consultants SA

November 2003

Keywords: Fractal, fracture network, multi-scale, power law, self-similar, tracer

Abstract

The present study belongs in the framework of the TRUE Block Scale Continuation project (BS2), following the TRUE Block Scale project (Tracer Retention Understanding Experiment at the Block Scale).

In the first part we have strived at developing a view of the fracture system at Äspö that encompasses all scales in a unified conceptual framework. Such a view, because it takes into account data at several scales, is likely to provide a more robust description of the fracture network. After a review of earlier related studies of the Äspö site, a multiscale analysis allows assessing the relevance of a power-law model for the fracture size distribution (exponent a), related to a Poissonian/fractal model for the fracture positions (dimension D). We found that two pairs of parameters could explain the data at hand: either a power-law exponent a_{3d} of 3.8 combined with a fractal dimension D_{3d} of 2.8, or a power-law exponent a_{3d} of 4 combined with a fractal dimension D_{3d} of 3. Having "$a_{3d} = D_{3d} + 1$" signifies that the network is "self similar": the distribution of large and small fractures is the same at all the scales considered.

In the second part, conservative tracer tests in the Block Scale rock volume are simulated. The configuration tested (CPT2) corresponds to a pumping point at borehole KI0025F03 in structure #19 and several possible injections points. The numerical model built from this theoretical framework shows how the choice of a probability distribution function for fracture size can affect the advective response of the network, and how such assumptions influence the relative interplay of the structures and the background fractures. The transport analysis here is nevertheless very much governed by the knowledge of the structures, in which (or close to which) the tracers tests will be performed.

Sammanfattning

Föreliggande studie ingår i projektet "TRUE Block Scale Continuation" som utgör en uppföljande studie till det tidigare genomförda TRUE Block Scale som ingår i Tracer Retention Understanding Experiments (TRUE).

Den första delen av denna rapport kännetecknas av en strävan att utveckla ett allomfattande angreppssätt på spricksystemen vid Äspö som tar hänsyn till alla skalor i ett samlat konceptuellt sammanhang. Ett sådant angreppssätt bör, då det tar hänsyn till data från ett flertal observationsskalor, ge en mer robust beskrivning av spricknätverket. Efter en genomgång av tidigare studier av Äspö, har en analys som tar hänsyn till flera skalor använts för att studera relevansen i utnyttjande av en potensmodell (eng. *power law*) för fördelningen av sprickstorlek (exponenten a), kopplad till en Poisson-modell (fraktal) av sprickläger (dimensionen D). Det befanns att två set av parametrar kunde förklara tillgängliga data: antingen en exponent $a_{3d} = 3.8$ för en potensfunktion kombinerad med en fraktal dimension $D_{3d} = 2.8$, alternativt en exponent $a_{3d} = 4$ för en potensfunktion kombinerad med en fraktal dimension $D_{3d} = 3$. Observationen att "$a_{3d} = D_{3d} + 1$" indikerar att det studerade spricknätverket är fraktalt (eng. *self similar*) vilket innebär att fördelningen av stora och små sprickor är densamma oavsett observationsskala.

I den andra delen av rapporten simuleras spårförsök med konservativa spårämnen i TRUE Block Scale volymen. Den aktuella konfigurationen (CPT-2) motsvarar pumpning i struktur #19 i borrhål KI0025F03 och injicering av spårämne i ett antal närliggande punkter. Den numeriska modellen, som är konstruerad med ovanstående teoretiska koncept som bas, visar hur valet av sannolikhetsfördelning (eng. *probability distribution function*) för sprickstorlek kan påverka den advektiva transporten i spricknätverket, och vidare hur dessa antaganden påverkar det relativa samspelet mellan större strukturer och till dessa kopplade bakgrundssprickor. Analysen av transport är i detta fall under alla förhållanden till stor del bestämd av kunskapen av läge och geometri hos de större (deterministiska) strukturerna, där huvuddelen av transporten av spårämne sker.

Table of contents

List of Tables

List of Figures

Executive summary

General Objectives

The present study belongs in the framework of the project TRUE Block Scale Continuation (BS2), following the TRUE Block Scale Project (Tracer Retention Understanding Experiment at the Block Scale). The general purpose aims at improving the understanding of tracer retention properties and to assess the predictive capabilities of numerical models at a 10-100 meters scale.

Overview and background

During the TRUE Block Scale Project a hydrostructural model was built, that includes deterministic definition of the main 100 meters scale conductive structures within the block studied. The hydrostructural model therefore serves as an essential basis for the ensuing in situ transport/retention experiments. During the "tracer test stage", several tracer tests were performed over distances ranging from 15 up to 100 m, with all the source and sink points located in the relatively high-conductive structures identified in the hydrostructural model. Therefore, during the TRUE Block Scale Project, tracer tests mainly sampled the network of highly conductive structures at the scale of interest.

The BS2 project is aimed at assessing the feasibility and at performing the modelling of tracer tests through the less conductive fracture network, in the above mentioned framework: tracer tests at the scale of a few meters, with an injection point in the less conductive network and a sink in the identified deterministic structures of the hydrostructural model. At the present time two phases have been defined:

- BS2A involves complementary monitoring, and modelling in support of in situ tests necessary to define the second phase (BS2B)
- BS2B, is defined to perform tracer tests partly involving background fractures and numerical modelling (prediction and evaluation)

It has been subsequently established that the main focus of the second phase (BS2B) of the BS2 project would be to perform tests in a single intermediate-sized structure over longer distances. Such a candidate exists in Structure 19, which constitutes a bounding structure to the rock volume previously investigated as part of TRUE Block Scale. In addition, limited tests involving background fractures close to structure 19 are planned.

The present study is part of BS2A.

Fracture network representation

In the present framework, flow and transport modelling of a fracture system involving small scale features/fractures raises the question of their representation. We therefore choose to *a priori* consider the medium as a network of discrete fractures whose statistical properties are assessed from new data analyses and synthesis of the numerous and well documented works already published. One underlying question here, in the specific context of BS2A, is the possible existence of a scale below which fracture representation could be stochastic or be represented as a homogenised continuum, or alternatively not represented at all.

Overview of fracture analyses at Äspö

A review of former statistical analyses of the fracture system at Äspö performed at various scales permits to highlight several general trends:

- Fractures are present at any scale of observation, from the centimetre up to tens of kilometres.
- Direct observations along boreholes and on the tunnel walls display the presence of numerous features with varying hydraulic properties.
- fracture size distributions data are often entailed by strong censoring and truncation effects, simply due to the multi-scale nature of the fracture system and to the limited range of length scales sampled on a map (maximum size is the system size, minimum size is given by the lower resolution scale of measurement devices). Hence this renders the characterization of a underlying power-law model very difficult, since it requires a large range of observation scales.
- Fracturing observed at Äspö outcrops and tunnel walls presents relatively similar characteristics. A few different fracture sets are clearly defined but no distinction can be made about the fracture length distribution from the different fracture sets.
- No obvious characteristic length scales (reflecting a change of underlying physical processes resulting in a variation of the size distribution shape) are clearly identified from the different fracture maps analysed.

Note that, depending on the underlying reports, opposing conclusions are found regarding the scaling behaviour of the fracture system, the existence of a "discontinuity" in the observation of fracturing over scales, and the possibility to use the knowledge of fractures at one scale as a useful predictor of fracture geometry at other scales.

Fracture length distribution modelling

Classical models for fracture length distributions are exponential, lognormal or power-law. The presence of fractures over a large range of scales and also the absence of any obvious characteristic length scale are two arguments in favour of the use of the power law model for fracture network modelling. The simplest power-law model predicts the number of elements $n(l)$, of length l, comprised between l and $l+dl$ such that:

$$n(l)dl \propto l^{-a}dl \,.$$

The power-law model is thus characterised by its scaling exponent, noted a, and the minimum and maximum fracture lengths below which and above which there is no fracture. Represented in a log-log diagram, the power-law distribution corresponds to a straight line with a slope equal to $-a$.

A combination of a power-law size distribution of fractures with a fractal scaling of the fracture spatial density can be expressed through the model:

$$n(l, L)dl \propto l^{-a} L^{D} dl \,,$$

where D is the fractal dimension and L the characteristic linear size of the system (for instance the edge length of a cube) at which the fracture system is observed. The fractal dimension D expresses the way the fracture network fills the space.

Statistical analysis

A multiscale analysis is performed (see figure below), by representing in a log-log diagram the variations of the number of fractures of a given length, normalized by the system characteristic size, as a function of the length.

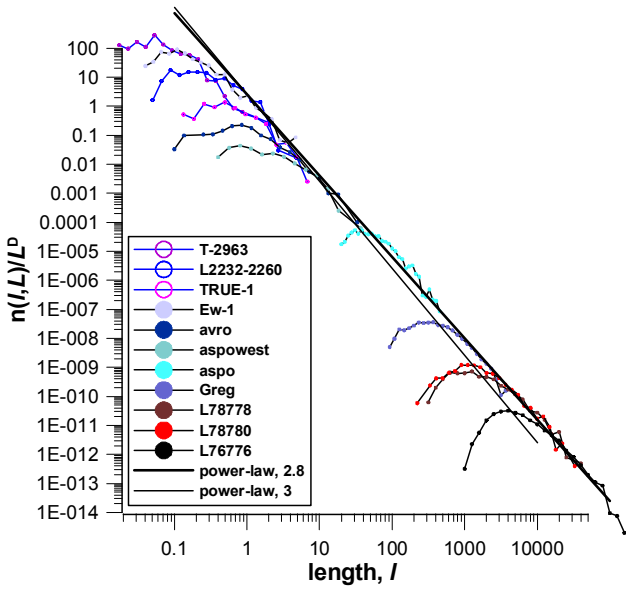

multi-scale analysis with D_{2d}=1.8.

We demonstrate that, although a precise determination of exponents remains difficult due to the numerous artefacts present in the available data, the fracture system in 2d is well fitted by the fracture density length model outlined above. In addition the qualitative similarity of the fracture patterns through all scales speaks in favour of the power law model, with parameters a_{2d} and D_{2d} such that $a_{2d}=D_{2d}+1$. Indeed, having $a_{2d}<D_{2d}+1$ (respectively $a_{2d}>D_{2d}+1$) implies an increase (respectively decrease) of the proportion of large fractures with the observation scale whereas only when $a_{2d}=D_{2d}+1$ the proportion remains scale invariant, as is observed on maps of Äspö fracture data.

The derivation of 3d parameters using stereological principles yields two pairs of parameters that could explain the data at hand: either a power-law exponent a_{3d} of 3.8 combined with a fractal dimension of D_{3d} 2.8, or a power-law exponent a_{3d} of 4 combined with a fractal dimension D_{3d} of 3. We have some indication that this model may be valid down to a fracture radius in the order of one meter. However, the scarcity of small scale fracture length samples with a high resolution prevents from fully assuring the validity of the statistical model below a fracture size of about 10 m.

Tracer test simulations

The analysis of transport here is very much governed by the knowledge of the deterministic structures, in which (or close to which) the BS2B tracer tests will be performed. Structure positions and transmissivity properties, positions of intersections coupled to conditioned transmissivities estimations along conditioned boreholes are indeed directly introduced in the model. The rest of the fracture network is stochastic and several fracture distribution models (power-law and lognormal, varying a_{3d}, varying smallest length cut-off) are considered. The configuration tested corresponds to a pumping point at borehole KI0025F03 in structure 19. Several injection points are tested, located along structure #19, the new "structure" 25 and at some other intersection points located between boreholes and background fractures. Hence conservative tracer tests are simulated to provide predictions of the travel times through the fracture network partly including the "secondary flowing network".

The simulations predict that 5% recovery times range from a few hours (short distances between pumping and injection points and injection directly in structure #19) to a few hundred hours (longer distances and injection in background fractures). Similarly, the 50% recovery times range from 10/20 hours to 1000/2000 hours. Also note that, as expected, the prediction variability increases with the proportion of the simulated tracer test flow paths forced to the stochastic fracture network.

More precisely the simulations show how the relative behaviour of a background fracture network varies when considering a lognormal or a power law fracture radius distribution (with the specific parameters corresponding to Äspö conditions). For the BS2 program, however, the differences resulting from the stochastic assumptions of the model are not of great concern, for one main reason: the main structures are known and strongly control the advective flow. They do not need to be assessed from other scales since they have been directly detected, characterized and modelled. In other words, we know enough at the scale of interest, such that no “interpolation” is needed between scales. This is likely not to be the case in most other set-ups, be it during site characterisation for a repository, or for performance assessment work on a larger-scale, not fully characterised site.

Conclusion

From this study we can conclude that tracer tests in the volume surrounding structure #19 are feasible provided injections in background fractures, if any, are operated close to the Structure 19, as in fact is planned (injections in “Structure 25”, a few metres from the structure).

After this necessary first step of advective transport modelling, one can try to understand how reactive transport is affected. Specifically, stepping back to the tentative hypotheses which constitute the rationale for BS2, we note that the possible differences in retention properties between smaller features (mostly background fractures) and larger ones (mostly structures) makes the understanding of the way they interact hydraulically all the more important.

Prospects

In performing this task, we have strived at developing a view of the fracture system at Äspö that encompasses all scales in a unified conceptual framework. Such a view, because it takes into account data at several scales, is likely to provide a more robust description of the fracture network, can help filling "voids" in observation scales, for sizes that are difficult to assess from field work, and may provide new insights in several directions, beyond the framework of the TRUE Block Scale Continuation project. The following imminent needs have been identified:

- detail mapping at the "lower scale" (metres to tens of metres) to improve models predictive capacities at the geologic barrier close to canisters, that is where properties of the smaller scale fractures become essential. Unbiased (i.e. systematic) mapping at this scale would then help confirm - or invalidate - the relevance of the power law model.
- More theoretical studies of the connectivity of such networks, using the fact that they show self-similarity, would yield estimates of the size of possible unconnected clusters within the network, and of the conductive/non conductive proportion of the fracture system.
- Our use of transmissivity data in this work was conceptually quite simple. In fact, more theoretical work on the interplay of size/transmissivity/connectivity properties of fractures would improve the robustness of our models for varying hydraulic conditions.

1 Introduction

The present study is part of project BS2, a continuation of the TRUE Block Scale (Tracer Retention Understanding Experiment at the Block Scale) project. These studies aim at improving the understanding of tracer retention properties and at assessing the predictive capacities of models at a 10-100 meters scale. During the characterisation stage of TRUE-Block Scale, the combination of numerous geological and geophysical methods of investigation and many flow tests has permitted to build a hydrostructural model including deterministically the main 100 meters scale conductive structures over the block studied. The hydrostructural model therefore serves as an essential basis for the ensuing transport/retention experiments. During the “Tracer test stage" of the TRUE Block Scale project, several tracer tests were performed with distances between source-sink pairs ranging between 15 and 100 m. More precisely all the source and sink points were located in the relatively high-conductive structures identified and deterministically represented in the hydrostructural model. Therefore, during the TRUE Block Scale project, tracer tests mainly sampled the network of highly conductive structures at the scale of interest.

At the Block Scale, although major flow paths are identified along the aforementioned structures, a network of significantly less conductive secondary flowing features (called background fractures) has been regularly observed (flowing intersections along boreholes). Until now the tracer tests performed have been restricted to major structures, such that transport/retention properties of the Block Scale represent in fact transport/retention properties of the main structures. However, in the perspective of underground storage of radioactive waste, radioactive canisters should as far as possible be positioned in weakly conductive regions. Therefore the "less conductive network" would probably be the first flowing path for escaping radionuclides before encountering the block-scale structures.

The first phase of the BS2 project, called BS2A, involves complementary monitoring, and modelling in support of in situ tests. BS2A already demonstrated that tests in complex fracture networks over longer distances will take a long time and are highly likely to show low breakthrough, particularly so when involving injections in background fractures. Therefore, the main focus of the second phase (BS2B) of the BSC project will be to perform tests in a single intermediate-sized structure over longer distances. Such a candidate exists in Structure #19, which constitutes a bounding structure in the interior of the rock volume previously investigated as part of the TRUE Block Scale Project. In addition, because the retention properties of the background fractures network may play a large role close to canisters, limited tests involving background fractures close to structure 19 are planned.

The work described here is aimed at assessing the feasibility of tracers tests through the less conductive fracture network, in the above mentioned framework: tracer tests at the scale of a few meters, with an injection point in the less conductive network and a sink in the identified structure #19.

Assessing in detail the flow and transport properties of the "secondary network" raises the question of the representation of features/fractures. Indeed, direct observations along boreholes and on the tunnel walls have shown the presence of numerous features with varying hydraulic properties (from flowing to non-conductive). Their exhaustive representation in a deterministic model is essentially impossible. One underlying question here is the one of the possible existence of a scale below which fracture representation could be stochastic or be represented as a homogenised continuum, or alternatively not represented at all.

In this framework we choose to *a priori* consider the medium as a network of discrete fractures whose statistical properties are assessed from new data analyses and synthesis of the numerous and well documented works already published. As will be apparent from the references noted in the text, the approach followed in analysing the data is in line with developments by the Geosciences Rennes group during the previous years. In fact, the analyses presented here were discussed with Ph. Davy and O. Bour during the course of the project.

The study is divided in 2 main parts. The first one focuses on the geometrical representation of the fracture network. The presence of fractures at any scale of observation (from meters up to tens of km) speaks in favour of trying to build a multiscale statistical geometrical model of the fractures at Äspö. Therefore the analysis is based on a global representation of the fractured media in the region of Äspö, including all the possible scales where fractures can be found. The statistical analysis is given in chapter 3, including a discussion of its theoretical background. Before undertaking the statistical analysis, a review of the previous works devoted to background fracturing and scaling relationships at Äspö (chapter 2) is presented; it permits discussion of the relevance of the general fracture representation chosen, in particular in the context of the specific scope of BS2A. Conservative tracer tests are next simulated to provide predictions on travel times of elements through the fracture network partly including the "secondary flowing network" (chapter 4) and results are discussed in chapter 5.

2 Overview of reports including a geometrical analysis of fracture network

Numerous studies have been dedicated to the fractures of the Äspö site, from the meter up to the kilometre scale, among them [Mazurek et al., ICR97-01, 1996], [Bossart et al., TR-01-21, 2001], [Andersson et al., TR-02-13, 2002] [Lapointe et al., TR99-03, 1999] and [Dershowitz et al., IPR-03-13]. Most data cited further in chapter 3 and *Table 3-1* are otherwise described and/or analysed in the reports cited below.

Before undertaking the review let us recall a few definitions currently used. Several **generic** terms are used to describe spatially consistent parts of the fracture system (apart from specific genetic terms joints, faults, veins): fracture, feature, structure. A general definition of the fracture system is that it is a population of fractures which are individual roughly planar elements in which the displacement is supposed to be spatially consistent [Bour et al., 2002]. When considering a population of fractures, fracture properties such as length or orientation can be defined. However in practice it often remains difficult to "individualize" fractures. For instance the term “structure” is in practice used at the scale of 100 meters to denote either one single large fracture or a set of fractures (swarm, zone) spatially coherent (connected, conductive) at the considered scale. The terms "fracture" and "feature" apply to individualized fractures, "feature" being more general than fracture. Several characteristic scales are also straightaway identified and frequently used as boundaries to subsequent fracture system analysis and modelling:

- The scale of a few meters, that has been investigated along the TRUE-1 project, especially designed to focus on one single flowing feature.
- The scale of about 100 meters or *block scale* was originally considered as the scale from which conductive pathways would be made up of clusters of connected features (network). The block scale can also be viewed as the length scale above which any radionuclide element released in the medium would have reached a large conductive structure. Down to that scale geological and hydraulic structures should be possibly identified.
- The scale of 1000 meters (regional scale) and more corresponds to regional structures.
- Below the block scale (50 meters and less) the conductive features can be made up of single fractures. In the following this population of fractures is often referred as "background fractures". For instance in the TRUE Block Scale Project, the term is used to define the very large fracture population whose characteristic lengths are less than the otherwise observed structures.

Due simply to the respective amount of fractures, as a function of their length and of the scale of observation, the deterministic representation of large features is possible at the regional scale and mostly at the block scale, whereas at lower scale the huge quantity of data needed, as well as detection capacities strongly limit the possibility to perform a deterministic representation.

According to their specific objectives the different reports provide information at one of the aforementioned scales, and even some multiscale analysis. We give in the following a brief and non-exhaustive review of these studies, with a special attention to the specific scales, considered *a priori* or highlighted by the analyses, and to the small scale fracturing. As already mentioned these scales are more typically scales of interest, not intrinsic characteristic length scales of the fractures at the Äspö site.

2.1 FCC – Fracture Characterization and Classification

2.1.1 FCC I and II [Mazurek et al., ICR97-01, 1996]

The object of the FCC project was to classify and characterize the water conducting structures in the Äspö tunnel at the scale of a meter up to decametres and to provide a conceptualisation of the fracture system with respect to radionuclide transport. One specific scale is studied, the one that corresponds to trace lengths that cross-cut the entire tunnel. Furthermore the study is restricted to water conducting fractures, as mentioned above.

The database is made up of 88 conducting features mapped between tunnel coordinate 600 and 3050. Trace lengths between 7 to 25 meters were investigated. The rest of the structures were not mapped, i.e. conductive structures that did not cross-cut the entire tunnel were deliberately not mapped. It is noted that at this scale, meter to decametre, almost all fractures are conducting and are related to faults.

At the scale of interest, the authors indirectly raise the question of the fracture "individualization": indeed, they distinguish 5 types of water-conducting features, among them the "single fault" or "fault zone" (Figure 2-1). The internal geometry of fractures may change along the fractures. They find that "the application of the classification scheme is limited to smaller-scale considerations, while in the case of large-scale transport, results of the study indicate that due to the common history, water flow in the underground of Äspö is dominated by one single family of water-conducting features."

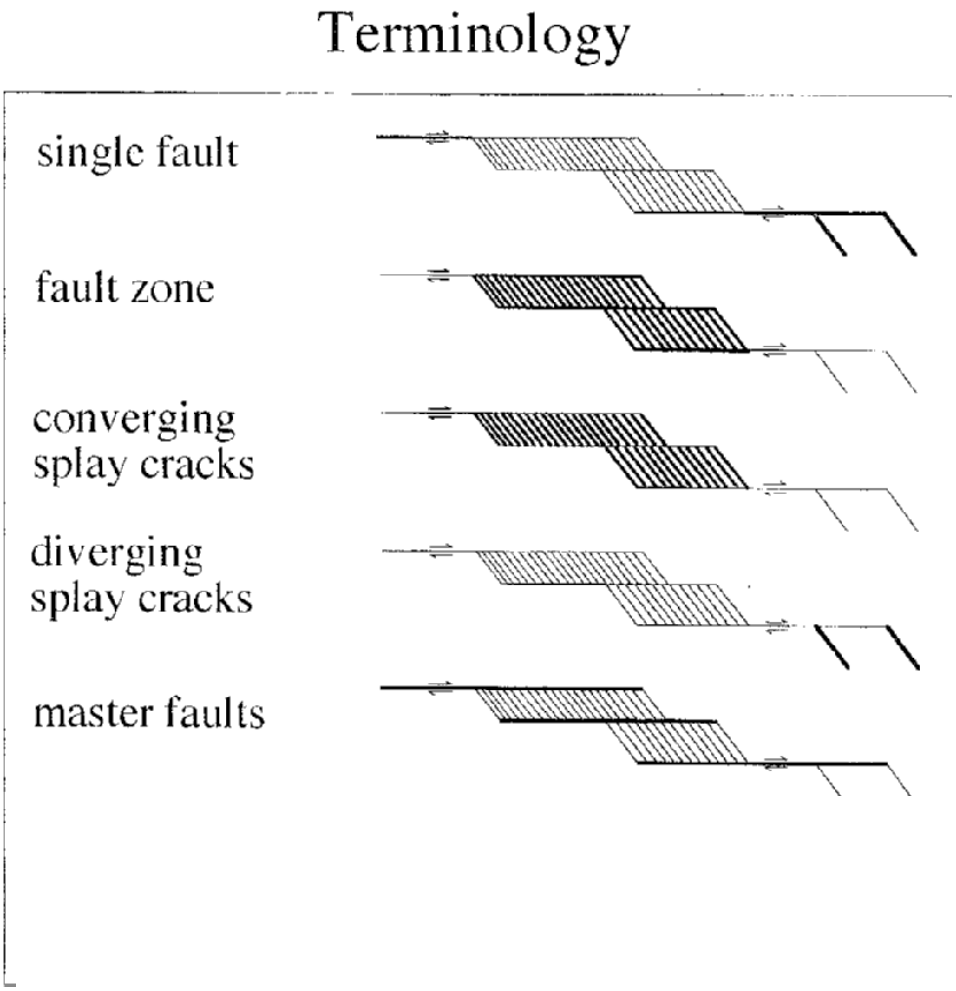

Figure 2-1: *Types of water conducting features at Äspö, from [Mazurek et al., 1996]*

Several different lithologies are present along the tunnel. Mazurek et al. note that no differences exist between Småland granite and Äspö diorite, contrary to the fine-grained granite where higher fracture frequencies are found. However this last rock type does not host faults over more than a few meters (it is not relevant for the larger-scale transport properties of the faults).

The common genetic history of all conductive structures here (faults) leads to expect common hydraulic and transport properties for all these conductive structures.

Finally, the authors suggest extending the analysis both to larger and smaller scales, by smaller they mean from centimetres to meters. This is done in the phase III of the FCC (section below).

2.1.2 TR-01-21, phase III of FCC

The scope of the study here was twofold: it comprised firstly the characterization of small scale Water Conducting Features coupled with fracture network modelling of the TRUE-1 small scale area and next a multi-scale analysis of the fractures from the meter up to the kilometre scale.

BIPS borehole data (with borehole lengths going from 17 m up to almost 60 meters) and 2d-tunnel mapping and line counting in the vicinity of tunnel coordinates 2930 to 3020 (the map called elsewhere "TRUE-1" corresponds to tunnel coordinates 2944 to 3004.) are analysed to provide a consistent statistical model of fractures at a scale of 50x50x50m. The area of interest is located in the vicinity of the TRUE-1 rock block where the rock mass is highly fractured but where no so-called major faults are present. One important remark is that 85% of the fractures strike in the NW-SE direction, so that they are just sub-parallel to the tunnel map in that area (p43). The dominant fracture set is NW-SE. Accordingly a higher fracture frequency is observed for the boreholes oriented NE-SW. The possible distinction between water-conducting features and non-conducting fractures is performed from BIPS data (p10).

Two series of tunnel maps, corresponding to distinct campaigns are provided: the first set comes directly from the SICADA database (the SKB Site Characterisation Database). In that case, because of time constraints, only traces longer than 1m were mapped (p18 TR-01-21). The second set, called map "TRUE-1" has been performed specifically for the study, this time with a higher resolution and a truncation level of about 0.3 to 0.5 meter. 1d line-counting over the same map have been realized additionally with a truncation level of 0.1m (p 40). The authors underline the fact that during the mapping process it is frequently difficult to establish whether each individual trace is a separate fracture or if it can be treated as part of a fracture with an uneven trend. Noticeable results (*for our purpose*) of the study are listed below:

- Although an increased frequency is observed in zones with ductile precursors. there is no clear distinction in fracture frequencies as a function of lithology (Fine-grained granite, Äspö diorite and Småland granite).
- Fracture orientations are in good accordance with overall observations at Äspö.
- The fracture size distribution is dominated by the smallest fractures. The different levels of truncation for fracture trace mapping, permit to highlight this characteristic. For example the cumulative trace length measured on the maps with a resolution between 0.3 to 0.5 m is twice the one measured from 1m resolution lengths maps (table at p20 report [TR-01-21]) and the mean for trace length map is 1.33 whereas it is 0.64 for the line counting/sampling. Fracture lengths distributions coming from the different fracture sets are considered simultaneously. Indeed, data are too scarce, it was not possible to separate the different fracture sets. Size estimation analyses (section 2.5.3, p 39) rely on a trial and error method. They do not permit to distinguish a better model between lognormal, power-law or exponential length distribution. Finally the authors choose to dismiss the power-law model because of the dominance of rather small fractures.

- Here, in opposition with the authors, we notice that a power law model with $a_{2d} > 3$ is rightly characterised by the dominance of rather small fractures and that the lack of large fractures is simply due to the low probability to observe them, therefore the power-law model should not be neglected. One interesting point is that up to the higher scale of resolution (length equal to 1m), both the exponential, lognormal and power-law model could be interchangeably used to match the data, as illustrated in Figure 2-2. In particular the power-law model provides a scaling exponent between 3 to 3.5. Here again, cumulative density lengths distributions have been used to assess the parameters. The minimum length chosen for the power-law model lies within the range 0.1 to 0.4. It is clear that smaller fractures dominate the cumulative trace length distribution (see conclusions page p42) and that the traces length range available to analyse the data remain limited (tunnel transversal dimensions).

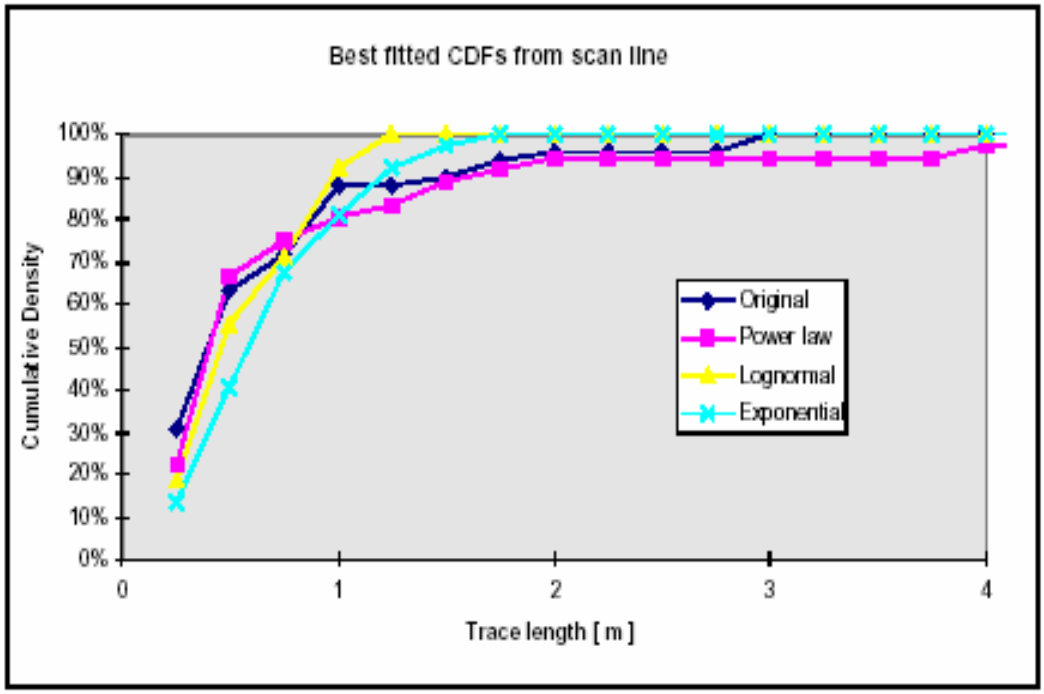

Figure 2-2: *Cumulative density functions of observed trace length data from the scanline measurements and simulated trace lengths generated with three different DFN models based on scanline measurements. From [Bossart et al., 2001].*

- In the area of concern, the boreholes present hydraulic interconnections. The corresponding conductive areas are interpreted as clusters of connected smaller structures because of the lack of observation of large fractures (p33). A former fracture model of TRUE-1 site had been based fracture model estimation of conductive structures ([LaPointe et al., 1995]). The present study considers the whole fracture network, that is both conductive and non-conductive fractures. Based on P_{10} comparison between 1d scan-lines over the tunnel map and direct borehole observations, the authors suggest that even typical fractures of characteristic length less or around 20cm could contribute to flow in the boreholes (p44).
- Fracturing over the TRUE-1 site is not singular, but it is found to be very similar to other areas such the one of the ZEDEX tunnel section (p43). Besides, the apparent P_{32c} here is significantly larger than the estimated value of the TRUE Block Scale area which is equal to 0.29 m^2/m^3. However, the estimate of P_{32} from BIPS data could correspond to open fractures rather than conductive fractures. Then the difference between the two areas is not so significant.

To sum up, from the first part it was concluded that over the TRUE-1 site (~50x50x50 m) the fracture network (model) is dense and interconnected with in addition zones of higher frequencies. All the fractures observed are relatively small, and within the area studied no decametre-scale fracture (as in Mazurek et al., 96) is observed on the tunnel wall.

Scaling relationships and multiscale analyses are tackled in a second part. The maps analysed are comprised between $2m^2$ and $1200km^2$, five are outcrops and the rest are tunnel maps. The exponents characterising a possible power-law behaviour have been systematically and separately measured from log cumulative frequency distributions of fracture trace lengths. Results show a high variability, with cumulative exponents estimated between 0.52 up to 1.21 (add 1 for the non cumulative length distribution, leading here to 1.52 and 2.21). We notice that some of the exponents have been measured on very small samples (a few tens of fractures). In addition, such low values of the power-law scaling exponent are a sign of a fracture length distribution dominated by a large proportion of large fractures, a proportion that increases with the scale of observation. This is apparently in contradiction with the first part of the report, were it had been noticed that fracture length distributions were dominated by the smallest ones. The conclusion of the report is however that the fracture networks analysed are not self-similar (in the sense that the exponent of the length distribution varies significantly from one map to another). It is argued that “a geological environment like Äspö, with a multiphase deformation history where many deformation phases have contributed to the final fracture network, is not a likely candidate for a self-similar fracture network” (p 97 of [TR-01-21]). We note that this conclusion is in clear opposition with [Lapointe et al., TR99-03, 1999]. In Chapter 3 (p 97 of [TR-01-21]), called "Scaling Relationships", the conclusion is opposite to ours. However they do not compare different scales and use the cumulative distribution to measure the exponent, and do not consider finite size and truncation effects.

At all the scales observed fractures are structurally and hydraulically interconnected and may form parts of hydraulic pathways. The authors note that an important result is the finding of hydraulic interconnection over all fracture scales at Äspö. This property is corroborated by geochemical evidence.

2.2 True Block Scale rock volume

The TRUE Block Scale (noted TBS below) task was devoted to reactive transport experiments and modelling within a few conductive structures at the scale of 10-100m (complementary to experiment TRUE-1 that was designed to experiment and model reactive transport within a single structure). For that purpose, a volume of rock equal to 200x200x200m, rimed in the north by the TBM (Tunnel Boring Machine) tunnel and localized at a depth around –400m was selected. A preliminary investigation stage necessary to enable reactive transport tracer tests was to build and characterize a hydro-structural model over the rock volume. The hydrostructural model at the scale of TBS is controlled by a few hundred-meter scale structures (Figure 2-3) that were identified by a combination of several methods (geology, geophysics, hydraulic tests, etc.).

Ensuing tracer tests were designed to take place in the identified conductive network, which was by far the main focus of the characterisation program. Therefore, characterisation of the rest of the network was of secondary importance for the study. Several reports detail the whole experiment, from the fracture network characterization to the tracer tests analyses ([Andersson et al., TR-02-13, 2002], [Andersson et al., TR-02-14, 2002], [Poteri et al., TR-02-15], [Winberg et al., TR-02-16]). Also, within the framework of the Äspö Task Force on Hydrogeological Modelling, in the context of the Task 6 "PASC" Project (Performance Assessment modelling using Site Characterisation data) [Dershowitz et al., IPR-03-13] detail the conceptual framework of the TRUE Block Scale rock volume. Several intermediate progress reports treat specifically the background fracture network characterization. Among them details on the fracture size estimation analysis can be found in [IPR-01-71, IPR-01-70].

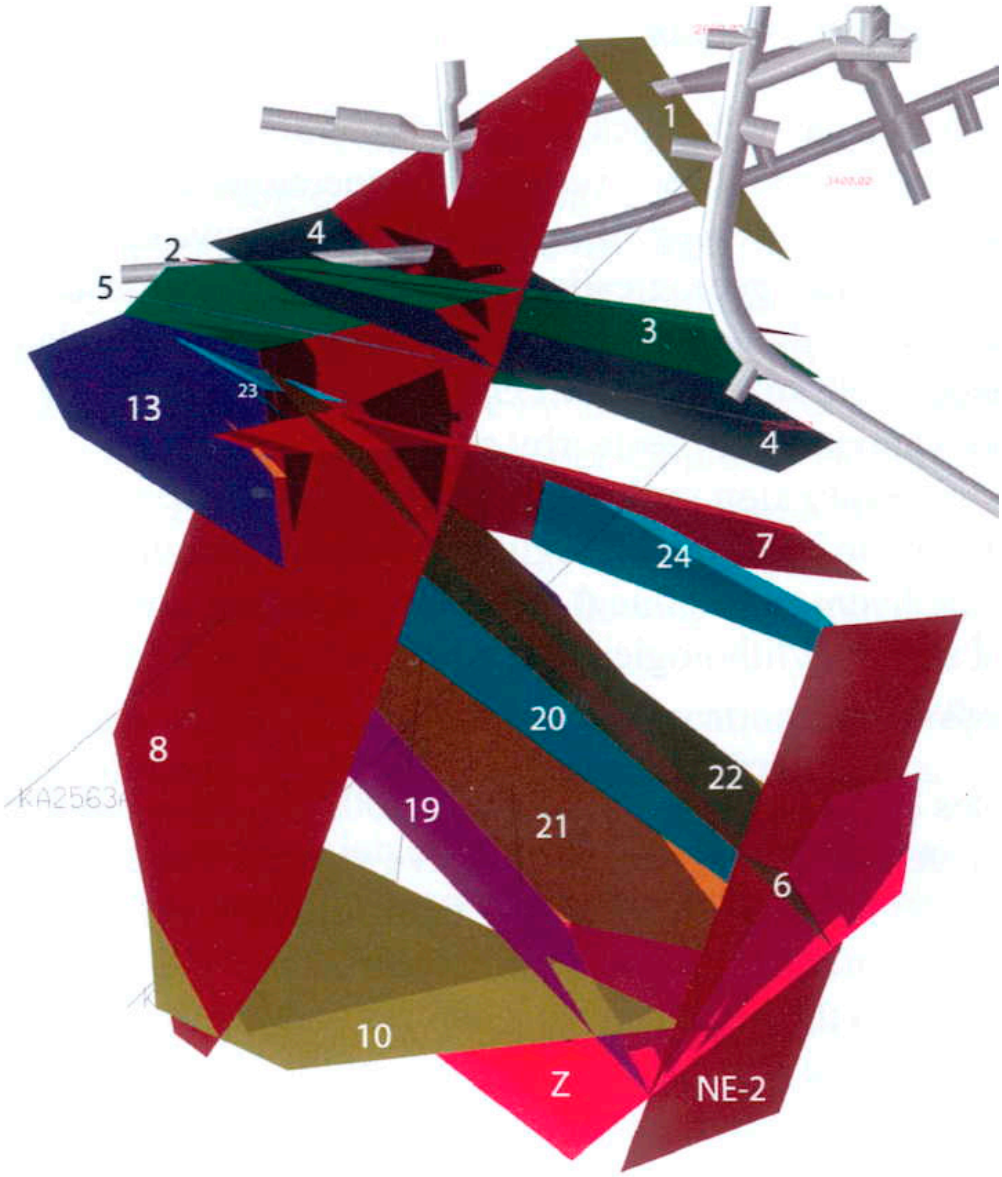

Figure 2-3: *Structures in the TRUE Block Scale volume from [Winberg et al., 2003]*

The fracture intensity and orientation distribution are deduced from intercept measurements along the boreholes crossing the TBS rock volume. According to [Hermanson et al., IPR-01-70] the potential three sets of fractures found in the boreholes are in good accordance with findings all over the Äspö HRL and there is no evidence for separating the length distribution in three different distributions according to orientations. For the background fractures, fracture size estimates come from tunnel map traces of the TBM. The lower cut-off for the fracture mapping is about 1meter. The fracture size distribution model proposed is lognormal. The original parameters, inferred directly from the TBM data [IPR-01-70], were a mean of 6 meters and a standard deviation of 3 meters. These parameters lead however to poor results in terms of simulations of hydraulic interference tests. For that reason a model of mean 2 meters and standard deviation 1 m was preferred. According to the report, these values are consistent with data from the Prototype Repository and FCC ([Bossart et al., TR-01-21, 2001] and [Mazurek et al., ICR97-01, 1996]).

Several methods are applied to characterise the fracture spatial pattern. A spacing distribution analysis indicates that a Baecher model (equivalent to a random distribution of fractures) may be used for background fracturing in the Tracer Test Volume (TTV – centre part of the TRUE Block Scale Rock Volume where the tracer tests will take place) whereas it would not be necessarily applicable for the full TRUE Block Scale Rock Volume [TR-02-13]. Furthermore a fractal analysis (box dimension, spectral analysis and Mass-Lévy) indicates that the fractures of the TRUE Block Scale Rock volume are fractal in their spatial arrangement with a fractal dimension in 3D around 2.5-2.6 [TR-02-13]. The authors notice also that these values are in good accordance with results from trace map analysis of the Äspö island.

Background fractures are made up of 2 sets of distinct orientations, between which the only difference is a slight intensity difference (set 1 is $0.16 m^2/m^3$ and set 2 is $0.13 m^2/m^3$, see p 48 in report [Dershowitz et al., IPR-03-13]). The third set, corresponding to more or less horizontal fractures, was found to be non-conductive and is consequently not considered further. Only conductive background fractures are included in the model, i.e. the fracture density is estimated from the conductive fractures only. This is contrary to what was done in phase III of FCC [TR-01-21], where the background fracture network density was based on the sum of open and conductive fracture.

Besides, deterministic structures are the result of geological, geophysical and hydraulic test evidence. Their hydraulic parameters have been successfully adjusted to match the hydraulic tests at the scale of interest. This is however not a proof that background fractures have no effect on the hydraulic properties. In that context, it seems that no attempt was made to relate the background fracture model to the upper scale fracture model (deterministic structures). The differentiation between background fractures and deterministic structures is nevertheless not the result of an intrinsic characteristic scale of the fracture system.

Finally, the possible absence of a geometrical characteristic length does not prejudge the possible existence of a characteristic scale from the transport properties point of view. Indeed, two fracture types are defined in [IPR-03-13], named structures type 1 (fault) and 2 (non-faults). "These two structure types should be regarded as two end members of a spectrum of possible structure compositions in the real system. According to the definition of type 1 and 2, type 1 fractures are filled by cataclasite and fault gouge, characterized by a significant shear movement along the main fault plane, whereas type 2 fractures are open with mineral coating, but show no typical shear indicator." The authors indicate that features of size 0.5 meter are type 2 while features of size 100 meters are type 1, and also that either type 1 or 2 can be found at any scale in between.

2.3 Fracture system and earthquake predictions [TR-99-03]

[Lapointe et al., TR99-03, 1999].

The study aims at assessing the safety of canisters through earthquake predictions. The necessity to consider fractures at many different scales is presented as obvious for earthquake prediction. The authors notice that only a small subset of fractures should be modelled for fluid flow and transport prediction at the scale of interest. They also mention that determination of the scaling properties of the fracture network may make it possible to properly model fractures at scales that are poorly represented in existing data sets. For that purpose an analysis of lineament trace data in order to quantify the scaling properties of the fractures is provided. Both the fracture length distribution and the spatial fracture repartition (measure of the fractal dimension) are analysed.

The multiscale analysis is performed using data from three sites: Aberg (contains the Äspö Island), Ceberg and Beberg regions, with several maps from a scale 1:7000 up to 1:1000000. Trace maps from the Äspö HRL tunnel are also included in the study. The method used to measure the exponent of the power-law is based on the CCDF (Complementary Cumulative Density Function). The analysis of the Aberg data set shows that a single power-law model can match the data with a well defined exponent of 1.6 for the cumulative length distribution function (this corresponds to 2.6 for the length probability distribution function) of all the maps including the area (Figure 2-4). A small-scale departure from the power-law model is approximately observed from a size of 50m. Indeed, the smallest outcrop map trace length distribution analysis shows a departure from the power-law model from this length. Moreover, an exponent of 1.45 is measured from the Äspö HRL data, with a lower cut-off for the trace length equal to 1 meter. Slightly larger exponents of about 1.7 to 1.8 are found for Ceberg and Beberg regions.

Note that with regards to the statistical analysis provided in Chapter 3, we do recommend to measure the power-law exponent from the probability density function (PDF) rather than from the CCDF. Our analysis leads to slightly larger exponents. In fact the fractal dimension, when measured from the classical box dimension method, is always found to be roughly equal to, or slightly larger than, the fracture length exponent obtained from the cumulative distribution.

The authors conclude that "rock breakage due to tectonic forces, uplift or glacial unloading produce fracturing over a large range of scales" and that consequently the "knowledge of fracturing at one scale is a useful predictor of fracturing geometry at other scales". "It implies that it is not unreasonable to assume that a single scaling model applies also for traces belonging to 1 to 50m" and that "there is no evidence of a discontinuity in the fracturing over these scales."

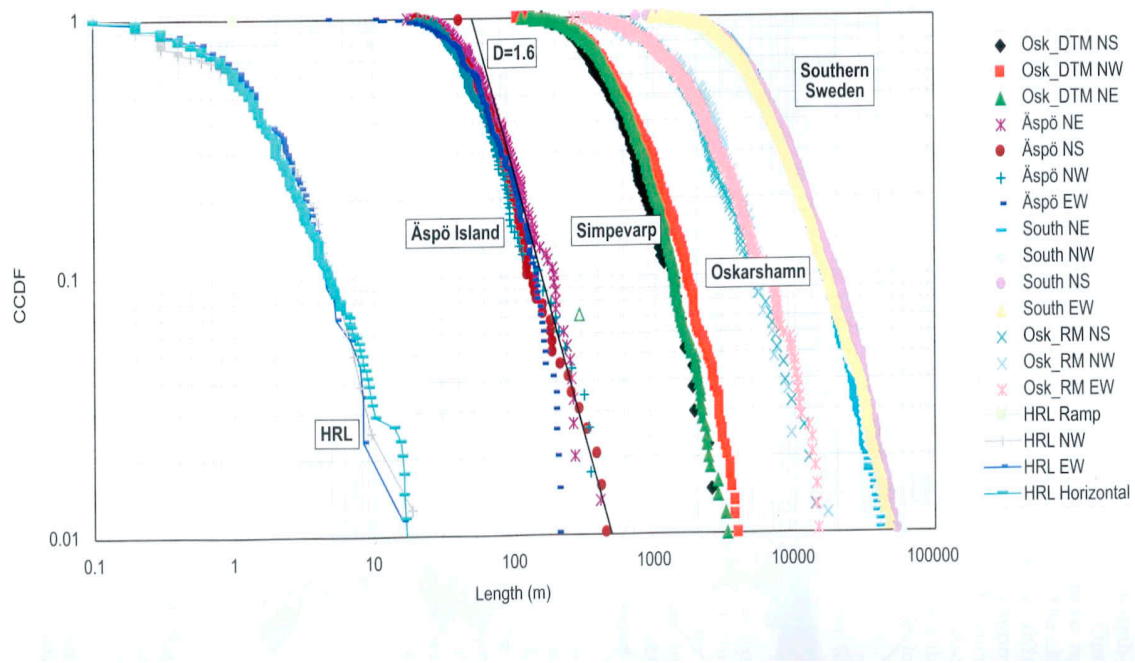

Figure 2-4: *Trace length CCDF for Aberg and surrounding region. From [Lapointe et al., 1999].*

2.4 Summary

The former brief review of fracture characterization efforts at Äspö allows highlight of several general trends. They are listed hereafter:

- fracturing on Äspö outcrops and tunnel walls presents relatively similar characteristics. A few different fracture sets are clearly defined and can be identified over the different zones studied. However no distinction can be made on the fracture length distribution model from the different fracture sets.
- The individualization of fractures is not obvious, fault zones can alternatively be viewed as one fault zone or a cluster of smaller fractures. A fault zone at small scale can appear as one single fracture at a larger scale.
- Small scale fractures are numerous, fractures exist at least down to the 10 cm scale. However, the range 10 cm to 50 m is really difficult to sample, because it is below the scale of resolution of most existing maps.
- There is no firm evidence that the separation of fractures in two categories, i.e. background fractures (<50m) and deterministic block scale structures (around 100m), has a physical meaning.
- Due to the difficulty to obtain statistically relevant data, fracture length analyses are often entailed by strong censoring and truncation effects that make the estimation of a power-law exponent very difficult.
- Depending on the individual reports, opposing conclusions are found regarding the scaling behaviour of the fracture system, the existence of a “discontinuity” in the fracturing over scales, and the possibility to use the knowledge of fractures at one scale as a useful predictive tool of fracture geometry at other scales.

3 Statistical analysis of fracture network

3.1 Theoretical background

The presence of fractures over a large range of scales and also the absence of any obvious characteristic length scale are two arguments in favour of the use of the power law model for fracture network modelling. Theoretical background for the power-law fracture network model and the corresponding parameters are recalled in this chapter.

This part is voluntarily restricted to the geometrical characterisation, without *a priori* consideration of cut-off lengths under which fractures do not contribute to flow. This question will be tackled in Chapter 4.

3.1.1 Density length model of fracture network

Length distribution

Classical models used to model fracture length distributions are either exponential, lognormal or power-law. Among them, the power-law model has the particularity to be entirely defined by l_{min} and l_{max}, the minimum and maximum lengths of fractures, and a scaling exponent a (see illustration in Figure 3-1, where a power-law distribution is represented alongside a lognormal distribution). Depending on the value of a, the moments of the distribution (mean, variance, …) are dominated either by the largest fractures (l_{max}) or by the smallest ones (l_{min}) [Dreuzy et al., *in press*]. Let $n(l)$ be a power-law distribution model for the fractures of characteristic length l:

$$n(l\ ) = \frac{a-1}{l_{min}^{-a+1} - l_{max}^{-a+1}} l^{-a} \cong \frac{a-1}{l_{min}^{-a+1}} l^{-a}\ ,\ l \in [\ l_{min}\ ;\ l_{max}]$$

The exponent a fixes the respective proportion of large and small fractures. The exponent a can have any value in the range $[1; \infty]$. The power-law model encompasses two classical end-member models: all fractures have the same constant length l_{min} if $a \to \infty$. On the opposite, for a=1 all the fractures have a length l_{max}. Between these two extremes, as a decreases, the proportion of large fractures increases. Finally a lower than 1 is geologically irrelevant since this predicts more large fractures than smaller ones [*Bonnet et al*, 2002]. Represented in a log-log diagram, the power-law model appears as a straight line whose slope is equal to $-a$.

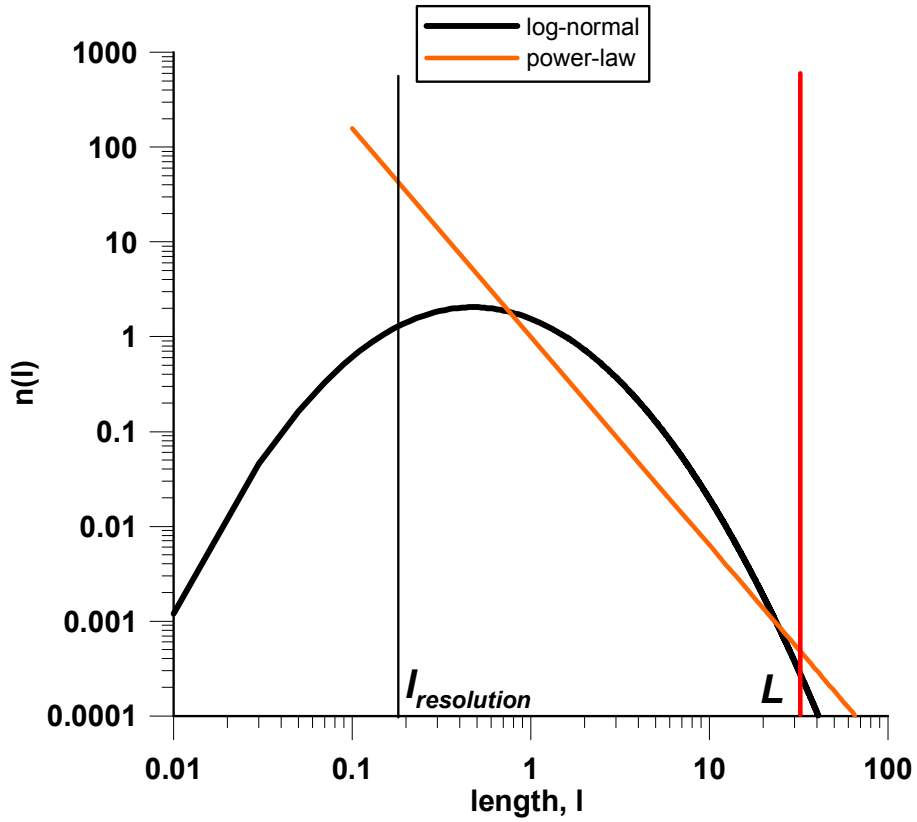

Figure 3-1: *Power-law and lognormal model. The power-law results in a straight line of slope –a when represented in a log-log diagram. The thick red line represents the system size at which the fracture network is observed and the thin black line an hypothetical low resolution scale. In the present case* $l_{min} << l_{resolution} << L << l_{max}$ *so that* l_{min} *and* l_{max} *can not be observed .*

In practice the fracture network is characterized within a given system size of observation. Let us note L the linear size of the system. It corresponds to the scale of observation or the scale at which the system should be modelled. A common situation corresponds to $l_{min} << L << l_{max}$. Therefore fractures larger than L appear truncated at the scale of observation and moments of the truncated length distribution possibly depend on L when the model is dominated by large fractures (for details, see [Dreuzy et al., *in press*]).

The power-law and lognormal models are frequently two competing models for the representation of fracture length distributions. Furthermore, resolution effects[1] imposed on a power-law length distribution can result in an apparent lognormal distribution if small fractures are underrepresented (Figure 3-1). The lognormal distribution model can nevertheless be the right model, for instance in fractured systems with lithological layering [Odling et al., 1999]. To complete the power-law model description, we notice that values of a depend on the geological nature of the fractured medium. Compiling many field studies, Bonnet et al. [2001] or Renshaw [1999] reported power-law exponents a for 2-D fracture maps in the range 1.5 to 3.5.

[1] The apparent decrease of fracture intensity toward shortest lengths comes from resolution limitations: shortest fractures are missed either by the eye of the observer or simply by the technical limit of resolution of a camera.

Spatial distribution, fractal dimension

The measure of the fractal dimension of a system allows characterization of its spatial distribution over scales, i.e. the way it fills space. In other words, it is a scaling model for heterogeneity. The usual definition of a fractal dimension, D, is given from the variation of the number of segments, disks or spheres of Euclidean dimension equal respectively to 1, 2 and 3, and of characteristic length scale r, necessary to cover the part of a fractal object included in a volume R^d. This number of objects varies as $N(r,R) \sim (r/R)^D$.

The fractal dimension obtained for a fracture pattern first depends on the way the fracture pattern itself is described: indeed, it can be considered as a whole, or as a set of individualized fractures. In the latter case, fracture lengths and positions are identified, where the position is generally given by the fracture mid-point or barycentre. This way to describe fracture networks is convenient since it permits definition of the number of fractures, as the number of fracture centres, noted $N(L)$, present in a system of linear size L.

Although the barycentre of a fracture trace is typically taken as representative of its position, any arbitrary position on the fracture could have been taken as the representative point [Bour et al., 2002]. As a consequence, the measure of the fractal dimension can be performed only if, for a given map, the majority of fractures have a small extent compared to the system size. In this case the choice of the representative point of a fracture can be taken anywhere along the fracture, since the induced variation of the fracture "position" will be small compared to the scale at which the position is defined. Therefore, the distance statistics we wish to use for computing the fractal dimension can be obtained only on condition that the number of fractures whose length is lower than r remains significant. This also implies that, in terms of the number of fractures, the fracture network should be dominated by small fractures to enable the measurement. On the contrary, a fracture length distribution dominated by large structures can prevent the measure of the fractal dimension associated with the scaling of fracture numbers, even in a fractal system [Bour et al., 2002].

For illustration of the difference between two types of sets of points, Figure 3-2 shows a Poisson point process and a fractal one. Both can be viewed as a set of fracture centres. If the point spatial distribution follows a Poissonian model, it follows directly that the number of points included in a system of linear size L is simply proportional to the observation area in $2d$, that is L^2 (left column). A set of points has a fractal repartition if the density scaling is proportional to L^D, with $D<d$ (where d=2 for the plane in Figure 3-2).

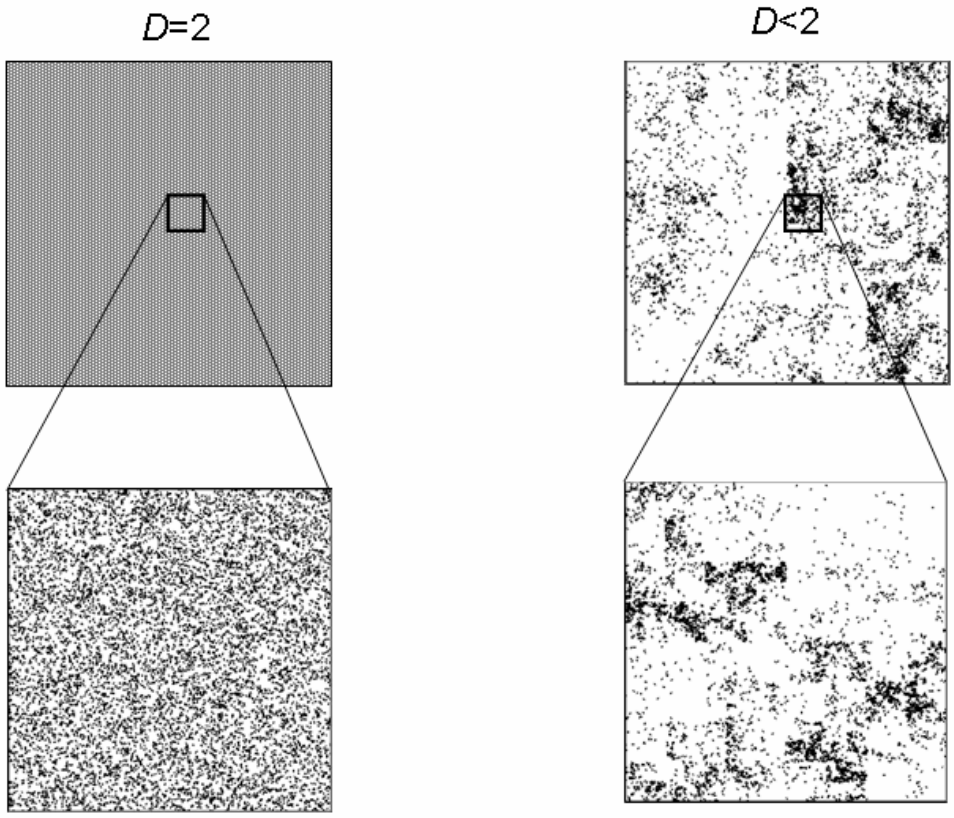

Figure 3-2: *Illustration of two stochastic sets of points. In the left column the set is Poissonian. In the right column the system is fractal.*

Several methods exist to measure the fractal dimension of an object (box-counting, mass method, correlation integral, multifractal analysis). Since they refer to different geometrical properties of the object measured, they do not necessarily provide the same value of fractal dimension. Details on the different methods used and different fractal dimensions obtained can be found in [Bonnet et al., 2001]. For the fractal dimension of a natural fracture set, it has been demonstrated that the best method to characterize the system is the measure of the correlation integral. The pair correlation function $C_2(r)$ is defined as:

$$C_2(r) = 2N_p(r)/\left[N(N-1)\right]$$

where $N_p(r)$ is the number of pairs of points whose distance is less than r and N the total number of points in the system. It follows then that the correlation dimension is equal to:

$$D_2 = \lim_{r \to 0} \frac{\log C_2(r)}{\log r}$$

D_2 is called the correlation or mass dimension. It will be simply called the fractal dimension in the following.

Analyses of numerous natural fracture fields have provided fractal dimensions varying between 1 and 2, with a majority of exponents between 1.5 to 2 [*Bonnet et al*, 2001] for 2d outcrops, underlying the difficulty to measure fractal dimension of natural fracture systems.

Density length fracture distribution model

Both scaling properties, reviewed briefly above, (i.e. length distribution and spatial distribution) are now integrated in the statistical fracture model described here. It indeed provides simultaneously the length distribution and the fracture density scaling or spatial heterogeneity of a fracture system. The model was originally proposed by Davy et al. [1990] and was recently validated by Bour et al. [2002] over a fracture network mapped from the metric scale up to almost the kilometric scale in the Hornelen basin (Norway). The model simply gives the number of fractures centres, $n(l,L)\mathrm{d}l$, observed within an elementary volume of typical size L, and whose lengths belong to the interval l and l+dl:

$$n(l,L)dl = \alpha L^D l^{-a}\mathrm{d}l \quad \text{for } l\in[l_{\min}, l_{\max}].$$

We recall that a is the exponent of the power law length distribution, D is the fractal dimension, α a constant. The only intrinsic characteristic length scales of the model are the smallest and largest fracture length, $l_{\min}$ and $l_{\max}$ respectively. L corresponds to the scale of observation. In so far as some correlations between length and orientation can be neglected, the model can be easily extended to incorporate any fracture orientation distribution such as: $n(l,L,\theta)\,\mathrm{d}l\,\mathrm{d}\theta = \alpha\, L^D l^{-a}\, \Psi(\theta)\,\mathrm{d}l\,\mathrm{d}\theta$, were $\psi(\theta)$ represents the orientation distribution function.

The fractal dimension D fixes the level of heterogeneity. When D is equal to the Euclidean dimension d, (d=3 for a volume, d=2 for a plane and 1 for a line) the fracture network model is uniformly or regularly distributed. As soon as $D<d$ the system is said to be fractal. The total number of fractures, $N(L)$, present in a system of linear size L centred on the fracture network is expressed by :

$$N(L) = \int_{l_{\min}}^{l_{\max}} n(l,L)\mathrm{d}l = \frac{\alpha l_{\min}^{-a+1}}{(a-1)} L^D$$

Therefore the density of fractures, expressed by the ratio $N(L)/L^{\mathrm{d}}$, is equal to $L^{\mathrm{D-d}}$. It comes directly that $N(L)=d_c \cdot L^{\mathrm{D}}$. As a consequence, the apparent fracture centres density, defined by the ratio of $N(L)/L^3$, decreases with scale as $L^{\mathrm{D-3}}$, where D-3 is less than one as long as the fracture system is fractal, that is $D<3$ by definition of a fractal.

Stereological relations

The statistical model describes equivalently the trace length distribution in 2*d* or the diameter length distribution in 3*d*. Note that fractures are assumed to be isotropic planar shapes in 3*d*. Furthermore, the exponents of the 2*d* and 3*d* model can be related. Let $n_{3d}(l,L)$ be the 3*d* statistical model of fractures:

$$n_{3d}(l,L) = d_c \cdot \frac{a_{3d}-1}{l_{\min}^{-a_{3d}+1}} \cdot L^{D_{3d}} \cdot l^{-a_{3d}},$$

where l represents the fracture diameter of the 3*d* disk-shaped fractures and d_c the fracture centre density.

Scaling exponents

Several authors ([Berkowitz&Adler, 1998] [Piggott, 1997] [Darcel et al., *in press*]) have demonstrated that, either for a power-law or a lognormal model of the length distribution in 3*d*, the apparent distribution of fracture trace lengths on a 2*d* outcrop remains of the same nature (power-law or lognormal) and that the parameters of the trace length distribution and the real fracture length distribution are related in a simple way. In particular, for a power-law model of disc-shaped fractures in 3*d*, the relations between 3*d* and 2*d* parameters are:

$$a_{d+1} = a_d + 1$$

$$D_{d+1} = D_d + 1 \quad \text{if } a_d > 2$$

Note that these relations are established for the case of isotropic fractures (for instance disk-shaped). Strong fracture anisotropy would introduce bias in these relations.

Orientation distribution

A specific orientation distribution clearly influences the probability of intersection between fractures and also between the fractures and sampling areas (outcrops, tunnel walls, boreholes). As a consequence the sampling of a fracture network by a plane or a borehole is obviously dependent on the orientation distribution. However, as long as orientations are not correlated to fracture lengths, the relative proportion of the different fracture length classes is preserved. Therefore, under that assumption, the above stereological relations remain valid either for uniform or for non uniform fracture orientation distributions.

*Density extrapolation in 3*d

Besides the scaling exponents, the density, or the total amount of fractures within the bulk rock mass, remains to be estimated. The amount of fractures within the system of linear size L can be expressed as the total number of fracture centres, $N_d(L)$, or as the total fracture mass (cumulative length in 2d or cumulative surface in 3d), $M_d(L)$, present in the system, where d is the Euclidean dimension (1, 2 or 3). Both expressions are recalled here:

$$N_d(L) = \int_{l_{\min}}^{l_{\max}} n_d(l,L)dl$$

$$M_d(L) \propto \int_{l_{\min}}^{l_{\max}} n_d(l,L) \cdot \min(l^d, L^d)dl \equiv P_{d(d-1)} * L^d$$

Therefore the ratio of $M_d(L)$ by L^D corresponds to the so-called $P_{d,d-1}$ parameter commonly used in the Äspö context, which gives the fracture density in m^2/m^3 (P_{32}).

[Berkowitz and Adler, 1998] calculated the relation between 2*d* trace densities and 3*d* bulk densities of disk-shaped fractures for random orientation distributions. They show that the bulk density depends simply on the ratio of the areal trace density divided by the mean diameter length, times a factor equal to $4/\pi$, where the areal trace density is the number of fracture traces, not the cumulative length of traces. They provide a "complete method" to derive the complete diameter length distribution. To take simply into account the specific orientation distribution of fracture sets at Äspö, most studies have related values of P_{10} to P_{32} by a trial and error simulation method. The advantage is to take care in a simple way of the specific orientation distribution. Indeed, the assessment of P_{32} depends only on the orientation distribution, not on the nature of the fracture diameter length distribution.

For a fractal fracture system, the fracture centre density should decrease with scale as $N(L) \sim L^{D-3}$ where D is the fractal dimension in 3*d*. The fracture mass in the system (noted $M_d(L)$, see equations above) evolves similarly as long as a_{3d} is larger than 3. We notice that if the fracture density can be estimated directly at the scale of interest, the possible problem posed by the dependence of $M_d(L)/L^3$ with L (see applications in section 4.2) can be bypassed.

Finally, having estimates of both P_{32} and the scaling exponent of the power-law model is not sufficient to completely describe the model in 3*d*. Indeed, for systems dominated by relatively small fractures[2] ($a_{3d}>3$), we have:

$$M_{3d}(L) = \int_{l_{min}}^{l_{max}} d_c \cdot \frac{\pi}{4} \cdot \frac{a_{3d}-1}{l_{min}^{-a_{3d}+1}} \cdot L^{D_{3d}} \cdot l^{-a_{3d}+2} \cdot dl = d_c \cdot \frac{\pi}{4} \cdot \frac{a_{3d}-1}{l_{min}^{-a_{3d}+1}} \cdot L^{D_{3d}} \cdot \frac{l_{min}^{-a_{3d}+3}}{a_{3d}-3} = d_c \cdot \frac{\pi}{4} \cdot \frac{a_{3d}-1}{a_{3d}-3} \cdot l_{min}^2 \cdot L^{D_{3d}}$$

Then evaluation of l_{min} and d_c must be performed simultaneously (or rather l_{min} must be estimated to obtain d_c). In theory l_{min} corresponds to the lower cut-off of the fracture length distribution. Taking a purely theoretical case, the value of l_{min} in 3*d* can be deduced from the 2*d* trace length distribution. Figure 3-3, based on a numerical experiment where fractures are generated in 3*d* space, and their trace length along a given plane is recorded, illustrates how this can be done in principle. However in practice almost systematic resolution effects will hide the transition and the existence of fractures smaller than l_{min} (as it has been theoretically defined) also mask the transition. In practice, we assume that l_{min} corresponds, in 3*d*, to the length under which the power-law model is no more valid (decrease of the quantity of fractures by comparison to the theoretical value calculated according to the power-law model). In practice we need to assess the values of both l_{min} and of P_{32} in order to obtain the complete 3d model.

[2] Case corresponding to our analysis of Äspö fractures.

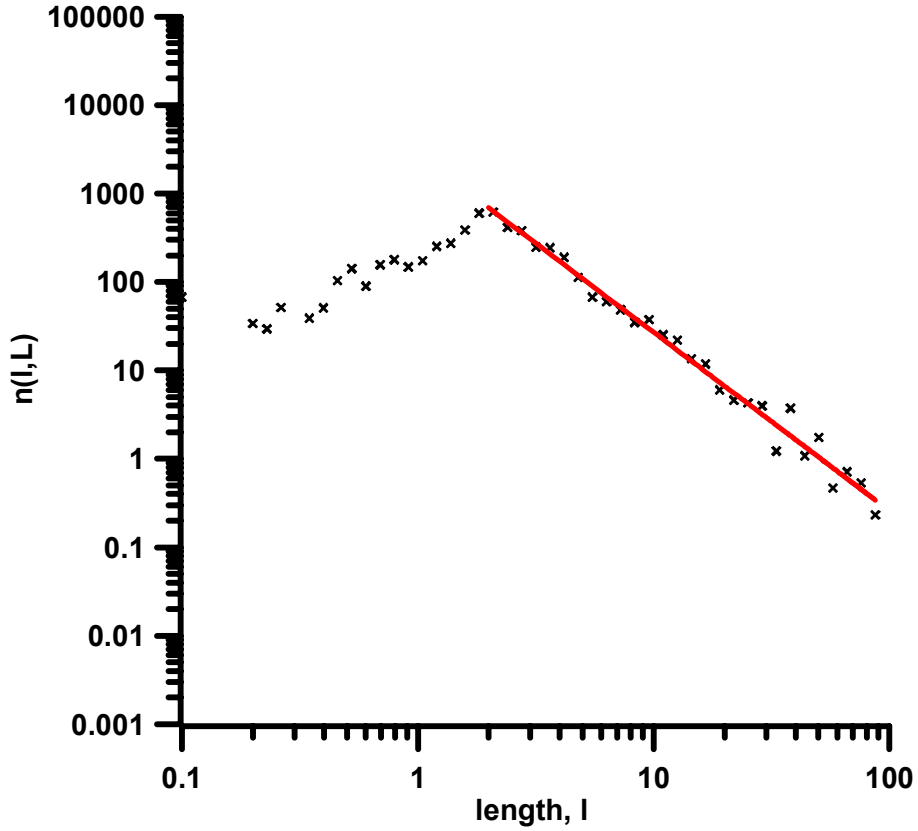

Figure 3-3: *Apparent trace length distribution arising from the intersection of a purely synthetic 3d fracture network by a 2d plane. The parent 3d length distribution corresponds to* $a_{3d}=3$ *and* $l_{min,3d}=2$*. For the trace length distribution* $a_{2d}=2$ *(red straight line with slope -2) and* $l_{min,3d}=2$ *can be easily identified.*

3.2 Database

3.2.1 2*d* maps and 1*d* borehole maps

A total of 15 2*d* maps of fracture traces and 5 1*d* borehole logs were analysed. The 2*d* maps are either outcrops or tunnel maps. The map names and references are summarized in Table 3-1.

a)

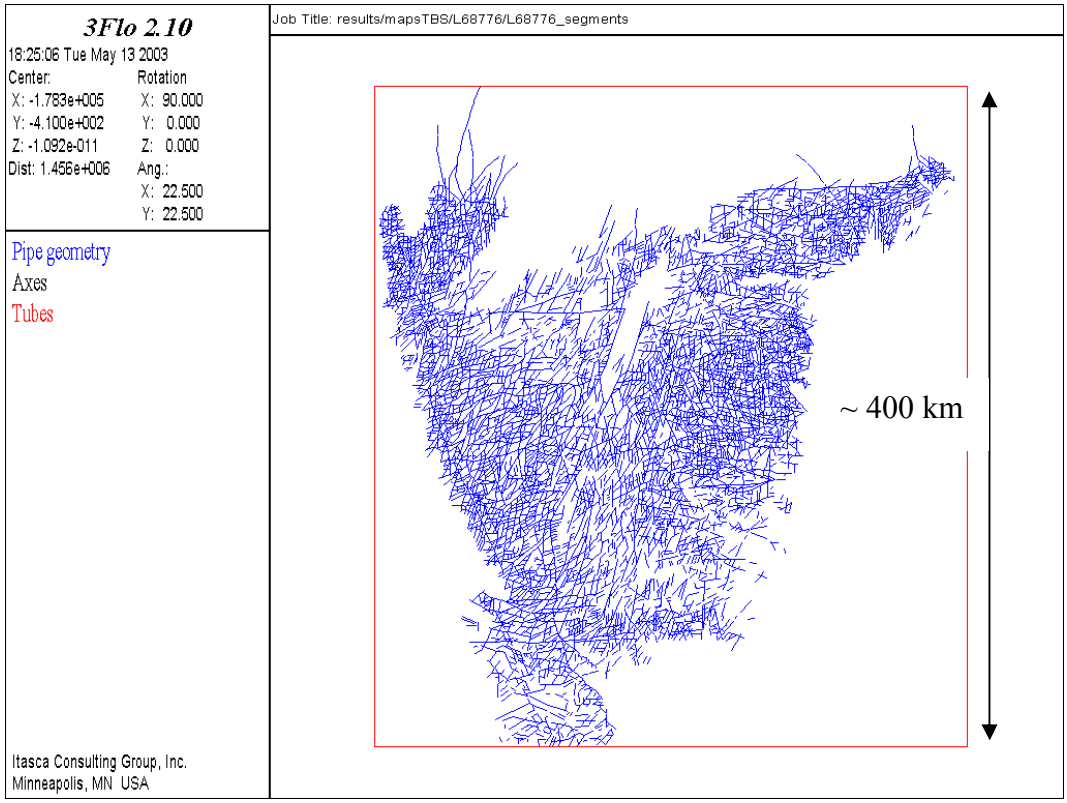

b)

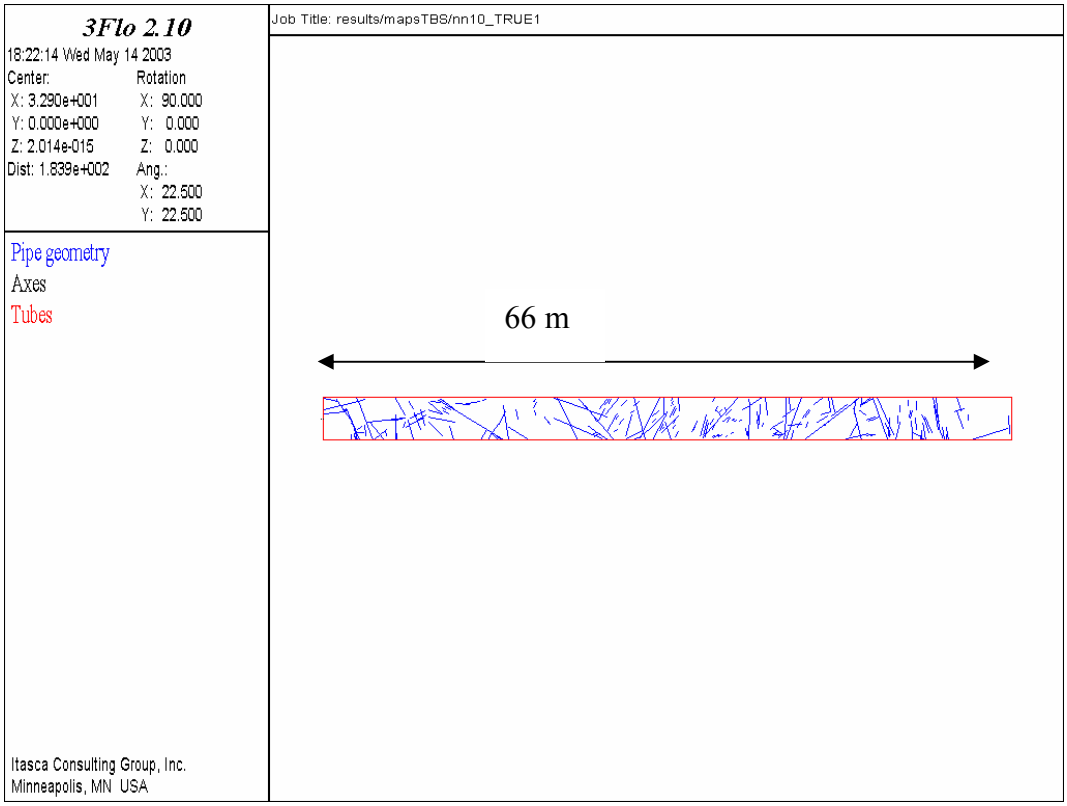

Figure 3-4: *Two maps, a) L68776 (south of Sweden), around 400x400 km and b) TRUE-1 tunnel, 66x4m.*

Table 3-1: References of all the data set analysed to assess the statistical properties of the Äspö fracture system. The "reference" column indicates former reports for which the data where collected or in which they were already treated.

Map name	Type	Reference	Scale	# Traces
L68776	2*d* outcrop	[Lapointe et al., TR99-03, 1999]	**~ 400 km**	**3614**
L68778	2*d* outcrop	[Lapointe et al., TR99-03, 1999]	**~ 50 km**	**449**
Greg	2*d* outcrop	[Lapointe et al., TR99-03, 1999]	**~ 25 km**	**1357**
L78780	2*d* outcrop	[Lapointe et al., TR99-03, 1999]	**~ 55 km**	**1123**
Äspö	2*d* outcrop	[Lapointe et al., TR99-03, 1999]	**~ 1 km**	**759**
Äspowest	2*d* outcrop	[Bossart et al., TR-01-21, 2001]	**75 m x 30 m**	**173**
Avro	2*d* outcrop	[Bossart et al., TR-01-21, 2001]	**60 m x 30 m**	**415**
Ew-1	2*d* outcrop	[Mazurek et al., ICR97-01, 1996] [Bossart et al., TR-01-21, 2001]	**< 7 m x 6 m**	**386**
TRUE-1	2*d* tunnel	[Bossart et al., TR-01-21, 2001]	**66 m x 4 m**	**229**
T-1978-2003	2*d* tunnel*	[Mazurek et al., ICR97-01, 1996] [Bossart et al., TR-01-21, 2001]	**25 m x 6 m**	**50**
T-2232-2260	2*d* tunnel	[Bossart et al., TR-01-21, 2001]	**28x2 m**	**395**
T-2050	2*d* tunnel	[Bossart et al., TR-01-21, 2001]	**1.325 x 1.5 m**	**52**
T-2963	2*d* tunnel	[Bossart et al., TR-01-21, 2001]	**2.75 x 2 m**	**144**
T-3124	2*d* tunnel*	[Mazurek et al., ICR97-01, 1996] [Bossart et al., TR-01-21, 2001]	**2 x 4 m**	**32**
T-3580	2*d* tunnel	[Bossart et al., TR-01-21, 2001]	**2 x 2 m**	**94**
KI0025F02	1*d* borehole**	[Andersson et al., TR-02-13, 2002]	**204.2 m**	**180 open+conducting features**
KI0025F03	1*d* borehole**	[Andersson et al., TR-02-13, 2002]	**141.7 m**	**45 conducting features**
KA2563A	1*d* borehole**	[Andersson et al., TR-02-13, 2002]	**263.4 m**	**88 conducting features**
KA2511A	1*d* borehole**	[Andersson et al., TR-02-13, 2002]	**293 m**	**91 conducting features**
KA3510A	1*d* borehole**	[Andersson et al., TR-02-13, 2002]	**150 m**	**41 conducting features**
: water-conducting features** *: water-conducting and non water-conducting features**				

The different outcrop maps cover a very large range of scales, going from about four hundreds kilometres (Figure 3-4a) for the largest one, down to a few tens of meters. The tunnel maps have an obvious limited lateral extension due to tunnel shape, whereas their length goes from 2 m up to almost a hundred meters (Figure 3-4b). At a given scale of observation, the number of fractures observable is mainly dependent of resolution effects (scale under which fractures may be present but are invisible).

3.2.2 Overall density

By consulting the different reports various values of fracture intensities have been collected. At the Äspö site, the density of fractures is usually expressed in terms of P_{10} (number of fracture intersections per meter of observation) along a borehole, P_{21} (in m^{-1}, summed trace length of fractures per square meter) for 2*d* measurements and P_{32} (in m^{-1}, summed fracture area per cubic meter). The apparent variability observed (Table 3-2) may be due to actual variations of fracture intensity through the fracture system. However the measured intensity also depends on the different methods of data acquisition and is subject to resolution effects. In particular, the conductive fracture intensities were originally measured from packer tests with a 5m interval. A more recent method (Posiva Heat Pulse Flow Log) provides almost continuous measurements of flow rates (resolution equal to 0.1m) between $2\ 10^{-3}$ and 5 l/min.

Fractures under the resolution limit are considered as non-conductive (open) features. Therefore, as a consequence of resolution variations, fractures that would have been labelled as "conductive" with one method may be labelled as "non-conductive" when using another method. Note that analyses for estimation of fracture transmissivity distributions will be recalled in Chapter 4. Transmissivity values do not directly interfere with the fracture size distribution estimation, which is *a priori* considered for the whole network, that is for all fractures, whether they conduct water or not.

Table 3-2: Summary of measured values of fracture intensities (P_{10}, P_{21} and P_{32} in m^{-1} see text for details. Subscript "c" indicates a measure of conductive features).

Object	Report	Reference	P_{10}	P_{21}	P_{32}	P_{10c}	P_{21c}	P_{32c}
			Non conductive **- open** **- open & closed**			**Conductive**		
TrueBlockScale Borehole KA2563A	IPR-01-70		3.2		5.1-6.4	2		3.2 - 4.0
True Block Scale	TR-02-13	p122, from Posiva flow logs				0.16 to 0.21 average 0.19		0.29
	IPR-03-13	p31, for the background fractures						0.16 (set 1) + 0.13 (set 2)
TBS The TBM tunnel	IPR-01-71			0.546	0.47			
	TR-01-21	p 38. Previous work Dershowitz et al.,96						2.45
		p39, Mazurek et al.,96 tunnel section near TRUE-1, trace map		1.27				
		p39, scan line on trace map	1.63					
		p44, Tunnel wall map P_{32}: try/error, until $P_{21,sim} = P_{21,obs}$			2.1			
		P 44, from dershowitz et al.,96 Log analysis from KXTT boreholes				1.55		3.17
		Along ten simulated scanlines on tunnel wall, p 44	0.8					
		p44, **Open** fracture frequency in boreholes, dershowitz,96	1.3 to 2					
		p44, Borehole BIP evidence, **open and closed fractures**	4.5		6.7			

3.2.3 Orientations and fracture sets

The global fracture system at Äspö is made up of different fracture sets distinguished by different orientation distributions. Within the Äspö HRL, orientation distributions are deduced from borehole logging (BIPS, TV imaging). Corresponding results are illustrated in Figure 3-5.

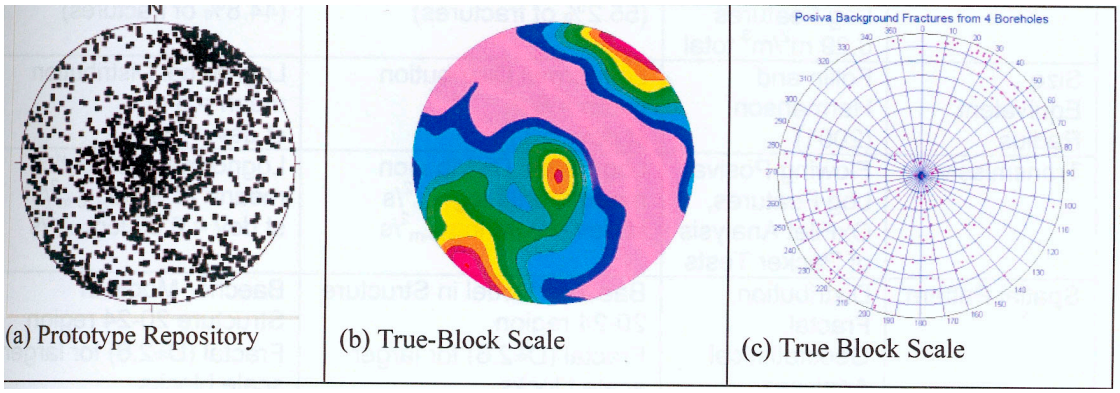

Figure 3-5*: Orientations of background fractures throughout Äspö HRL, from [IPR-03-13].*

Distinct fracture families are also observed at various scales, as illustrated on the outcrop map of the Äspö island (Figure 3-6). Although different fracture sets have been systematically observed, no clear distinction in terms of fracture length can be made between the different fracture sets. This is illustrated in Figure 2-4 (extracted from [Lapointe et al., TR99-03, 1999]. Cumulative Complementary Distribution Functions are shown for different fracture orientation families, on different maps at scales from the HRL up to the kilometre scale. Equivalent exponents can be deduced from the slope of the linear part in these CCDF's. The various curves of orientation families yield the same exponents, and therefore their length distributions can not be distinguished. As a consequence, in the following statistical analysis of fracture lengths, the different fracture sets are treated as one single population.

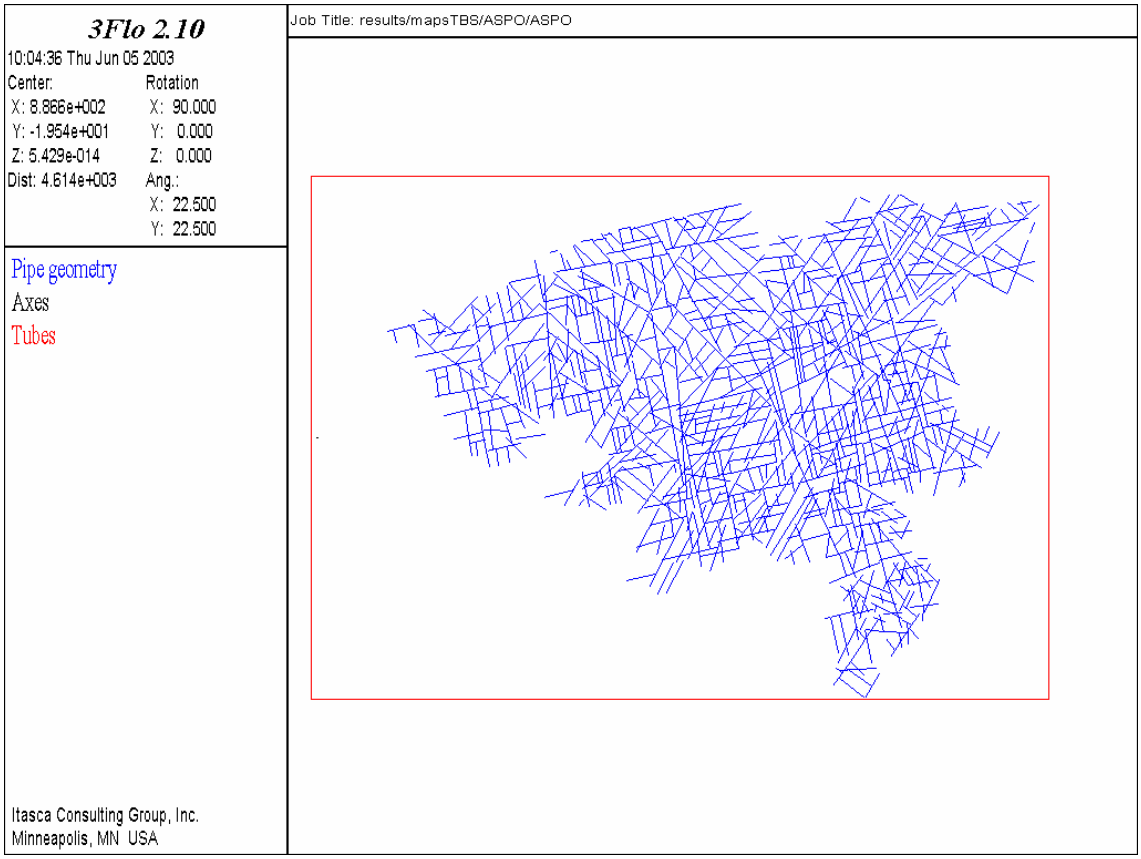

***Figure 3-6**: Map of the Äspö island showing several families of fracture orientations (red rectangle frame size : 1657 by 1174 meters). See also [TR-99-03] page 23).*

3.3 Methodology

As underlined in the review of existing reports, contradictory arguments exist pro and against the validation of a multiscale or power-law model to represent the fracture sizes at Äspö. Here we propose to analyse the data described above, first separately (in terms of observation scale not fracture set, see previous section) and then simultaneously to provide a complete multiscale analysis. The method excludes any *a priori* characteristic size within the system and aims at integrating all scales of observation. We note that whether or not the power-law model can be validated, the multiscale analysis provides a complete analysis of the fracture system, and should highlight the possible existence of characteristic length scales if they exist. In the following, fractures coming from different fracture orientation sets will be considered as one single population. Indeed, the reports reviewed indicated neither any correlation between fracture lengths and orientations, nor a dependence of the orientations with spatial position.

Both the spatial arrangement and the length distribution are studied simultaneously. Data from each map are first separately considered before the integrated multiscale analysis. Indeed, by doing an appropriate normalization, data from the different maps can be represented simultaneously thus allowing a multiscale analysis that reduces the strong effects of finite size.

3.4 Spatial analysis

The spatial analysis is performed on the 1*d* borehole data and on the 2*d* outcrop maps.

3.4.1 1*d* analysis

In the case of 1d boreholes, a data set is made up of the list of the fracture intercept positions (i.e. positions of the intersections between the borehole and the fracture system). The analysis of conductive, open and open & conductive (sample of size 180) fracture intercept positions is performed using data from borehole KI0025F02. Results show that for each of these 3 sets, a fractal character (slope less than 1 for 1*d* data) appears, with a fractal dimension around 0.7-0.8 defined over more than one order of magnitude (Figure 3-7). Note that the same analysis performed over the **sealed fractures** and the **veins** (from BIPS data and around 200 fracture intercepts for each sample) led to a dimension close to 1. This difference may be due to a structural difference between the conductive/open fracture network and the sealed/veins fracture network. Note that the flow path heterogeneity combined with physical/chemical processes (i.e. change in ambient conditions, chemical interactions, precipitation and dissolution…) govern the geometry of the conductive network, as compared with the geometry of the overall (conductive, sealed, and so on… fractures) network. Also, such a comparison between open&conductive and sealed fracture intercept positions along a borehole was performed for only one borehole (KI0025F02). The result should therefore be taken cautiously. The analysis indicates nevertheless that the fractal dimension of the conductive fracture network is similar to the fractal dimension associated with the potentially conductive fracture network (i.e. conductive + open).

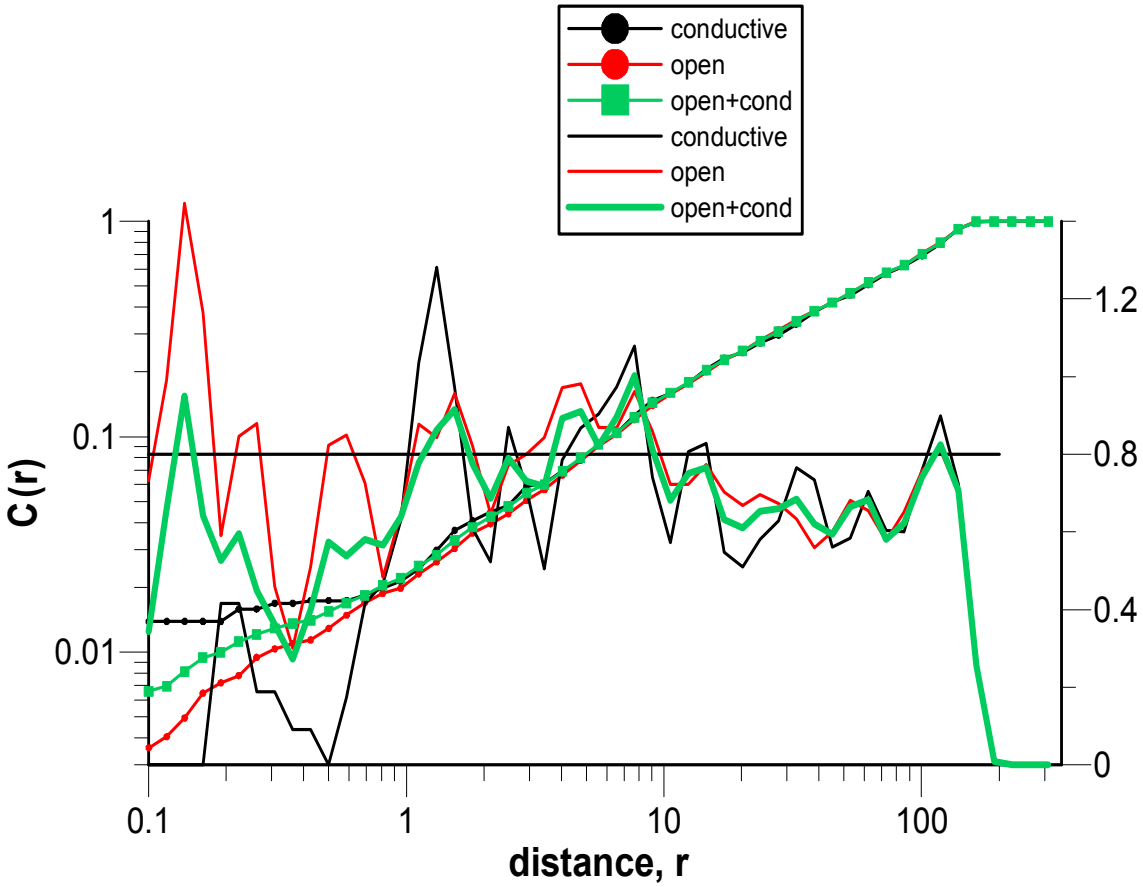

Figure 3-7: *Diagram of the correlation integral C(r) for borehole KI0025F02. r is in meters. Lines with symbols correspond to the evolution of C(r) (left axis). Simple lines represent the local slope of C(r) (right axis). The local fractal dimension is directly read on the right axis. The black straight line represents a constant value of 0.8 for reference. The sample size of conductive + open fractures is equal to 180 intersections along a 170 meter long line).*

Next, the analysis of the fractal dimension of conductive fracture intercept positions is performed over the 5 boreholes indicated in *Table 3-1*. Since the 5 data sets cover the same length range, they can be directly averaged to produce one more robust sample. The resulting correlation integral function shows an exponent *D* equal to 0.85 well defined over more than one order of magnitude (over distances between 1 and about 30 meters). Individual correlation integrals were also checked separately and provide similar results.

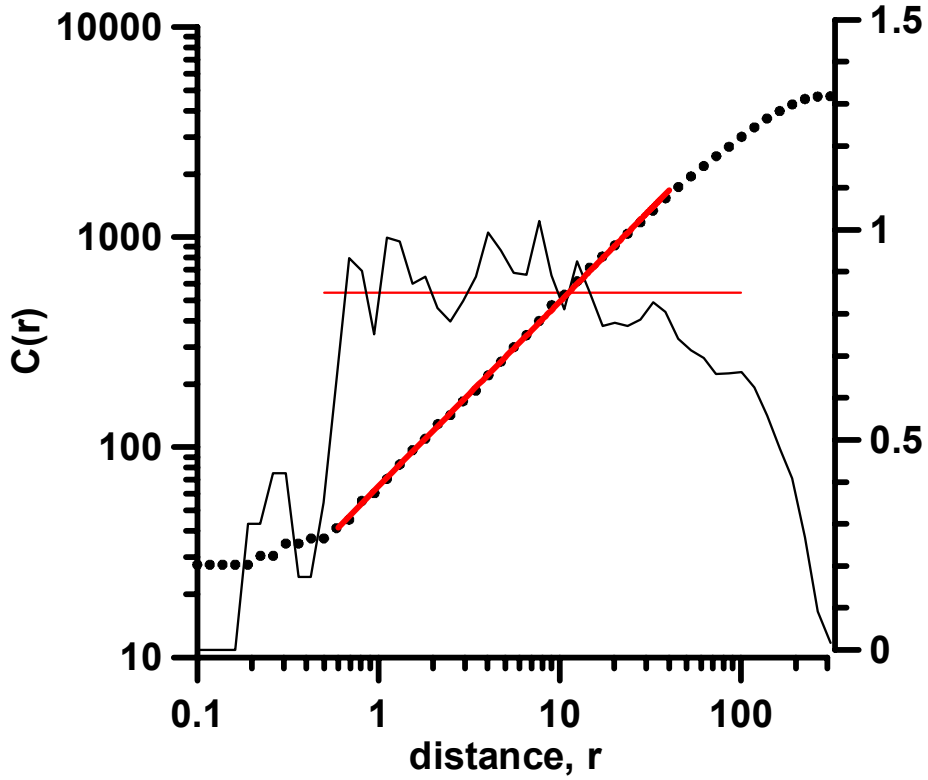

***Figure 3-8**: Diagram of the correlation integral C(r) for the boreholes described in Table 3-1. r is in meters. The line with black dots corresponds to the variations of C(r) (left axis). The thick red line represents the corresponding power law fit with D_{1d}=0.85. The local fractal dimension can be read on the right axis. The thin red line represents the power-law fit (right axis).*

In summary, the fractal dimension deduced from 1*d* samples of the conductive fracture network at Äspö is less than one. Therefore it does not support a purely random Poisson model of spatial distribution. The fractal dimension is well defined at about 0.8±0.5. Moreover, the more complete analysis performed on borehole KIF0025F02 data indicates that the fractal dimension of the conductive fracture network is similar to the one of the complete fracture network (conductive + open). Let us recall that due to instrumentation limitations an open fracture could be conductive with an undetectable flow rate (less than 2 10^{-3} l/min).

3.4.2 2*d* analysis

The second part of the spatial analysis is devoted to the 2*d* outcrop maps. The tunnel maps could not be analysed here because of data scarcity and strong finite size effects: maps are very elongated, *i.e.* the ratio between scan length and transverse length is >>1. Moreover, as explained in section 3.1.1, the measure of the fractal dimension also depends on the relative amount of small fractures by comparison to the system size. Hence, the fractal dimension is measured over the most robust remaining 2*d* maps. These correspond to fracture maps called Äspö (the whole Island), GREG, L68778, L68780 and L68776 (see *Table 3-1*).

The slopes measured over the five data sets vary between 1.85 and 1.95 (Figure 3-9). As can be readily seen in the figure, the range of stability of the fractal exponent is very short, or even missing. The tendency is more to have a continuous variation of the local slope. This effect can be either intrinsic to the fracture system, or simply due to the possibility/impossibility to measure the fractal dimension of the fracture network with the available data.

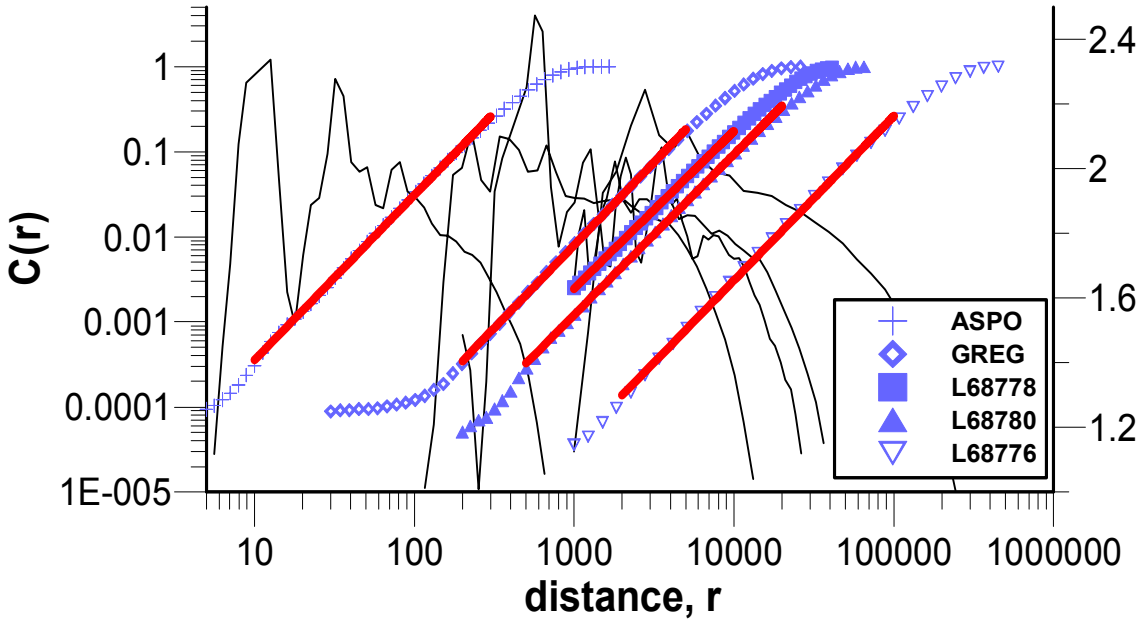

***Figure 3-9**: Diagram of the correlation integral C(r) corresponding to the five outcrop maps (see legend) described in Table 3-1. r is in meters. The lines with symbols correspond to the variations of C(r) (left axis). Power-law fits are represented in red. Black single lines represent the local slope of C(r) (right axis).*

In summary, the fractal dimension D_{1d} is about 0.8±0.5, the fractal dimension D_{2d} is between 1.85 and 1.95 (almost 2). [Darcel et al., *in press*] have shown that in the case of a power-law density length distribution model, the relation $D_{d+1}=D_{1d}+1$ occurs if the exponent a_{d+1} of the power-law length distribution is larger than 2. We will see in the next section that the exponent a measured remains larger than 2. Therefore, the fractal dimensions measured on 1*d* and 2*d* samples are consistent. Moreover, this indicates that in 3*d*, the fractal dimension of the 3*d* fracture network should be within the range 2.8 to 3.

3.5 2*d* trace length distribution

3.5.1 Sampling maps

We recall that here the purpose is to bring out a robust statistical and geometrical model for the fracture system of Äspö and to estimate its range of validity over scales. Ideally, the range of correctly sampled length classes, *l*, should be such that:

- $l_{censoring} << l << l_{truncation} < L$,

- the number of fractures in the length class is statistically relevant.

Note that from a methodological point of view, to perform the length distribution analysis, a logarithmic bin is chosen and a density distribution representation is chosen since they allow us to measure an exponent that is independent of the binning choice (linear or logarithmic) [Bonnet et al., 2001]. Then we have:

n(l) = l^(-a). dl , therefore *n(l)/dl = l^(-a)*, where *dl* represents the bin size and *n(l)* is the density distribution.

When studying each map individually, numerous effects appear, that severely limit the range of analysis. They are listed below:

- the number of fractures within a map is often severely limited, especially for small tunnel maps.
- Statistical effects such as truncation are pervasive. The probability to entirely sample a fracture of a given length at a given system size can be low, meaning that we will not get much significant information on some fracture length size classes.
- The determination of the characteristic - or linear - size for a map can be difficult/arbitrary. This is needed to enable the comparison between maps. Also, how does the characteristic size of the map relate to the truncation scale for this map? For instance, in the simplest case of a square-shaped map, the characteristic size is obviously its side length, from which the area, and the truncation scale can be directly deduced. The question is however more complex for a rectangular, anisotropic or irregular pattern, where the square root of the area does not correspond necessarily to an obvious characteristic length of the map. In such a case, the apparition of truncation effects from a certain fracture length can not be simply related to the characteristic length of the map. In the present study several maps have a complex shape, very irregular, or elongated.
- A sampling bias appears in the choice of the small scale tunnel maps, whose locations may have been chosen especially to contain fractures that cross the entire map, and/or conduct water. In this case, smaller fractures are partially sampled only in the vicinity of the main local structure.

Because of all these effects, we shall see that several maps among the ones listed in *Table 3-1* can hardly help to build a robust statistical model of fractures. We recall that the main point when considering each map, is to assess whether or not one can find a fracture length class with a robust statistical representation.

3.5.2 Individual maps

Maps **T-3124** and **T-1973-2003** were specifically designed, for the purposes of FCC I and II, to study one conductive zone (one or several fractures) at the decametre scale (or "mesoscale"). They therefore can not be used in the statistical analysis.

a)

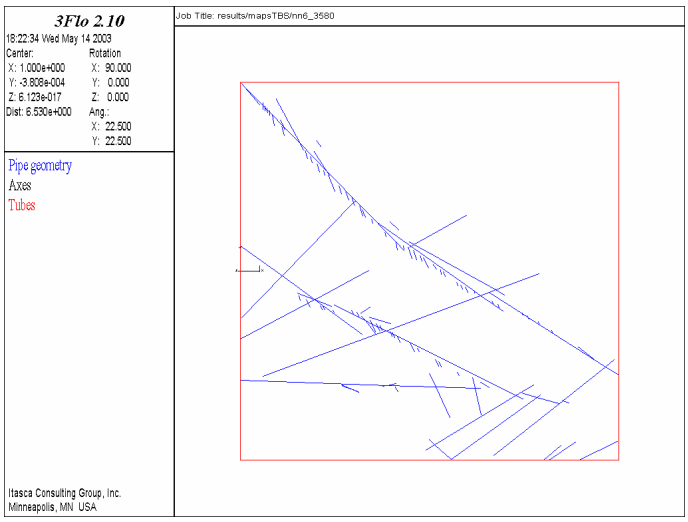

b)

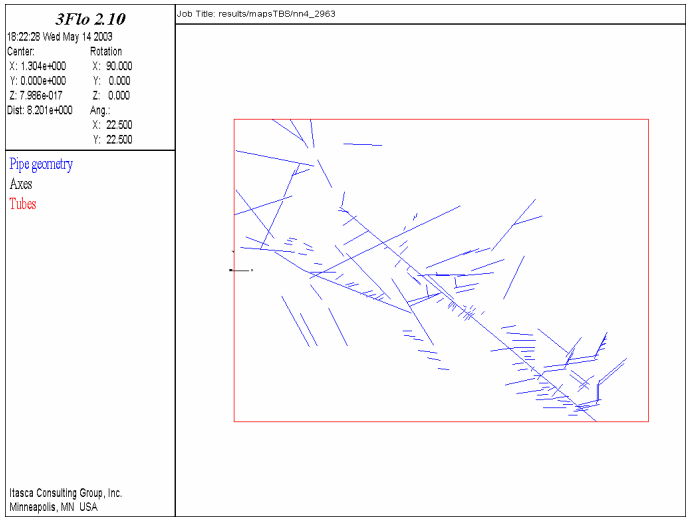

c)

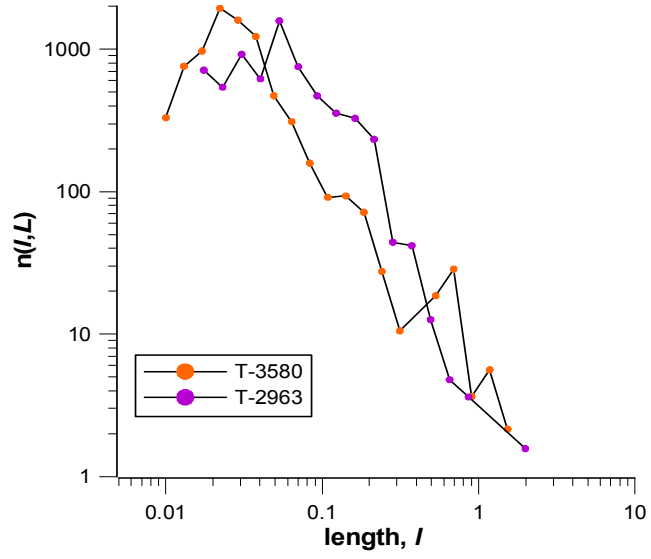

Figure 3-10: *a) map T-3580, 2 by 2 meters. b) map T-2963, 2.75 by 2 meters. c) length distribution for maps displayed in a) and b). Note that fractures are represented as idealized straight segments, not exactly as they actually look like.*

Maps **T-2050**, **T-3580** and **T-2963** were designed to study small-scale fracturing during FCC III. They contain fracture traces with lengths ranging from 0.01m up to the map scale, here 1 to 2 meters. By looking at the visual fracture repartition, it seems that here again smaller fractures have been sampled only in the close vicinity of main local structures. For that reason, the direct estimation of a power-law exponent or more generally of any theoretical length distribution remain questionable for these maps. Therefore here we choose to retain only map T-2963 because it presents a larger distribution of fractures with different sizes. We retain only one point over the length distribution, as the point were the probability to have the right sampling of the fracture trace lengths is the stronger.

Maps **T-2232-2260** and **TRUE-1** are two vertical maps of distinct orientations. Although both map scales are of the same order of magnitude, the density of fractures on **T-2232-2260** is significantly larger than on **TRUE-1**. This could be due to their different orientations (**T-2232-2260** is better oriented to catch NW fractures than **TRUE-1**) or simply to the fact that the spatial density of fracturing is heterogeneous at the scale of a few meters. Furthermore, both maps are rectangular with a ratio of about 15 between scan and transverse length. This particular shape may entail strong finite size effects. Indeed, as discussed above, it renders difficult to define a characteristic linear size of the system. Should it be the scan length, l_s, the transverse length l_t, the minimum value $\min(l_s , l_t)$, the arithmetic mean $(l_s+ l_t)/2$ or the geometric mean $(l_s \cdot l_t)^{1/2}$? It is beyond the scope of the present study to treat in details this effect on the power-law sampling.

Nevertheless, if we take into account the worst possible finite size effects, the characteristic size of the system should be $\min(l_s , l_t)$. For a trace length class to be adequately sampled it should lay between the censoring length scale and 10% of the characteristic size of the system ([Bour et al., 2002]). For the TRUE-1, map the truncation length of the sampled traces is within the range 0.3 to 0.5 meters [Bossart et al., TR-01-21, 2001]. As a consequence, since in that case $\min(l_s\text{-},\text{-}l_t)=4$, the range of adequately sampled fracture lengths on the TRUE-1 map is empty, or extremely small (centred around 0.4 meter). We notice that over a very restricted range of scales, an apparent exponent could be estimated at 2.25±0.25 (red line in Figure 3-11).

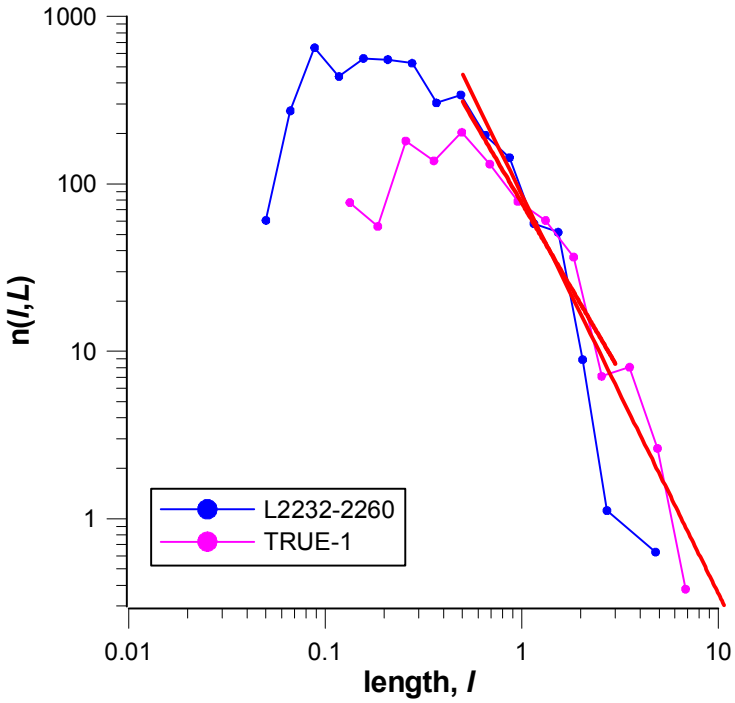

Figure 3-11: *Length distribution for maps TRUE-1 and T-2232-2260. Straight red lines corresponds to hypothetical power-law fits of slopes equal to -2 to -2.5.*

The remaining maps sample the fracture system from the meter scale up to about the hundred kilometre scale. They generally contain significantly more fractures. They are also all horizontal outcrops (identical orientation) so that a possible density variation could not be explained by the dependence of the probability of intersection on the orientation. Each map presents a classical "bell" or "dome" shape resulting from a mix of censoring truncation effects on the real (observation scale independent) fracture traces distribution (Figure 3-12). Measurements of a length exponent *a* for the five largest maps (“Aspo”, “Greg”, “L78778”, “L 78780”, and “couth,L76776”), with at least a thousand fractures each, lead to consistent values of *a* between [2.8 ; 3.1]. The three remaining intermediate maps (i.e. Ew-1, Avro and Aspowest) contain about one hundred fractures and display apparent *a* values about 2.4 to 2.6.

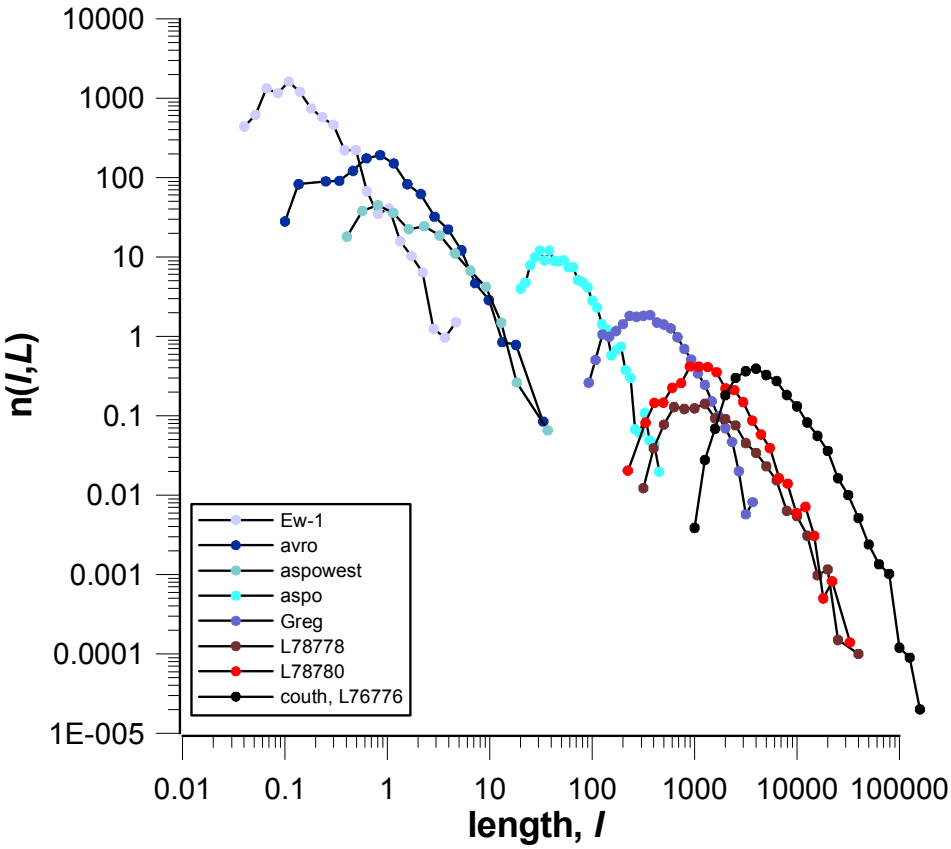

Figure 3-12: *Length distributions deduced from the horizontal outcrop maps (see legend on the Figure).*

Summary

In general, by looking at each of the previously described maps separately, a large range of exponents *a* can be measured, from 2 up to 3, that is almost all the plausible values found elsewhere for natural fracture systems [Bonnet et al., 2001]. In addition each measure is marred by strong uncertainties.

This demonstrates that the maps taken independently are hardly adapted to enable the measure of the amount of fractures belonging to a well defined class of lengths. We notice however that although apparent fracture length distributions always show a maximum, with on both sides a decrease of the amount toward smaller and larger scales, this effect is observable for each map, whatever the scale of observation. For that reason we go further in the analysis by mutually comparing the maps.

3.5.3 Normalization and cross-scale analysis

The cross-scale analysis relies on the assumption that at least a narrow range of lengths is correctly sampled on each map. Only the comparison between maps permits confirmation or not of the relevance of a multi-scale model and to distinguish partly the finite size effects.

Two procedures are applied :

- a direct comparison of the normalized length distributions,
- the identification of the "best sampled length scale" over each map and comparison on a diagram.

Both methods require a proper normalization. Indeed to compare the maps sampled at different scales, it is necessary to represent the quantity:

$$\frac{n(l,L)}{L^D} = d_c \cdot \frac{a-1}{l_{\min}^{-a+1}} \cdot l^{-a}$$

The relation simply means that in order to compare length distributions at various scales they must be expressed in term of fracture densities, that is the number of fractures of a given length per unit of area. This is exactly the case when D_{2d} is equal to 2. For a fractal fracture network, the apparent density decreases with scale and the correct normalization factor is L^D (for details see [Bour et al., 2002; Darcel et al., in press]). Here again the complex shape of several maps may entail some adverse effects. Indeed for several maps the only known parameter is the map area A. To pursue the analysis we assume that the characteristic system size L can be defined as $L = \sqrt{A}$. Note that we could have cut the different maps (at least the largest ones) to obtain regular shapes and thus avoid the pitfall of the shape on the characteristic size determination. It would have however led to a severe increase of finite size effects and a decrease of statistical robustness. The former analysis of the fractal dimension has shown that D_{2d} is included between 1.8 and 2. Both these limiting values will be used to perform normalization.

The normalisation is first performed with a fractal dimension D_{2d} equal to 2. Results of the subsequent normalized density length distributions are represented in Figure 3-13a, where the evolution of $n(l,L)/L^D$ is plotted for each map. If the fracture systems were perfectly described by a power-law, all curves should be well lined-up along the underlying straight line, with slope $-a_{2d}$, departing from the theoretical curve at both ends because of finite size effects. This is in fact what is qualitatively observed along the straight line (in black) with a slope of –3. The representation leads however to some visual confusions: it is hard to discern if any specific curve is tangent to the theoretical curve and, whether the range over which it is tangent is consistent with ranges for censoring and truncation effects.

To improve the analysis, a second procedure is used: we try to look at each map separately, and to mark the best sampled length class. This amounts to choosing the best pair (l_c, $n(l_c,L)$) for each map. Then we use the following relation:

$$\log(\alpha) = a \log(l_c) + \log(n(l_c, L) / L^D)$$

This enable the following graphic construct: straight lines with a slope of $\log(l_c)$ and original ordinate $\log(n(l_c,L)/L^D)$ are plotted on a ($\log(\alpha)$; a) diagram. In theory (i.e. for a perfect power-law model without sampling effects), all the lines deduced from distinct observation scales, should intersect at one single point, with coordinates $(\log(\alpha); a)_c$ on the graph. This procedure thus provides the power-law parameters directly. However, the estimation of l_c for each map is inevitably partly subjective. For each map we kept the best sampled class length l_c according to the following criterions:

- l_c should be significantly smaller than the characteristic length scale of the sample.

- the number of fractures within the corresponding class length should be at least a few tens of fractures to ensure statistical robustness.

Results are plotted in Figure 3-13b and can be compared with the results from the first procedure as shown in Figure 3-13a. Note that the a) plot show curves that are qualitatively well lined up along a line of slope a=-3. Below the one meter scale, however, things on this first plot are less obvious. The Figure 3-13b plot provides clarification. Indeed we notice there the orange lines representing the outcrop maps (with l_c down to 0.5 to 1 meter) all do intersect at a single point with a_c between 2.8 and 3. The apparent density term α_c is between 0.8 and 2.

The lines stemming from vertical tunnel walls, "TRUE-1" (intense pink) and "T-2232-2260" (blue), do not intersect the previous point. Their slopes are close to each other because of their similar scale of observation. The gap between them expresses the difference in density we already noticed. This may be due to small scale spatial density heterogeneity and/or to the distinct map orientations (angle between the maps: approximately 45°), which directly impact on the trace density P_{21}. Both maps are almost at the same scale of observation. Putting them together, that is treating them as only one map, is a (crude) way of minimizing the orientation bias. As a consequence an average is obtained from differently oriented maps. By doing this (with l_c chosen such that it is just above to 0.5, the resolution scale of "TRUE-1" and much smaller than the transverse length of "T-2232-2260"), we obtained a new line (not represented) that cross-cuts the outcrop map lines (in orange) close to a=3. This exemplifies the fact that data coming from maps whose orientations are distinct should be properly corrected for the corresponding orientation effect.

Finally, the pink lines in Figure 3-13b correspond to the small scale tunnel walls. They clearly do not fit with the rest of the data and do not intersect at another single point. However the determination of l_c for these maps led to very poor length classes, and it was shown in the previous section that these maps were probably only sampled around a system size scale structure.

The same analyses were performed with a normalization factor equal to $L^{D=1.8}$. Results are presented Figure 3-14. Again, both representations are closely related and show that even if a power-law model approximately fits the data, the precise definition of the parameters (figures b) remains difficult because of the data quality.

A more precise characterization would require more important trace maps and a better definition of the truncation lengths. As a comparison, all the maps treated in Bour et al. [2002] contain more than 2000 fractures and all the maps except one have a regular shape that enables the unique definition of a characteristic size. We finally notice a slightly better fit on Figure 3-13b), by comparison with Figure 3-14b). The best apparent fit on Figure 3-14a) is this time for a_{2d} equal to 2.8. (by comparison to 3 for Figure 3-13b).

a)

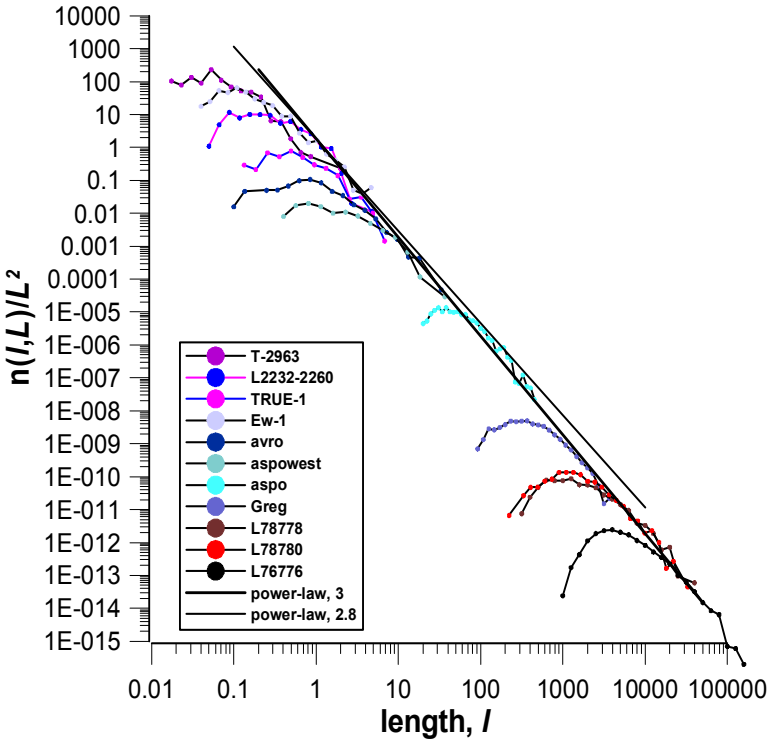

b)

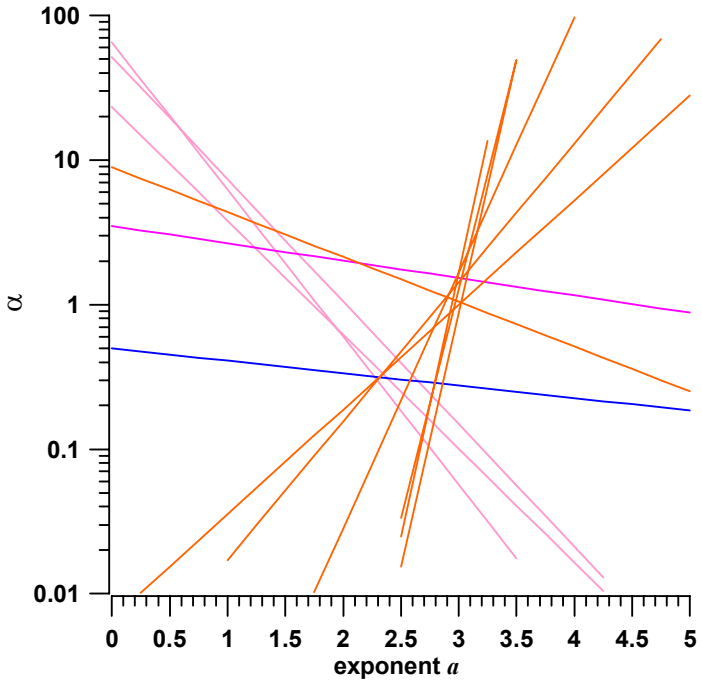

Figure 3-13: *Multi-scale analysis with D_{2d}=2. a) see inlet legend. b) Three sets are distinguished. The three pink lines correspond to small scale tunnel maps, the blue and intense pink lines respectively correspond to T-2232-2260 and TRUE-1. Orange lines correspond to outcrops. See text for further details.*

a)

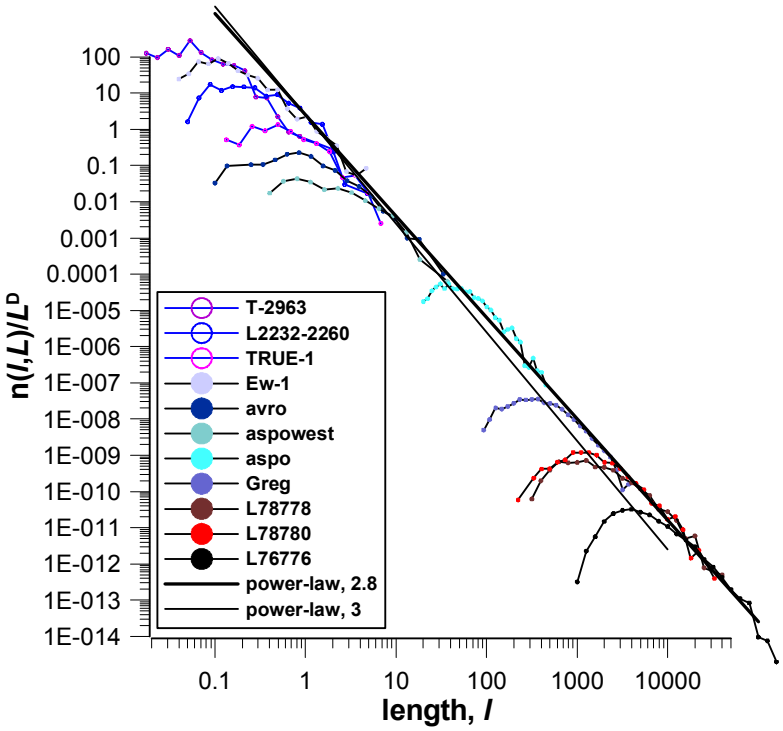

b)

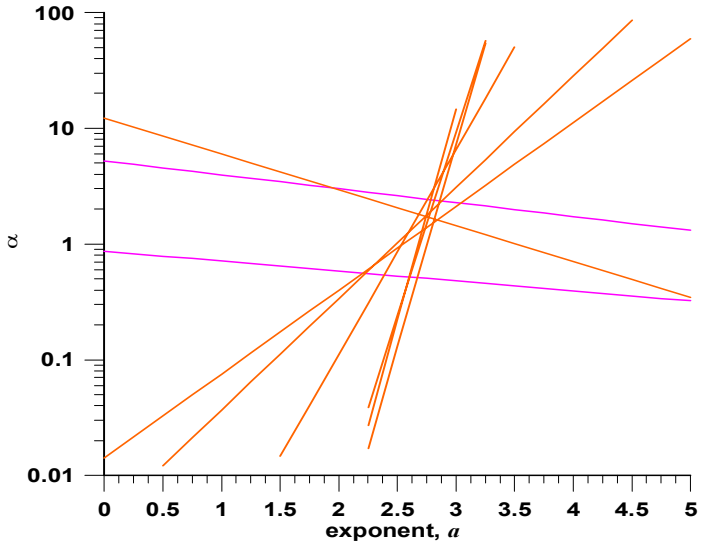

Figure 3-14: *Multi-scale analysis with D_{2d}=1.8. a) see inlet legend. b) Three sets are distinguished. Both intense pink lines respectively correspond to T-2232-2260 and TRUE-1. Orange rights correspond to outcrops. See text for further details.*

3.5.4 2*d* Conclusion

In the first part of the present study, we aimed at testing the validity of a power-law distribution to model the fracture system at Äspö. A compilation of existing reports shows that contradictory arguments are proposed for or against the validity of the power-law model and the possibility to use information collected at one scale to model fractures at another scale. However we did not find any previous real multiscale analysis that should provide additional arguments to confirm or not a power-law model and a range of validity.

The statistical analysis of a multiscale system requires robust statistical data and a sufficiently large range of observation scales. Many artefacts are however present in the available data (2*d* maps to characterize the fracture length distribution), displaying strong censoring and truncation effects. Moreover, the analysis of the maps becomes more and more difficult as their size decreases, such that the hardest interpretations occur right at the scale of interest of this study, the so-called background fractures. We first considered each map separately before applying the multiscale analysis that enables comparison between maps.

By doing so, we demonstrated that, although the apparent lower length of validity, l_{val}, from the outcrops remains difficult to clearly define, at least for the outcrops maps a power-law model could be validated. The precise determination of exponents however remains difficult and we propose a range for the parameters. If $D_{2d}=2$, then we obtain $a_{2d} \in [2.8, 3]$ and $\alpha_{2d} \in [0.5, 0.8]$. For $D_{2d}=1.8$, $a_{2d} \in [2.8, 3]$ and $\alpha_{2d} \in [1, 2]$. This result and conclusion (validation of the power-law model) are contrary to the second part of report [TR-01-21] in which several exponents, measured from cumulative length distributions and coming from several scales of observation, have been compared without a direct comparison of the different data. In fact we do recommend the use of the probability density function (pdf) representation instead of the ccdf (cumulative complementary density function) used in [TR-01-21] to measure the scaling exponents: the pdf avoids the mixing of several fracture length classes sampling, and also avoid the integration of resolution effects.

In addition, we chose to give up on the analysis of some of these maps because of strong sampling biases and data scarcity. Furthermore, Bossart et al. [TR-01-21] found power law exponents varying between 1.52 and 2.21, even for the smallest maps, which is contradictory with their observations (first part of the report) that at least for the TRUE-1 tunnel map, the fracture length distribution were dominated by small fractures, up to a size around 10cm (*1*d scan-line along tunnel map). Our conclusions are in good agreement with LaPointe et al. [TR99-03], although we found a slightly larger exponent a_{3d}, between 2.8 and 3 whereas it was given as 2.6 in the cited report. This discrepancy could be due to the fact that cumulative length distributions are analysed in LaPointe et al. [TR99-03].

Very few, if any, studies have been devoted to the study of centimetre to meter-scale fractures. Indeed, the presence of small fractures was noticed but deliberately not sampled, because it led to much work. To our knowledge, the only time it was reported is in the first part of report [TR-01-21], where it was qualitatively observed from *1*d scan line analyses that the smallest fractures dominated the total mass (cumulative length) of fracture traces. This argument speaks in favour of a power-law model valid at least down to the meter scale.

Finally, we noticed that for each outcrop map considered, the maximum trace length l_{max} observed within a map remains in the order of the map characteristic size and that the density of large fractures (i.e. fractures with a size close to the system size) remains constant. The only variation is that l_{max} is about $L/2$ for the largest maps whereas it is equal to (or larger than) L for the smallest maps. These observations were difficult to perform on elongated and narrow tunnel maps at a meter scale because of the strong sampling biases mentioned earlier.

The qualitative similarity of the fracture patterns through all scales speaks in favour of the power law model, with parameters a_{2d} and D_{2d} such that $a_{2d}=D_{2d}+1$. The arguments in favour of the relation $a_{2d}=D_{2d}+1$ for Äspö data are the following:

- $a_{2d} < D_{2d}+1$ implies an increase of the proportion of large fractures with the observation scale; whereas
- $a_{2d} > D_{2d}+1$ implies a decrease of the number of large fractures with the observation scale.
- Only when $a_{2d}=D_{2d}+1$ the proportion remains scale invariant, as is observed on Äspö maps.

In that case only, the fracture system is said to be self-similar, it "looks" the same at all scales.

3.6 3*d* geometrical parameters

Let us recall the definition of the power-law density distribution function in 3*d*:

$$n_{3d}(l, L) = \alpha_{3d} \cdot L^{D_{3d}} \cdot l^{-a_{3d}}$$

"$n_{3d}(l, L)\ dl$*"* is then the number of fractures with a length lying between l and $l + dl$ in a system of characteristic length L. By combining the 1*d* and 2*d* statistical analyses with the stereological rules provided in section 0, we deduce simply that:

$$a_{3d} \in [3.8;4]$$

$$D_{3d} \in [2.8;3]$$

The extrapolation of the density term α_{2d} to α_{3d} can not be so direct since corrections due to both map and fracture set orientations should be taken into account. We therefore must deduce α_{3d} from the available density measure, P_{32}. Note that the fracture surface intensity of **conductive** fractures, P_{32c}, has been determined by a trial and error method from boreholes measurements (P_{10}) and found equal to 0.29 m^2/m^3 at the scale of the TRUE Block (200m side cube).

In the specific case of a power-law length distribution, relating P_{32} to α_{3d} requires the knowledge of l_{min}. Indeed, over the range of a_{3d} values found ($a_{3d}>3$), the first moments of the fracture length distribution are dominated by the lower boundary l_{min}. In particular, the cumulative surface of fracture, $M_{3d}(L)$, in a system of size L is given by:

$$M_{3d}(L) = \int_{l_{min}}^{l_{max}} \alpha_{3d} \cdot \frac{\pi}{4} \cdot L^{D_{3d}} \cdot l^{-a_{3d}+2} \cdot dl = \alpha_{3d} \cdot \frac{\pi}{4} \cdot L^{D_{3d}} \cdot \frac{l_{max}^{-a_{3d}+3} - l_{min}^{-a_{3d}+3}}{-a_{3d}+3}$$

As long as a_{3d} is larger than 3, $M_{3d}(L)$ is dominated by the amount of small fractures (boundary l_{min}). Therefore α_{3d} , P_{32} and l_{min} are related through:

$$P_{32}(l_{min}, L) = \frac{M_{3d}(L)}{L^3} = \frac{L^{D_{3d}}}{L^3} \alpha_{3d} \cdot \frac{\pi}{4} \cdot \frac{l_{min}^{-a_{3d}+3}}{a_{3d}-3} = \alpha_{3d}(L) \cdot \frac{\pi}{4} \cdot \frac{l_{min}^{-a_{3d}+3}}{a_{3d}-3}$$

The determination of l_{min} is difficult, as illustrated in Figure 3-15 below.

- l_{min} is precisely defined as the real lower boundary of validity of the power-law. Below that scale the number of fractures is expected to decrease as the length decreases, as illustrated by the dotted line in Figure 3-15. There is no evidence that this scale corresponds to the scale below which there is no fracture.
- if this limit would exist for the 3*d* fracture network, then the observation of the corresponding trace lengths on a map should yield a power-law down to that scale and rapidly vanish below that scale (see Figure 3-3 in section 0 devoted to stereology). In 3*d*, l_{min} is defined as the smallest fracture diameter of the power-law length distribution. We assume that below that scale, the number of fractures rapidly vanishes. From a theoretical point, this parameter could be measured on a 2*d* outcrop (Figure 3-3), however in practice the measure is impossible because of resolution effects.
- This low boundary is not necessarily observable since it can be below the limit of resolution. To our knowledge it has not been precisely defined. The reason is simple, since these fractures are not expected to be significantly conductive or even open. However, and as already mentioned above [TR-01-21], the centimetre-scale to meter-scale fractures may dominate the cumulative trace length of fractures.
- The measure of P_{32} is dependent of resolution effects. The measure of P_{10} (leading to P_{32}) is performed from for a lower cut-off length that we call l_{app} (for "apparent length"). Hence the following questions remain: what is the value of l_{app}? Is the power-law model valid at least down to this length scale?

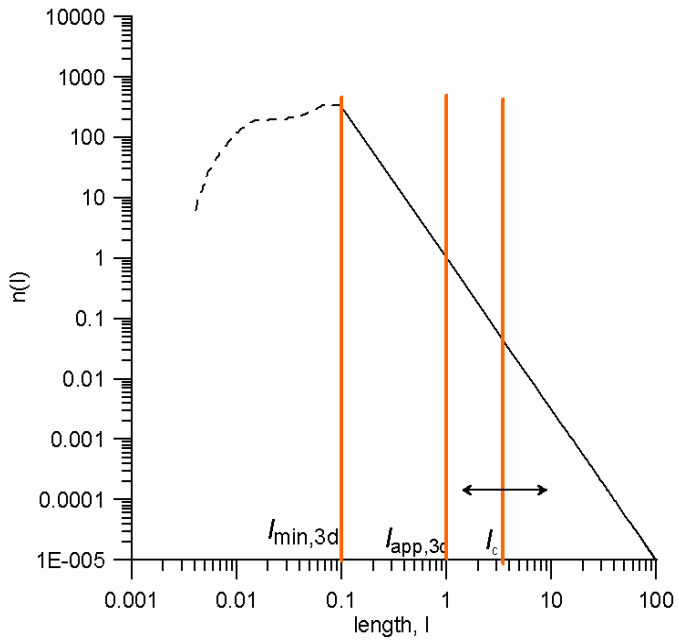

Figure 3-15: *Schematic representation of the 3d density length distribution model. l_{min} is the lower cut-off of the power-law model, l_{app} is the resolution scale and l_c is the length under which fractures could be neglected for the flow and transport predictions (see next section).*

It is therefore necessary to make an assumption on the apparent value of $l_{min,app,3d}$ that contributed to the measure of P_{21} or P_{10}. Two pieces of information can be used to sustain this assumption. First, the ratio between conductive and non-conductive open fractures is known from borehole measurements. In borehole KI0025F02, we have $P_{10} \cong 3^* P_{10c}$, where subscript "c" is used for a statistic considering only conductive fractures Second, we know in 3*d* the number of 100 meter scale structures, as given by the number of deterministic structures: about 15-20 conductive structures (depending on the size we chose) have been identified in the TRUE Block Scale block (200m side), with probably some more existing and not detected/identified. Both data are useful to propose the α_{3d} and $l_{min,3d}$ values.

Note that from here on, we use the fracture radius *r* as the characteristic length of a fracture in 3*d,* i.e. we are discussing r_{min} as a substitute for $l_{min,3d}$.

To conduct our evaluation of the pair of values (r_{min}, α_{3d}) based on conductive/non conductive fracture intensities, we use an empirical and direct verification approach. We generate synthetic fracture network models with various r_{min} values, computing α_{3d} from the value of P_{32} or P_{32c} for the background fractures. We test two kinds of models. Either we use the conductive density and verify that all fractures are conductive in that case, or we use the total fracture density and try to reproduce the ratio between conductive and non-conductive fractures in borehole KI0025F02.

- On one hand we use the value of P_{32c} to estimate the "overall" fracture density. The corresponding minimum radius r_{min} must then be the value above which all fractures size classes are connected and significantly conductive (i.e. as detected by Posiva flow measurements). Such a threshold is likely to exist, as indicated by the observation [Mazurek et al., 1995] that above a certain fracture trace length, all the features in the tunnel are conductive. In that case, fractures smaller than r_{min} are directly neglected. Accordingly, all the fractures in our model that intersect the boreholes must then be conductive (otherwise the P_{32c} measured on the simulated fracture network will be different from the P_{32c} value used as input in the model).
- On the other hand, we consider the whole network, and take a much higher P_{32} value. In this case, among the stochastic fractures that intersect the boreholes the ratio of conductive to non-conductive must match the measured one. As a consequence, the ratio between conductive and non-conductive fracture intercepts enables us to check the choice of the minimal fracture length in the model.

In practice, we assume that having no measurable flow in a fracture (open, non-conductive fracture) is equivalent to having a non-connected fracture, whereas having a connected fracture is equivalent to a flowing fracture, i.e. we assume that all the connected fractures are conductive. This assumption mixes up connected fractures having very low flow rates with non-connected fractures. A more thorough theoretical analysis would permit to refine this first order analysis.

These simulations yield the following results:

- For r_{min}=3 m, all the intersecting fractures are connected.
- For r_{min}=0.8 m, the total number of simulated fracture intercepts in boreholes corresponds to the number of fracture intercepts due to both open and conductive fractures.

As a conclusion, we expect that the minimum fracture radius above which all fractures are connected within the fracture system is about 3 m, and that the resolution scale for P_{10} measurements is consistent with a fracture radius of 0.8 m. This preliminary study enables us to provide a value of α_{3d}. In fact, for simulations, we will directly use the pair of values (P_{32c} = 0.29 m^2/m^3; r_{min} = 3 m), which yields the proper density function, together with a truncation value for the effectively simulated radii. It would have been equivalent to use the pair (P_{32} = 3 * 0.29 m^2/m^3; r_{min} = 0.8 m), as long as the r_c value is chosen the same.

We then check the number of 100 m scale fractures predicted by our model in the TRUE Block Scale block using this value. We find that if a_{3d}=3.8 then the number of fractures with a radius between 50 and 100 meters within the TRUE Block Scale block (200m side) is between 10 and 60 fractures. Similarly, if a_{3d}=4 we obtain between 1 and 10 fractures. In both cases the order of magnitude is correct, although case a_{3d}=4 tends to underestimate the proportion of 100 metres deterministic structures, whereas the case a_{3d}=3.8 may slightly overestimate the quantity of 100 meters structures. Therefore, the "true" fracture model should have properties bounded by the two models (a_{3d}=3.8, D_{3d}=2.8) and (a_{3d}=4, D_{3d}=3).

3.7 Conclusions

The statistical analysis of the fracture network yielded the relevance of a power-law model for fracture sizes, related to a Poissonian/fractal model for fractures positions: we found that two pairs of parameters could explain the data at hand: either a power-law exponent a_{3d} of 3.8 combined with a fractal dimension of D_{3d} 2.8, or a power-law exponent a_{3d} of 4 combined with a fractal dimension D_{3d} of 3. We have some indication that this model may be valid down to a fracture radius (r_c) of the order of one meter. However, we lack small scale samples to be fully assured of the validity of the statistical model below a size of about 10 m.

The fact that "$a_{3d} = D_{3d} + 1$" indicates that the network is "self similar": the distribution of large and small fractures is the same at all the scales considered. In fact, small fractures dominate the "mass" of fractures (i.e. the cumulative area) in any domain. Such a system, with a_{3d} equal or close to 4, is likely to follow closely the percolation theory behaviour, with a connectivity proportional to density and strong finite size effects.

The length model yields an overall r_{min} of 0.8 m, and a "connectivity cut-off radius" of 3 m. In order to assess the effect of the smaller fractures, we will test several assumptions on the minimum radius r_c that must be accounted for in the model to properly simulate the network behaviour. Can we safely take only the connected fractures (i.e. r_c = 3 m), do we need to go much lower (r_c = 1 m), or can we take only the larger background fractures (r_c = 10 m)?

4 Tracer test simulations

4.1 General Framework

Several questions/points motivate the present study of tracer test simulations:

- Assessment of tracer tests feasibility in the framework of project BS2A and BS2B, with several pre-determined configurations CPT-1, -2 and -3.
    - Mass recovery rate and arrival time prediction,
    - feasibility of performing tracer tests partly in background fractures (especially "Structure #25")
    - quantification of background fractures pathways,
- role of small fractures:
    - scale of deterministic/stochastic representation and role of small background fractures (value of r_c)
    - uncertainties due to stochastic fracture parameters

Because of the practical scope of the present study (tracer test simulations with a determined configuration), the role of small fractures and possible characteristic scales is assessed only over the specific case of the TRUE Block Scale block, that is within the hydrostructural model validated elsewhere [Andersson et al., TR-02-13, 2002]. Hence, all the simulations are constrained by strong condition and deterministic information. They are detailed in the next section.

4.2 Specific framework

As already mentioned, the tracer test configurations have been pre-selected (at the second BS2 Technical Committee meeting in Stockholm in April). For practical reasons, the neighbourhood of structure #19 was chosen to be the tracer test area. The tracer test area is characterized by:

- several boreholes that go through the whole domain,
- identified deterministic structures (mainly #19, #13, #21 that are close to injection/pumping sections), including extension, position and transmissivity estimates,
- positions of fracture intercepts (along boreholes) and corresponding transmissivity estimates,
- presence of fractures in the rock mass, whose statistical property distributions are estimated from indirect observations.

Structure related data, as well as fracture intercept positions and transmissivities along boreholes are directly included as deterministic data in the model. They obviously constrain the possibilities for locating both the injection and the pumping sections. Note that what is called "deterministic information" includes both real deterministic data (intersection positions, connectivity pathways) and already interpreted data (transmissivity estimates, structure exact extents).

The rest of the fracture network (i.e. background fractures that do not intersect the boreholes) is represented as a stochastic model with statistical geometrical properties as recalled and/or assessed in Chapters 2 and 3.

4.3 Connectivity

In Chapter 3 we showed that the fracture system at Äspö can be well represented by a self-similar fracture power-law model, $a_{3d}=D_{3d}+1$. Connectivity properties of such systems should be close to percolation theory ([Stauffer&Aharony, 1992]). In practice, the percolation threshold is reached when one cluster (set of connected fractures) spans the system, so that there exists one connected pathway between the system boundaries. For Poissonian fracture systems, a percolation parameter can be defined and the value of the percolation parameter at the percolation threshold remains invariant ([Bour&Davy, 97, 98], [Dreuzy et al., 2000], [Darcel et al., *in press*]). One correction must nevertheless be introduced to take a specific orientation distribution into account ([Robinson, 83, 84]), but this does not entail effects on the scaling invariance of the value of the percolation parameter at threshold. As a consequence, the connectivity state of the system can be described by the so-called percolation parameter. Percolation theory predicts that, for a system above percolation threshold, finite size clusters (not connected to the overall infinite cluster, that is the fracture network connected to the system boundaries) are present in the system up to a critical scale called the correlation length. Above that scale the fracture systems appears always connected. In addition, the correlation length decreases as the fracture density increases.

Experimental evidence has shown that the fracture system at Äspö in general is strongly connected (Chapter 2). Moreover, numerous observations along the tunnel show that fracture traces with a length above a threshold in the meter-decametre range are almost always flowing [Mazurek et al., ICR97-01, 1996]. At the TRUE Block Scale volume size of observation, the fracture system is obviously above the percolation threshold. Indeed, at the scale of interest (TRUE Block Scale volume), the structures - features that go through several boreholes - form several connected pathways. However, intensive hydraulic cross-hole interference tests and/or tracer dilutions tests and geochemical measurements have shown that not all the structures are interconnected and that some flow compartmentalization is likely to exist. Besides, by looking at the flow rates measured along the boreholes, one observes that not all the fractures intersecting the boreholes are conductive: for instance the ratio between conductive and open-non conductive fractures is about 0.33 for borehole KI0025F02. Note that open fractures could be flowing fractures whose flow rate is under the limit of resolution of instruments.

All these observations are in good agreement with the expected behaviour of a self-similar fracture system above the percolation threshold. Determining more precisely the statistics of finite size clusters and correlation scale is beyond the scope of the present study, but could constitute a more general continuation of the present work to assess the possibility to find finite or isolated areas within fractured systems.

4.4 Model specification

The geometrical model used here is based on the hydrostructural model that best fit the overall data available from the TRUE Block Scale rock volume ([Andersson et al., TR-02-13, 2002] [Dershowitz et al., IPR-03-13, 2003]). Deterministic data are used to place the structures and to condition the background fracture field to known intercepts with boreholes. The geometrical statistical properties of the general fracture network model are taken from the analyses presented in Chapter 3. Several tracer test configuration are proposed. The three next sub-sections detail the model specifications.

4.4.1 Deterministic structures

The following structures, #05, #06, #07, #10, #13, #19, #20, #21, #22, #23, #24 are included in the model. Their positions and properties were taken from IPR-03-13 and are used without any changes. Note that the definition of structures as perfectly planar features yields minor discrepancies in the position of their intersections with boreholes.

Table 4-1 gives the transmissivities used for the structures in the model.

Table 4-1: Transmissivity properties of structures, in m^2/s.

#05	#06	#07	#10	#13	#19	#20	#21	#22	#23	#24
4.020E-07	1.910E-07	9.760E-08	2.980E-08	1.380E-08	1.020E-07	1.430E-07	6.020E-08	2.190E-08	1.660E-07	8.510E-08

Flow paths within structures are represented by two superimposed square grids of channels [Rachez and Billaux, 2002], the second one oriented at 45 degrees from the first as shown in Figure 4-1. The spacing for the first square grid of channels is 12 m (the spacing for the second square grid of channels is then $12/(2)^{1/2}$). Using two superimposed grids greatly improves the accuracy of transport calculations in a large feature.

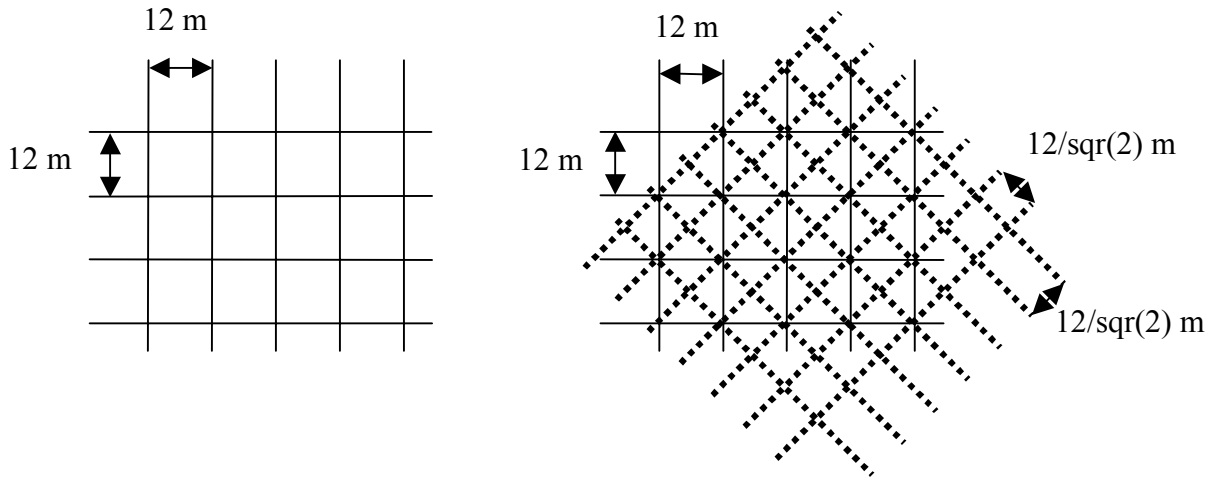

Figure 4-1: *2 square grids of channels on each structure, after [Rachez and Billaux, 2002]*

Varying conductivities are generated for the channels in a given structure. The mean conductivity ***C*** is computed from the mean structure transmissivity ***T***, using the following equation:

$$C = T * \frac{g}{shapef},$$

where:

> g is the grid size (length of the square edges, here 12 m), and *shapef* is a shape factor, with a value of "$1+\sqrt{2}$" for the "squares plus diagonals" grid that is used here (two superimposed square grids, with relative spacings 1 and $\sqrt{2}$).

It can easily be verified that the transmissivity – conductivity relationship above yields, for a homogeneous regular grid, flow properties equivalent to those of a *2*d continuum with transmissivity ***T.*** Figure 4-2 shows the log-conductivities we obtain, and outlines structure 19 where most of the tracer tests will occur.

Note: we assume that within each structure, channel conductivity is distributed according to a truncated normal law, with a mean as given by *Table 4-1* and the above equation, a coefficient of variation equal to 10%, and a minimum value equal to 1% of the mean.

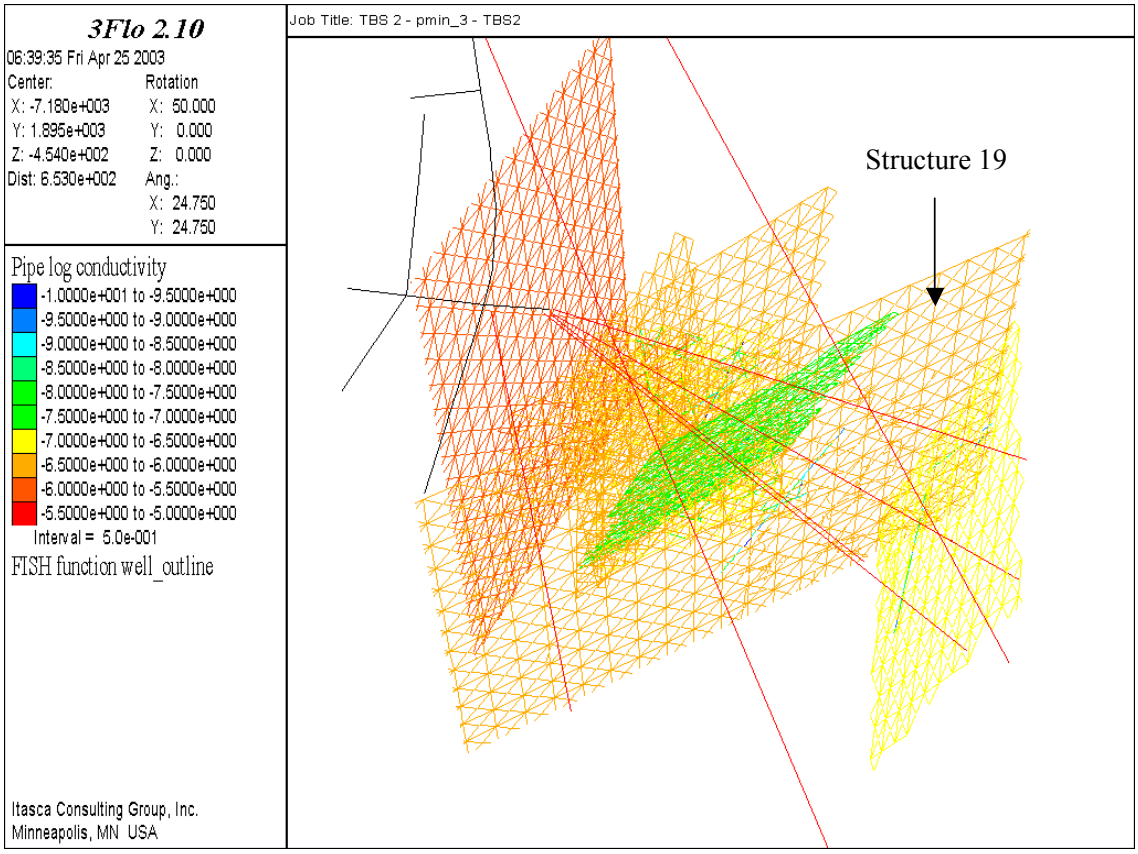

Figure 4-2: *Log-conductivities of the structures in the model. View is due East, looking from above at a 50° angle. Tunnels in black and boreholes in red.*

4.4.2 Stochastic fractures

The "stochastic fractures" comprise all the "non structure" fractures included in the model, that is both fully stochastic and borehole conditioned fractures. The stochastic fractures therefore correspond to the background fracture population.

As already mentioned, data available are mainly expressed in terms of statistical representations. For instance over the Block Scale rock volume, the mean density of fractures has been estimated to be P_{32c}=0.29m^2/m^3 ([TR-02-13]) for the conductive background fractures. From that point, two models of the fracture radius distribution will be considered in the following:

- the lognormal model proposed in [Dershowitz et al., IPR-03-13]. There the authors proposed to distinguish the fracture network model according to fracture scale, so that the stochastic model of the background fractures is not related to largest scales and is modelled by a lognormal radius distribution with a mean of 2 m and a standard deviation of 1 m. [Dershowitz et al., IPR-03-13] also propose that at small scale the spatial pattern of fractures is random (D_{3d}=3) whereas it should be fractal at higher scales (D_{3d}=2.5 to 2.6).

- the power-law model proposed in Chapter 3, whose parameters are the scaling exponent a_{3d} and fractal dimension D_{3d}. We found a_{3d} between 3.8 and 4 and D_{3d} between 2.8 and 3.

The fractal nature of the fracture network quantified by the fractal dimension D_{3d} renders both the evolution of fracture density with scale, and the fracture heterogeneity at each scale. In the present case, the fracture density has been estimated directly at the scale of interest since the boreholes used go through the whole area of interest. Therefore, we do not need to predict the evolution of fracture density with scale. Furthermore, in the framework of scaling law models for fractures, a two-dimensional study of fracture effective connectivity (see [Dreuzy et al., *in press*]) shows that above the percolation threshold (which is the case here) and with a fracture model $a_{3d} \cong D_{3d}+1$, the value of D_{3d} is of second order (the effect of fracture lengths is stronger that the spatial heterogeneity) to estimate the equivalent permeability of a fracture system at a given size of observation. Hence in the present study, we can consider in a first approximation that neglecting the fractal value of D_{3d} leads only to a relatively minor underestimate of the fracture network spatial heterogeneity. Therefore, in the following, all the simulations corresponding to the power-law model are performed with D_{3d} equal to 3, that is neglecting the spatial heterogeneity of the fracture network. This greatly simplifies fracture generation. Also, as will be seen in Section 4.4.3, conditioning to observed fracture intersections in boreholes is much easier in a Poissonian field.

Previous studies ([TR-02-13], [IPR-03-13]) have permitted to build models of fracture sets and corresponding orientation distributions for the background fractures (Table below). These models are used in the tracer simulations phase to generate the orientations of stochastic fractures.

Table 4-2: model of fracture set and orientation distribution deduced from TRUE Block Scale orientation estimations (from [TR-02-13] p125 and [IPR-03-13], p 48).

parameter	Basis	Set #1	Set#2
Orientation distribution	Two fitted sets	Fisher distribution Mean Pole (Trend, Plunge)=(211, 0.6) Fisher Dispersion κ=9.4	Fisher distribution Mean Pole (Trend, Plunge)=(250,54) Fisher Dispersion κ=3.8
Intensity P_{32}		0.16 m^2/m^3 55.2% of fractures	0.13 m^2/m^3 44.8% of fractures

Finally, the flow paths within fractures are represented by single square grids of channels and equivalent conductivities are calculated through the same procedure as schemed for the structures (section 4.4.1). The spacing for the square grid of channels is 2m.

4.4.3 Conditioning

Because the response to flow and transport tests can be largely perturbed by local conditions around boreholes it is essential to reproduce the exact arrangement and properties of the fractures that have been detected in boreholes, i.e. to condition the stochastic fracture field we generate on the borehole data. The data for a conditioned fracture along a borehole correspond to the intercept position, the orientation and the transmissivity estimate. Therefore the fracture radius and the position of its centre must be stochastically picked from the stochastic fracture network model. Also, during the generation process, stochastically generated fractures that would intersect the boreholes where no real borehole intercept appears, must be avoided.

In practice, conditioning is a simple matter when generating a Poissonian (i.e. D_{3d}=3) field, where all fracture locations can be considered independent from each other. During the fracture generation process, generated fractures are checked for intersection with one of the conditioning boreholes, and simply discarded if they intersect. In this way, we generate less "purely stochastic" fractures than should be included in the model volume. Then, for each "real" fracture intersection known on each of the conditioning boreholes, we generate one fracture with a radius taken from the radius Probability Distribution Function, located in the plane (position, orientation) of the fracture intersection. Note that we often generate only part of the pure stochastic fractures, by truncating the radius distribution and reducing the fracture density accordingly. In order to avoid bias, the radius distribution used for a conditioned fracture is picked up from the full radius distribution, corrected for stereological effects (i.e. for the fact that large fractures have a higher probability of cutting a well than small ones).

Provided the measured intercepts in boreholes obey the same statistics as the rest of the fracture population, the conditioning procedure outlined above has no bias when considering only one borehole. If several boreholes are used, a "conditioned" fracture in one borehole may intersect another borehole, thus creating one extra connection along this second borehole. The severity of this effect is governed by the relative positions of the boreholes and by the radius distribution. For the present case, we checked that the number of spurious fractures is insignificant.

Conditioning is much more difficult in an heterogeneous / fractal field, since in this case the positions of the fractures are not strictly independent of each other. We do not dwell further on this, since all simulations will be based on the hypothesis that $D_{3d} = 3$ (i.e. the fracture centres obey a Poissonian field).

To clarify the definitions used in the following, the discrete fracture network is made of two main kinds of features: the deterministic structures, whose position, extension and hydraulic properties are fixed and the stochastic fractures. These last ones contain both purely random fractures and conditioned fractures (i.e. intercept with a borehole, orientation, and transmissivity are known). In the following the terms "structures" and "fractures" are consequently used. Note that this difference in terms does not mean we are considering two differing populations in a statistical sense. In fact, we checked that the number of "structures" in the model is compatible with the "tail" of the power-law size distribution (see section 3.6).

4.4.4 Tracer test configuration

Three configurations have been selected for the CPT tests. Among them we choose to focus on CPT-2, with a pumping section at the intercept of structure 19 and borehole KI0025F02. In the pumping section, we fix a pump rate equal to 5 10^{-5} m^3s^{-1}. The injection rate in the tracer injection sections is fixed at 1 10^{-7} m^3s^{-1} (as suggested in the tentative proposal for pre-test program, at the same meeting).

Figure 4-3 and Figure 4-4 illustrate the configuration of the injection and pumping sections. *Table 4-3* gives more information on the various sections, such as the type (i.e. structure or background fracture) and number of the feature(s) they cut, and the Euclidean distance to the pumping section. Note that for sections straddling a structure, the actual position of sections in the model, as given in *Table 4-3*, may vary slightly from the real position of the structure intersection. This is to account for discrepancies as noted in section 4.4.1.

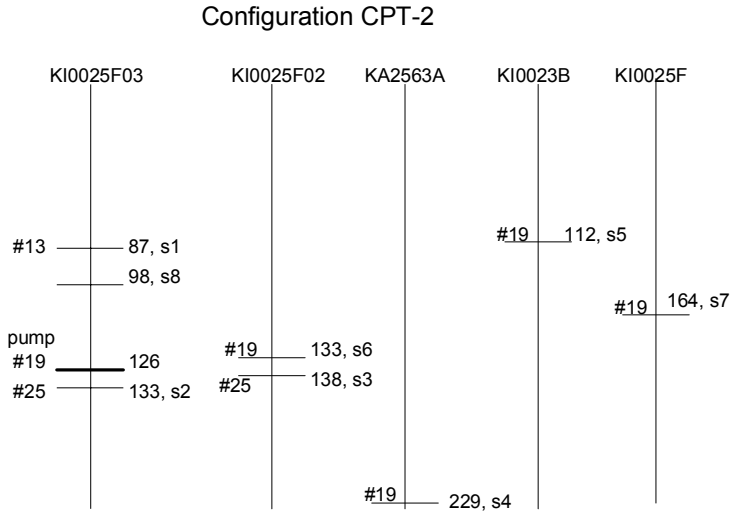

Figure 4-3: *Configuration CPT-2. Scheme of the 5 boreholes represented with the positions of pumping and injection sections. Intersections with deterministic structures #13, #19 and #25 are notified (position is approximate) and injection sections are identified from s1 up to s8.*

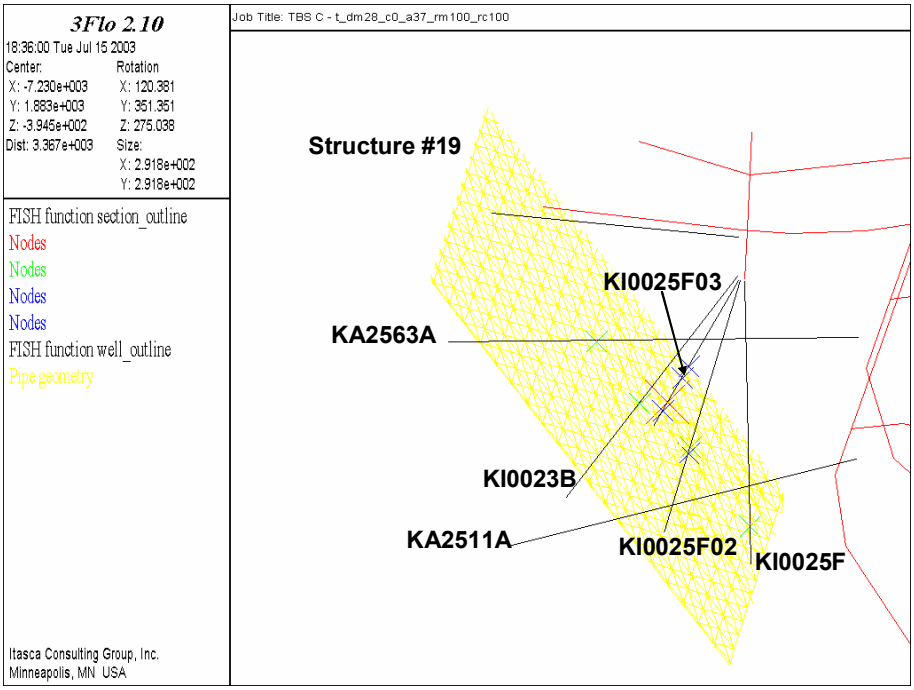

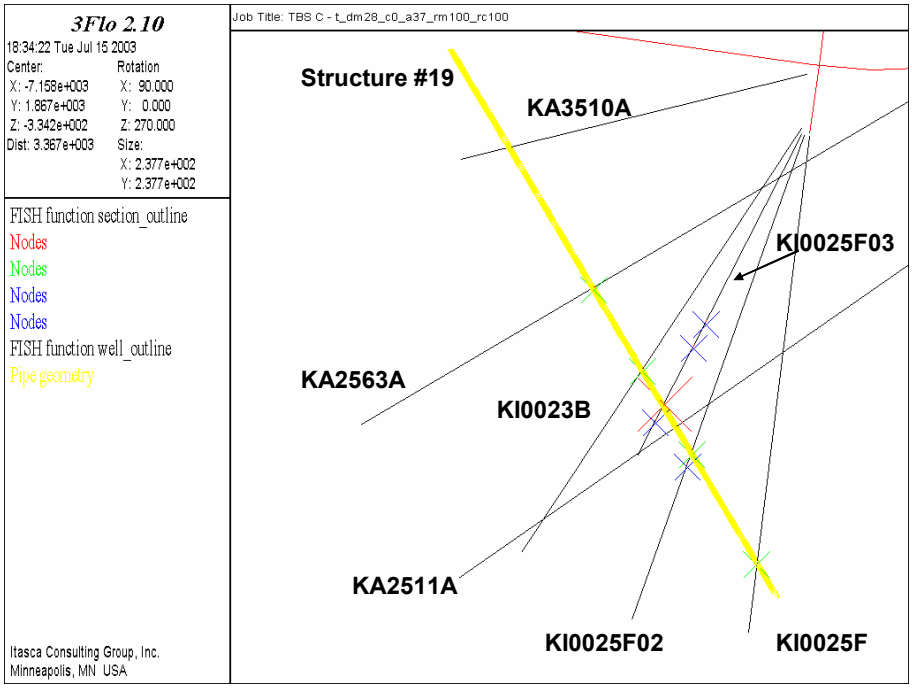

Figure 4-4: *Configuration of injection and pumping sections. The pumping section is symbolized by a red cross. Green and blue crosses symbolize injection points respectively in structure #19 and in stochastic/conditioned fractures.*

Table 4-3: The injection sections, CPT-2 configuration.

Test	1	2	3	4	5	6	7	8
Reference, borehole/section	KI0025F03 R5 #13	KI0025F03 R2 #25	KI0025F02 R2 #25	KA2563A S1 #19	KI0023B P2 #19	KI0025F02 R3 #19	KI0025F R2 #19	KI0025F03 25R03R4,.
Position (m from collar)	87 to 88	133 to 134	138 to 139	229 to 230	112 to 113	133 to 134	164 to 165	98 to 100
Euclidean Distance to pumping	39.9	6.7	24.2	55.7	25.6	21.2	61.9	27.1
Structure/ background fractures	S 13	BG (S 25)	BG (S 25)	S 19	S 19	S 19	S 19	3 BG fractures
Transmissivity (m^2s^{-1}) of the injection structure/fracture(s)	1.380E-08	1.36E-09	4.E-10	1.020E-07	1.020E-07	1.020E-07	1.020E-07	2.03E-09 4.74E-09 6.10E-11

The plane of Structure 19 is represented in Figure 4-5, illustrating for reference the relative positions of the injection and pumping sections in this structure.

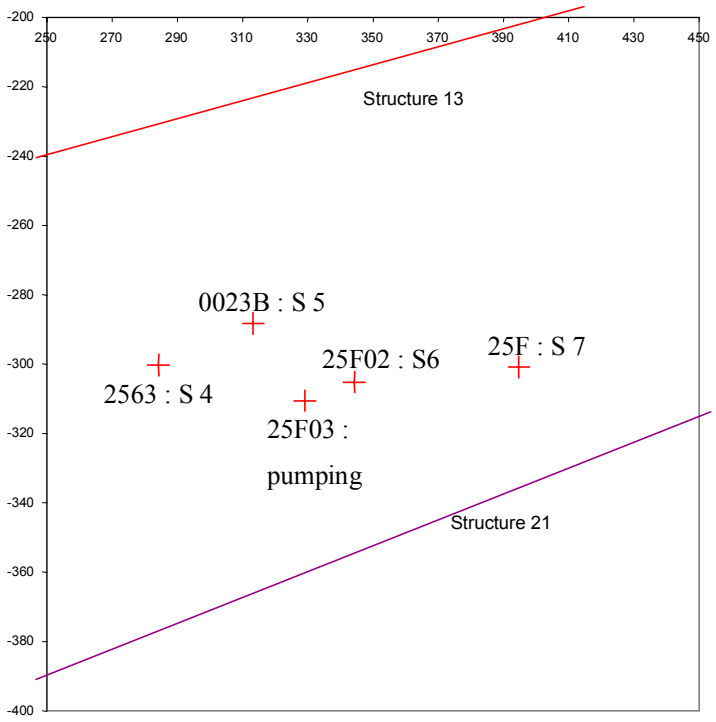

Figure 4-5: *Borehole intersections in Structure 19, viewed from South, from [Doe, 2002].*

Along the boreholes, three positions corresponding directly to "background fractures" were chosen to simulate tracer tests. Test Sections 2 and 3 correspond to the "structure 25" injections discussed at the TC2 meeting. We added test section 8 in order to experiment with a longer pathway in background fractures.

4.4.5 Flow and transport properties

Transmissivity

The transmissivity distribution of background fractures is deduced from the interpretation of flow rates measured by the Posiva flow logs. The derivation of the transmissivity distribution is performed by applying the radial flow equation to the flow in the Posiva flow logs (p125 in [TR-02-13]). This leads to:

$$T = \frac{Q}{2\pi \cdot \Delta H} \cdot \ln\left(\frac{R}{r_w}\right) \sim \frac{Q}{\Delta H},$$

where Q is the flow rate and ΔH is the head drop. Posiva flow logs cover a range of measured flow rates going from 0.002l/min to 5l/min. This corresponds to a minimum transmissivity at $8 \times 10^{-11} m^2/s$ (with ΔH equal to 410m, the TRUE Block Scale rock volume depth).

A compilation of the flow logs performed in the boreholes of the TRUE Block Scale rock volume lead to a lognormal distribution for the transmissivity with a mean = -8.95 $\log_{10}(m^2/s)$ and a standard deviation of -0.93 $\log_{10}(m^2/s)$ (Table 3-1 in [IPR-03-13]). Typically, conductive background fractures have a transmissivity between 10^{-11} and 10^{-9} m^2/s. Note that a unique transmissivity distribution is given for the two background fracture orientation sets, just as was the case for the length distribution.

Two hypotheses are considered regarding the correlation between fracture transmissivity and radius. We assume either no correlation between radius and transmissivity, or an univocal relationship between the probability distribution of the two parameters (see [de Dreuzy et al., 2001]).

If a one to one correlation is assumed between radius and transmissivity, we simply generate one of the two parameters, and compute the other one directly from the value of the generated one. In the case of a power law model for fracture radius r, and a lognormal model for fracture transmissivity T, [De Dreuzy et al., 2001] has shown that r and T are linked by the following equation:

$$r = r_{\min}\left[\frac{1}{2} erfc\left(\frac{\ln(T) - \mu_T}{\sqrt{2}\sigma_T}\right)\right]^{\frac{1}{-a+1}},$$

where:

a is the exponent, and $r_{\min}$ the minimum of the radius power distribution;

μ_T is the log mean and σ_T the log standard deviation of the transmissivity lognormal distribution.

If the model for the fracture radius r is lognormal, then the relationship between r and T is straightforward:

$$T = \exp\left(\mu_T + \frac{\ln(r) - \mu_r}{\sigma_r}\sigma_T\right),$$

where :

μ_T and σ_T are as defined above,

μ_r and σ_r are respectively the log mean and the log standard deviation of the transmissivity lognormal distribution.

The above equations enable us to generate perfectly correlated distributions of fracture transmissivity and radius, for either power-law or lognormal radius distributions.

By taking the two extreme cases, we are assured that our simulations will bound the real case, which is most likely to be an imperfect correlation between the two properties. Note that a correlation coefficient could be added to produce intermediate correlation ranges.

Also, note that the lognormal transmissivity model we use excludes the transmissivity properties of deterministic structures, which are discussed in section 4.4.1.

For the background fractures, flow paths are represented by a simple square grid, with a grid spacing of 2 m.

Transport

Once channel conductivities have been generated, channel cross sections S are chosen so that conductivities are proportional to the cube of sections (cubic law) :

$S = \alpha * C^{1/3}$, where α is constant for all the channels in a structure

This corresponds to flat "ribbons" within which Poiseuille's law may be applied. For the coefficient, we use the value $\alpha = 0.05$ for all the features, so that the total porosity of the in the rock volume is about 0,5%.

Note that transport simulated in each channel is purely advective, so that no other property is needed. Dispersion, however, will occur because of the complete mixing assumption used at channel intersections.

4.5 Numerical simulations

4.5.1 Building the model

The total network consists of the union of the structures, of the conditioned background fractures intersecting the borehole, and of the "purely stochastic" ones. Once channels have been projected on all these features, intersections between features are computed and stored. Such intersections are also considered as conductors, therefore permitting connection of the whole channel network. Any intersection between two features is assigned a conductivity taken from the distribution used for the most transmissive of the two features, and the corresponding section.

In order to keep the model at a manageable size, we do not model background fractures everywhere in the TRUE Block Scale volume. We define a fracture generation cylinder, with its axis normal to structure 19, and cutting structure 19 at the pumping point. The radius of the cylinder is 60m, which allows for inclusion of all borehole intercepts in structure 19, except the one with borehole KA3510A. The length of the cylinder is set so that flow paths from the "background injection" sections S2, S3 and S8 are included. From Figure 4-4 one can note that the cylinder needs to be longer towards the tunnel, and shorter towards the end of the boreholes. Measuring from the (structure 19 – KI0025F03 intercept), the cylinder extension is set equal to 35 m toward the tunnel and 10 m toward the end of the borehole. Background fracture centres are sampled only from this cylinder. Note that a fracture may extend outside of the cylinder

and will not be truncated at the cylinder boundary. Also, conditioned fractures are assigned on a borehole only along the portion of the borehole that is inside the generation cylinder.

The boundary conditions are taken from [IPR-03-13], and are shown in Figure 4-6, taken from this report. Note that after a first batch of simulations, and after discussion with the rest of the TBS team, we decided to change the boundary condition of the south face of the TBS cube (on Figure 4-6, left face of rightmost picture) to no-flow, in order to better account for the present understanding of the flow system. Also, these boundary conditions are applied mostly on the structures, shown in Figure 4-2 .

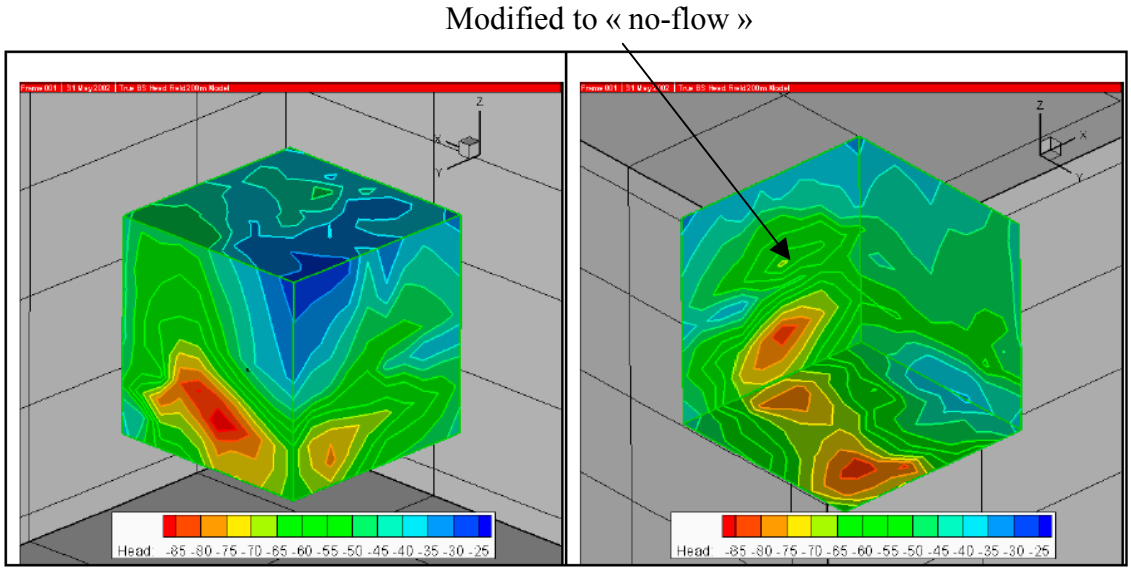

Figure 4-6: *Boundary conditions on the 200m block. X is Easting, Y is Northing, Z is vertical. After [Dershowitz et al., 2003]*

4.5.2 List of all the simulations

The main simulations performed are summarized in *Table 4-4*. In addition to these simulations, a number of verification runs were also done, in order to assess what are the main factors affecting the response of the network (see Appendix B). These various cases are outlined in *Table 4-5*. In the following, we concentrate on the "main simulations". Results for the cases listed in *Table 4-5* helped check the validity of the model. They are provided and briefly discussed in (Appendix B).

For ease of reference, we consider in the following that the "base case" is the first one indicated in *Table 4-4*, i.e. the "Power law distribution, a_{3d} = 3.8 case". In both tables, bold characters then point to the specific model property that differs from the "base case".

Table 4-4: List of the main simulations

Case	Correlation T/l	cut-off length r_c	Number of runs
Power law a_{3d}=3.8 $P_{32,c}$= 0.29 and r_{min}=3	yes	10	500
		3	434
		1	50
	no	10	475
		3	187
		1	26
Lognormal	yes	2	87
		0	88
	no	2	87
		0	88
Power law **a_{3d}=4** $P_{32,c}$= 0.29 and r_{min}=3	yes	10	94
		3	100
		1	20
	no	10	94
		3	100
		1	20
Power law **a_{3d}=3.6** $P_{32,c}$= 0.29 and r_{min}=3	yes	10	87
		3	200
	no	10	200
		3	200

Table 4-5: List of the verification/parameter assessment simulations

Case	Correlation T/l	cut-off length r_c	Number of runs
Power law a_{3d}=3.8 $P_{32,c}$= 0.29 and r_{min}=3 **grid spacing on fractures divided by 2**	no	10	200
		3	96
Power law a_{3d}=3.8 **$P_{32,c}$= 0.58 (double density)** and r_{min}=3	yes	10	100
		3	100
	no	10	100
		3	100
Power law a_{3d}=3.8 $P_{32,c}$= 0.29 and r_{min}=3 **BG transmissivity times 10**	yes	10	500
		3	500
		1	44
	no	10	500
		3	500
		1	50

4.5.3 Quantities measured

For each configuration, marked-particles are injected in the 8 sections defined above. Then a number of quantities are recorded independently for each of the 8 batches of particles.

Two characteristic recovery times are registered:

- t_{05}: time corresponding to the instant where 5% of the mass has been recovered.
- t_{50}: time corresponding to the instant where 50% of the mass has been recovered.

In addition, several quantities are quantified and registered. They are listed below:

- t_{st}: average (over particles) total time spent in the **structures** between injection and pumping.
- l_{st}: average (over particles) cumulative length spent in the **structures** between injection and pumping.
- t_{fr_ratio}: average (over particles) ratio of total time spent in the **fractures**[3] between injection and pumping to the total travel time.
- l_{fr_ratio}: average (over particles) ratio of cumulative length spent in the **fractures**[3] between injection and pumping to the total travel length.

These quantities are computed over particles recovered before t_{50}.

We therefore show 6 plots for each case. For each plot, the mean value of the quantity is displayed versus the injection section number. Runs with correlated and uncorrelated (Transmissivity/radius) distributions, as wall as the various cut-offs used for radius are grouped on the same graph.

In addition to the above results, we also give, for two of the main cases (power law, $a_{3d} = 3.8$; and lognormal law), a comparison of t_{st}, l_{st}, t_{fr_ratio} and l_{fr_ratio} for particles arrived before t_{50} to the same quantities computed for particles arrived after t_{50}.

4.5.4 Results

Base case: Power law radius distribution, $a_{3d} = 3.8$

The results as specified above are illustrated in Figure 4-7, which shows the mean values resulting from the Monte Carlo simulations (to lighten the presentation, means plus standard deviations are also provided in appendix A). First, we note that the 5% recovery times range from a few hours (test sections 5 and 6 in Structure 19, 20/25 m distance from pumping) to a few hundred hours (test section 1 in structure 13, and test section 8 in KI0025F03, background). The 50% recovery times range from 10/20 hours to 1000/2000 hours. The injections in structure 19 (sections 4 to 7) yield relatively fast travel times, with most of the paths in the structure itself (see plot e). Note that because of the full mixing assumption at fracture intersections, a small percentage of the paths (up to a few %) always sample the background fractures. Injections in "Structure 25" (sections 2 and 3) give intermediate results, with t_{50} in the 100 hours range.

Understandably, relative travel distances and times in fractures are lowest for injections in Structure 19. They are highest for Section 2 (injection in the background, close to the pumping section). Also, we predict a significant (15 to 50%) diversion of the tracer paths to the background when injecting in Structure 13 (Section 1). In this case, the path along structures is significantly longer than the Euclidean distance. For this section as well as for Section 8, we note that for correlated background fractures (circles), the paths in structures tend to be shorter, i.e. the tracer has a larger tendency to go through the background, and travel times are shorter: correlating fracture transmissivity with radius makes the background network more transmissive overall.

---

[3] Fractures include fully stochastic and stochastic/conditioned discrete fractures.

Still looking at long pathways (i.e. injections in Sections 1 and 8), we notice that the truncation radius r_c (see legend in plot b) has very little influence on the travel times in the correlated cases: larger fractures dominate the transport. In the non-correlated case, truncating the radius distribution decreases the travel times: tracers have more chances of going into low velocity paths when more small fractures are generated.

In order to look more closely at the paths followed by the tracer, we compare the behaviour of the "early" tracer (i.e. the first 50% of tracer recovered) to the behaviour of the "late" tracer. (last 50% of tracer recovered). Figure 4-8 and Figure 4-9 represent the behaviour of the tracer in structures and fractures respectively. The distance travelled in structures is marginally higher for late tracer, while time spent is mechanically larger. Here, differences in time spent are due to heterogeneity within structures (mostly structure 19). Relative distances and times travelled in fractures (Figure 4-9) are higher for late tracers: this part of the tracer is much more likely to have sampled the background fracture network over a significant portion of its path, even when tracer was injected in Structure 19.

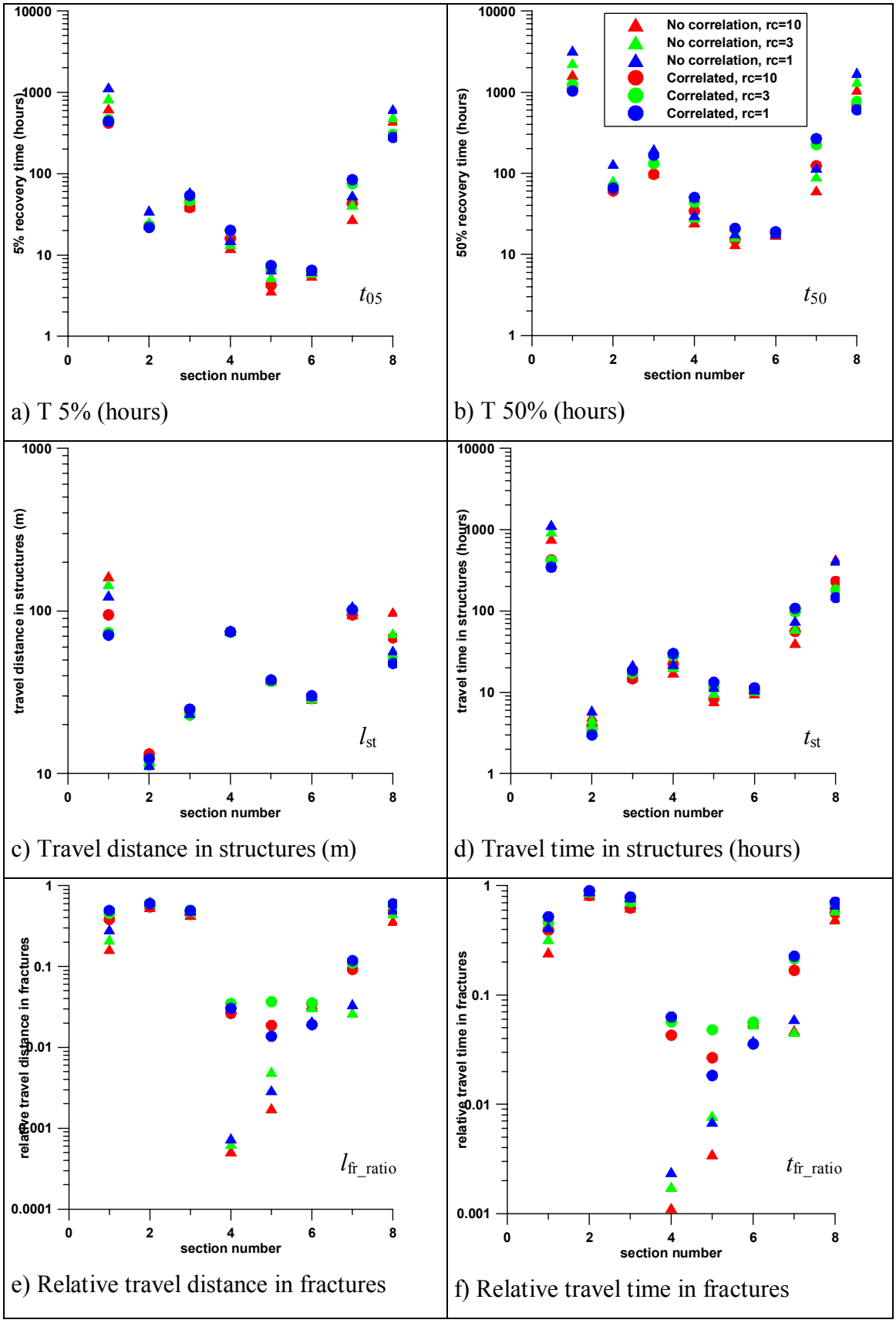

Figure 4-7: *Averaged results over Monte-Carlo simulations. Power law (a_{3d} = 3.8) radius distribution*

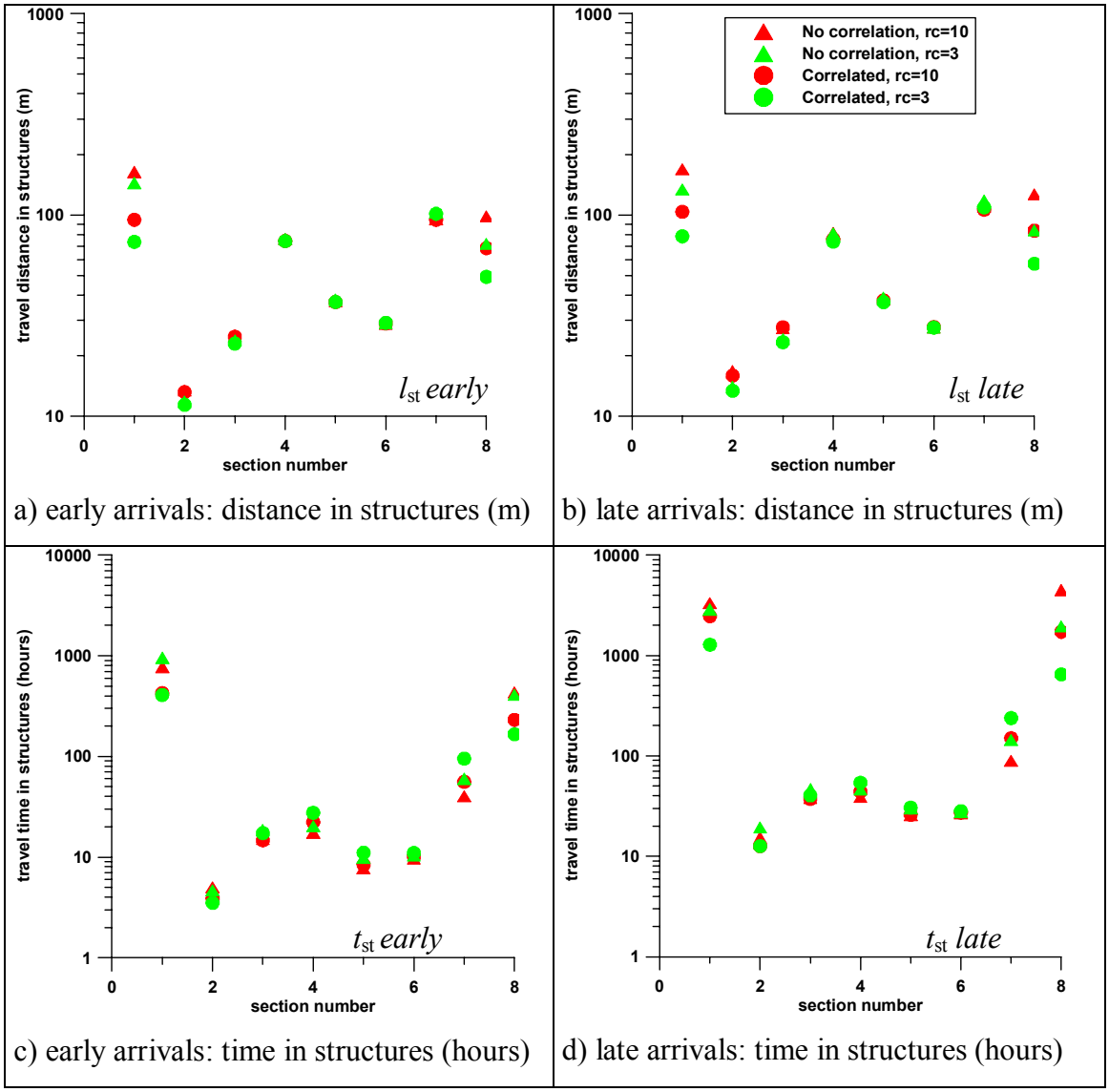

a) early arrivals: distance in structures (m)

b) late arrivals: distance in structures (m)

c) early arrivals: time in structures (hours)

d) late arrivals: time in structures (hours)

Figure 4-8: *Averaged results over Monte-Carlo simulations. Power law (a_{3d} = 3.8) radius distribution. Comparison between early and late arriving particles. Travel in structures.*

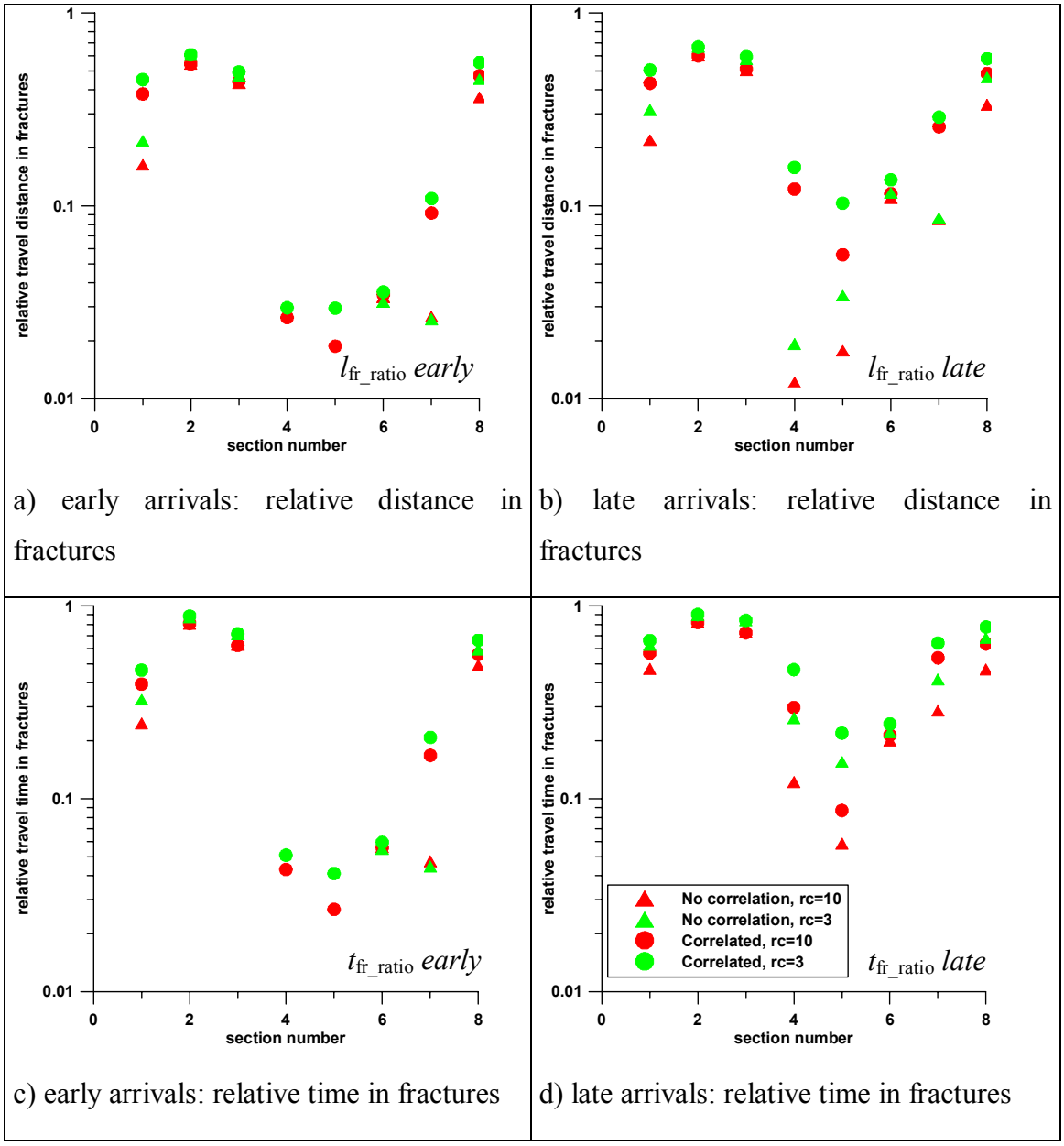

a) early arrivals: relative distance in fractures

b) late arrivals: relative distance in fractures

c) early arrivals: relative time in fractures

d) late arrivals: relative time in fractures

Figure 4-9: *Averaged results over Monte-Carlo simulations. Power law (a_{3d} = 3.8) radius distribution. Comparison between early and late arriving particles. Relative travel in fractures.*

Second main case: Lognormal radius distribution

In order to fix ideas on the differences between the radius distributions used, we show in Figure 4-10 the corresponding probability density functions. This figure shows that the lognormal distribution will generate more "medium size" fractures, and will tend to produce less small and less larger fractures. This is consistent with the property of this distribution, mentioned previously, that it is underlined by a characteristic scale. We can also already note that the three power laws distribution represented, with a_{3d} varying from 3.6 to 4, show little difference in the 3 metres to 20 metres range.

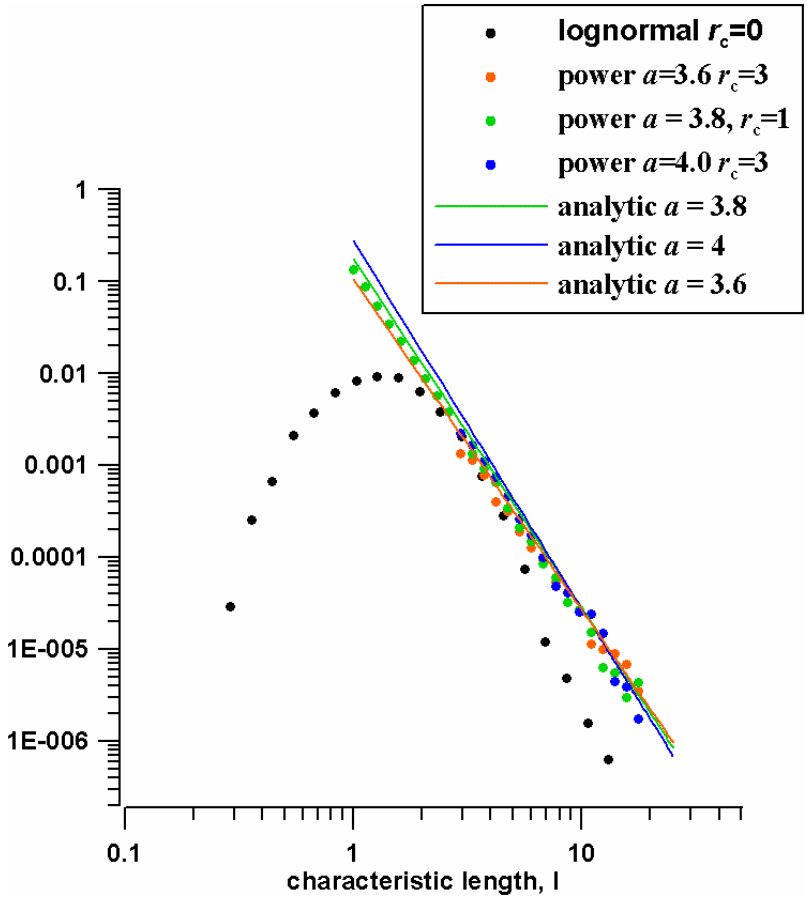

Figure 4-10: *Fracture radius distribution for the several stochastic fracture models.*

We show in Figure 4-11 the results of the lognormal distribution runs. Also, Figure 4-12 and Figure 4-13 detail the behaviour of the tracer depending on its ”early” or “late” arrival time, in the same manner as in the base case. Comparing the arrival times from this figure and Figure 4-7, we see that logically, results for the injection sections situated in Structure 19 (i.e. sections 4 to 7) are essentially unaffected.

Looking at sections 2 and 3 (injection in “Structure 25”, close to Structure 19), the lognormal model predicts arrival times at most half of the ones predicted by the power law model. Here, what governs the mean behaviour is the probability that the injection section be directly connected to Structure 19. Because the lognormal model has a lower proportion of small fractures, and because “medium” fractures are large enough to connect to Structure 19, it is more “efficient” in providing a direct connection. Note that as a consequence, the path travelled in fractures is shorter (see Figure 4-11, e).

We can see a somewhat opposite effect at larger scales. Tracer injected in test section 8 shows longer travel times, and a much longer distance travelled in structures. Because it predicts less “long range” background fractures, the lognormal model provides less connections through background at larger scale (i.e. tens of meters). Therefore, most of the tracer injected in test section 8 has to stay in structures 13 and 19.

Both “short range” and “long range” effects produce the same trend when looking at relative travel distances in fractures: the lognormal model predicts less travelled distance in background fractures.

When comparing “early” and “late” behaviour, we find, in structures (Figure 4-12) no significant departure from the “power-law” behaviour: quite similar travel distances, and longer travel times. The response in the background fractures (Figure 4-13) shows a more marked increase of the relative time in fractures than the power law model, specially for the structure-dominated tests. Still, late arriving tracer has spent in background fractures a much smaller part of the distance and time it travelled than with the power-law model.

Third and fourth main cases: Power law radius distribution, a_{3d} = 4, and a_{3d} = 3.6

Figure 4-14 shows the results obtained for the $a_{3d} = 4$. case. There is no significant difference between this case and the $a_{3d} = 3.8$ case. Note that we also ran simulations with $a_{3d} = 3.6$. These are illustrated in Figure 4-15 and again produce an almost identical response. The reason for this has been mentioned earlier (see Figure 4-10): within the range of radii we are sampling here (from 1 to about 50 m), differences between these three distributions are minimal, compared with the difference between them and the lognormal distribution.

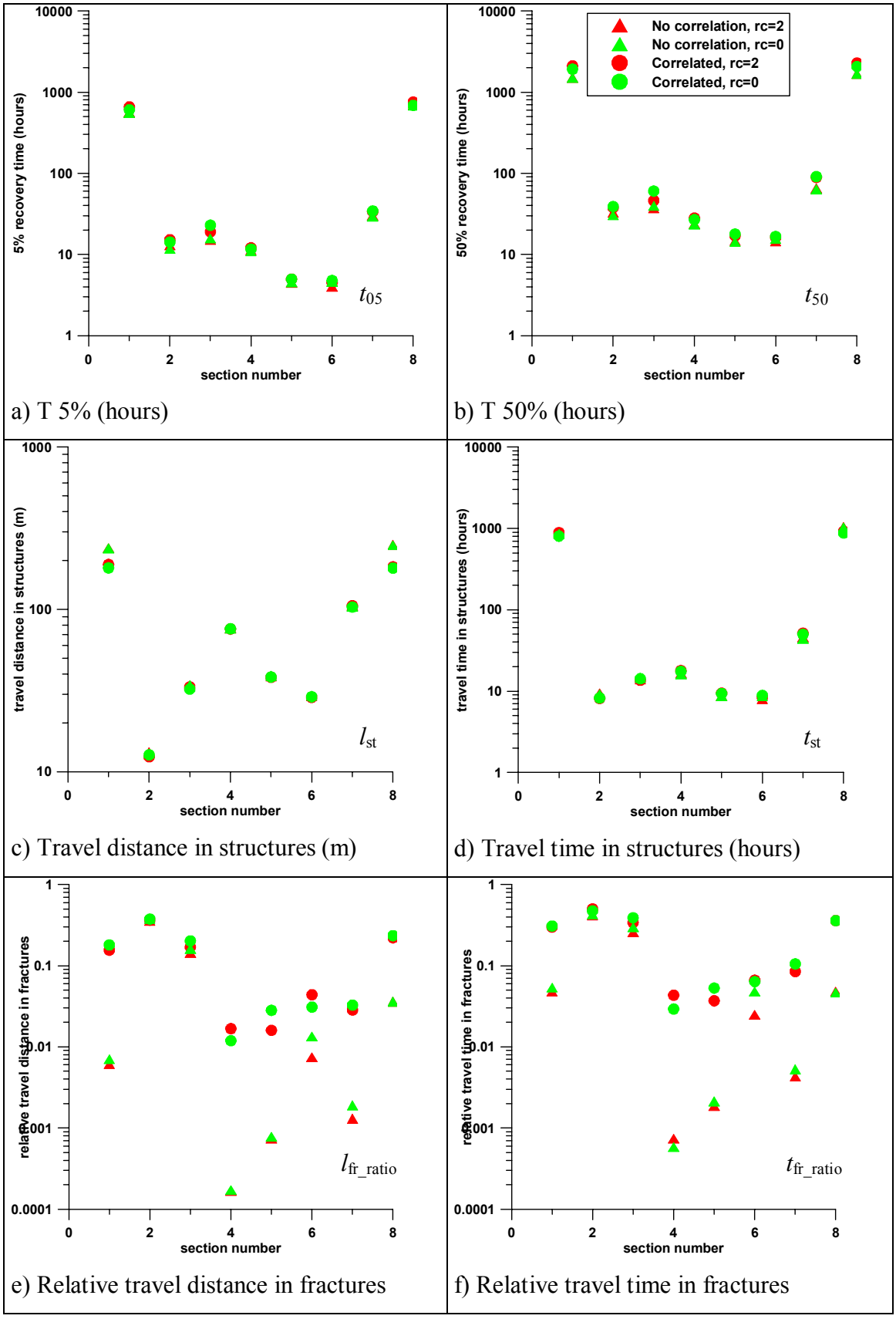

Figure 4-11: *Averaged results over Monte-Carlo simulations. Lognormal radius distribution*

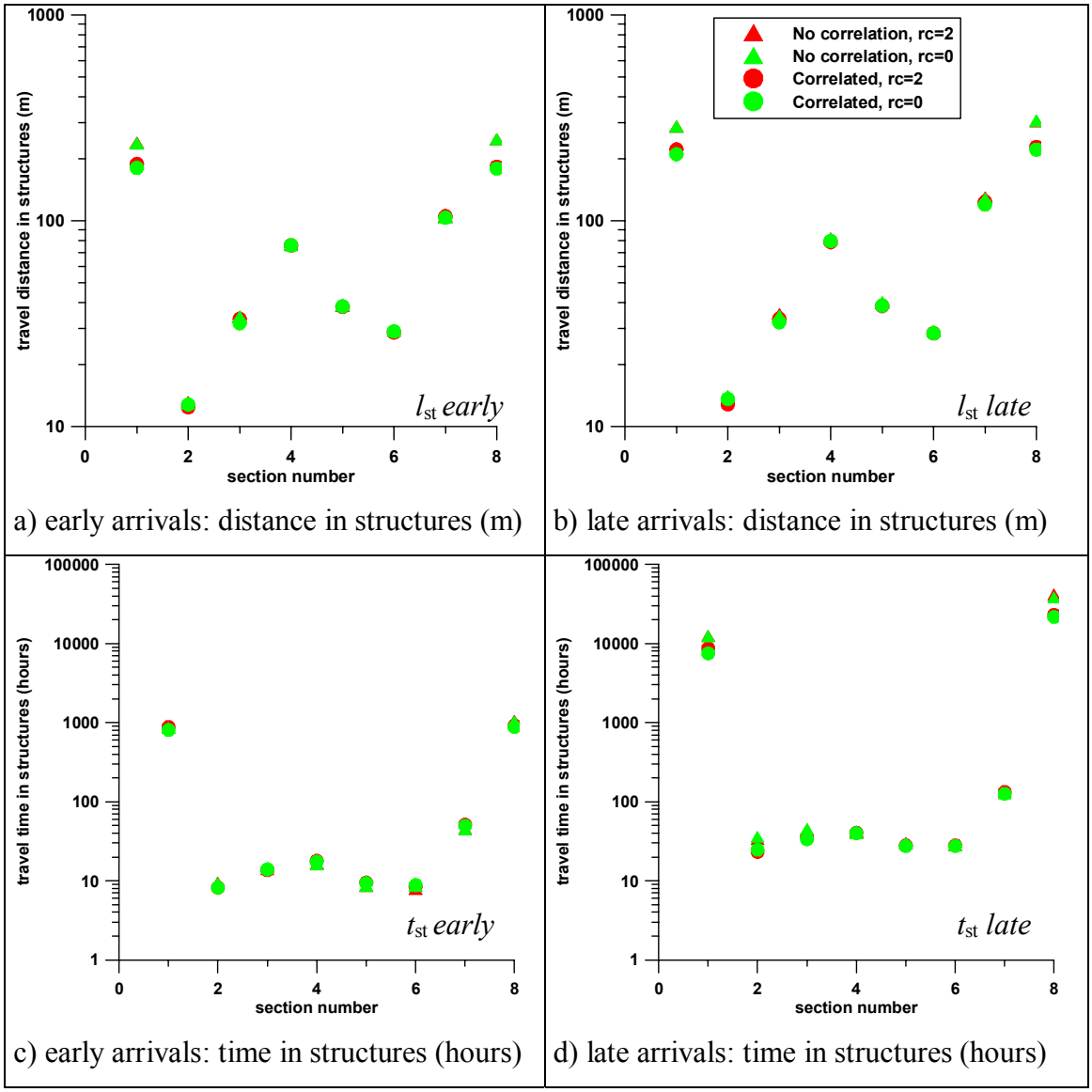

Figure 4-12: *Averaged results over Monte-Carlo simulations. Lognormal radius distribution. Comparison between early and late arriving particles. Travel in structures.*

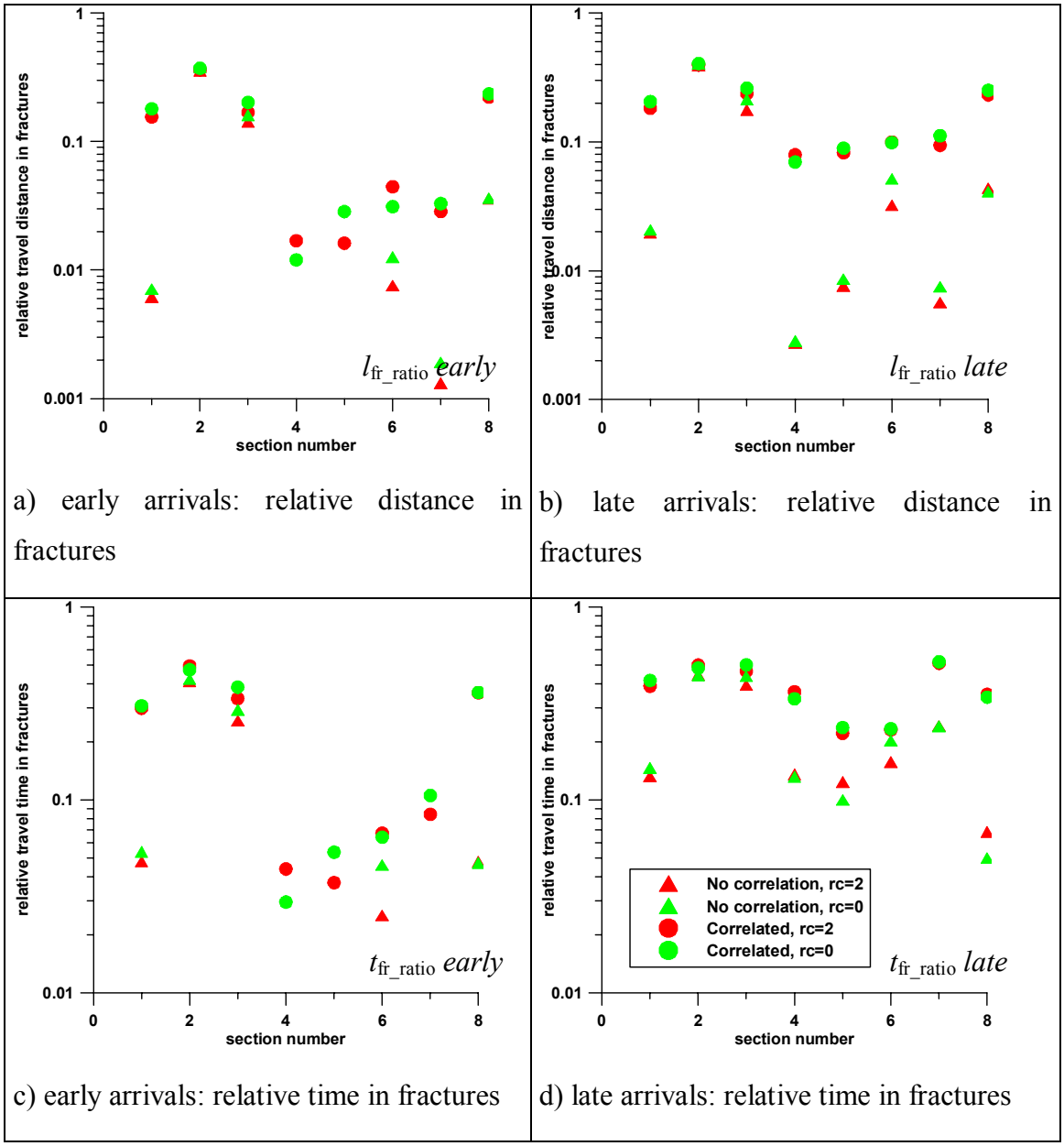

a) early arrivals: relative distance in fractures

b) late arrivals: relative distance in fractures

c) early arrivals: relative time in fractures

d) late arrivals: relative time in fractures

Figure 4-13: *Averaged results over Monte-Carlo simulations. Lognormal radius distribution. Comparison between early and late arriving particles. Relative travel in fractures.*

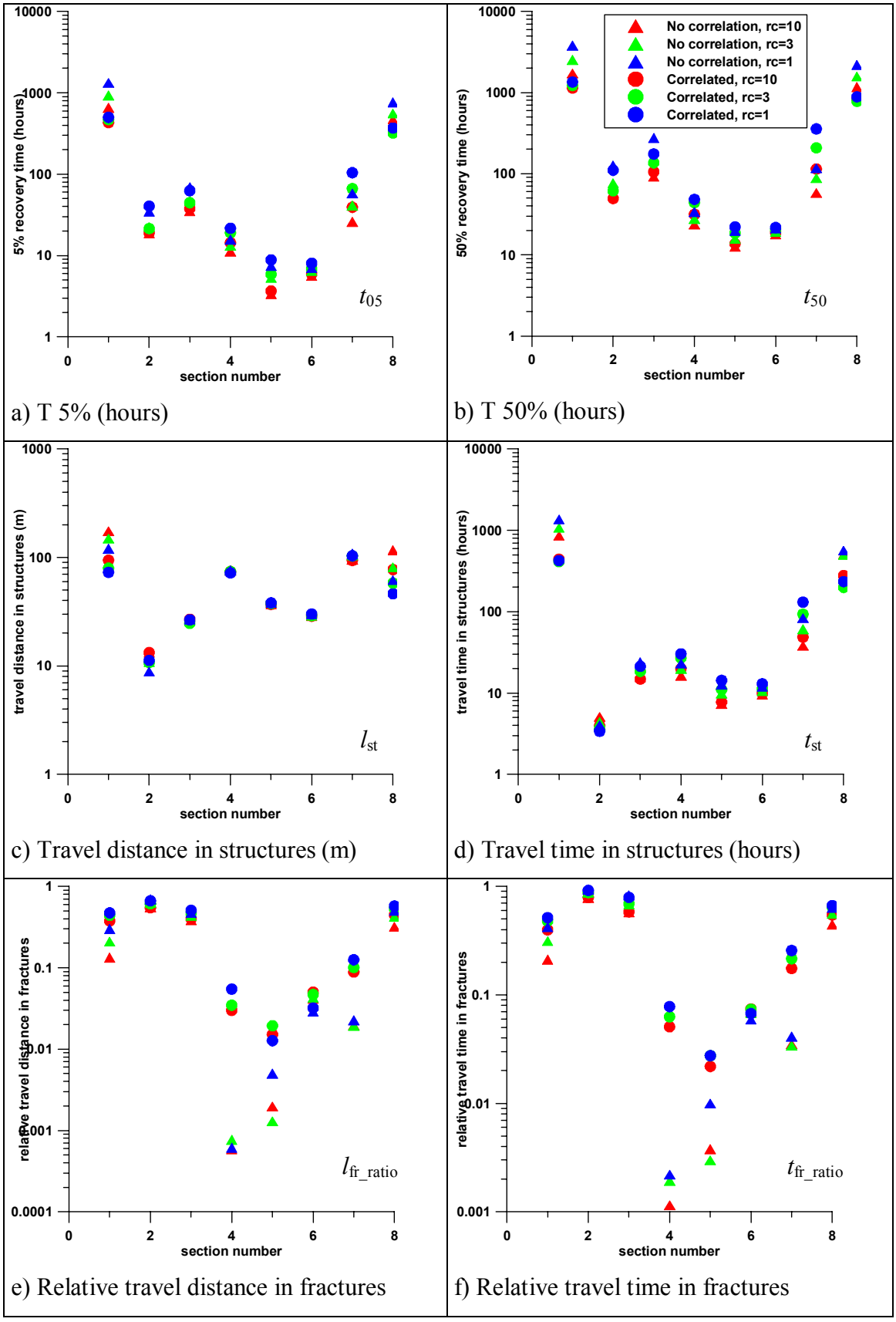

Figure 4-14: *Averaged results over Monte-Carlo simulations. Power law (a_{3d} = 4) radius distribution.*

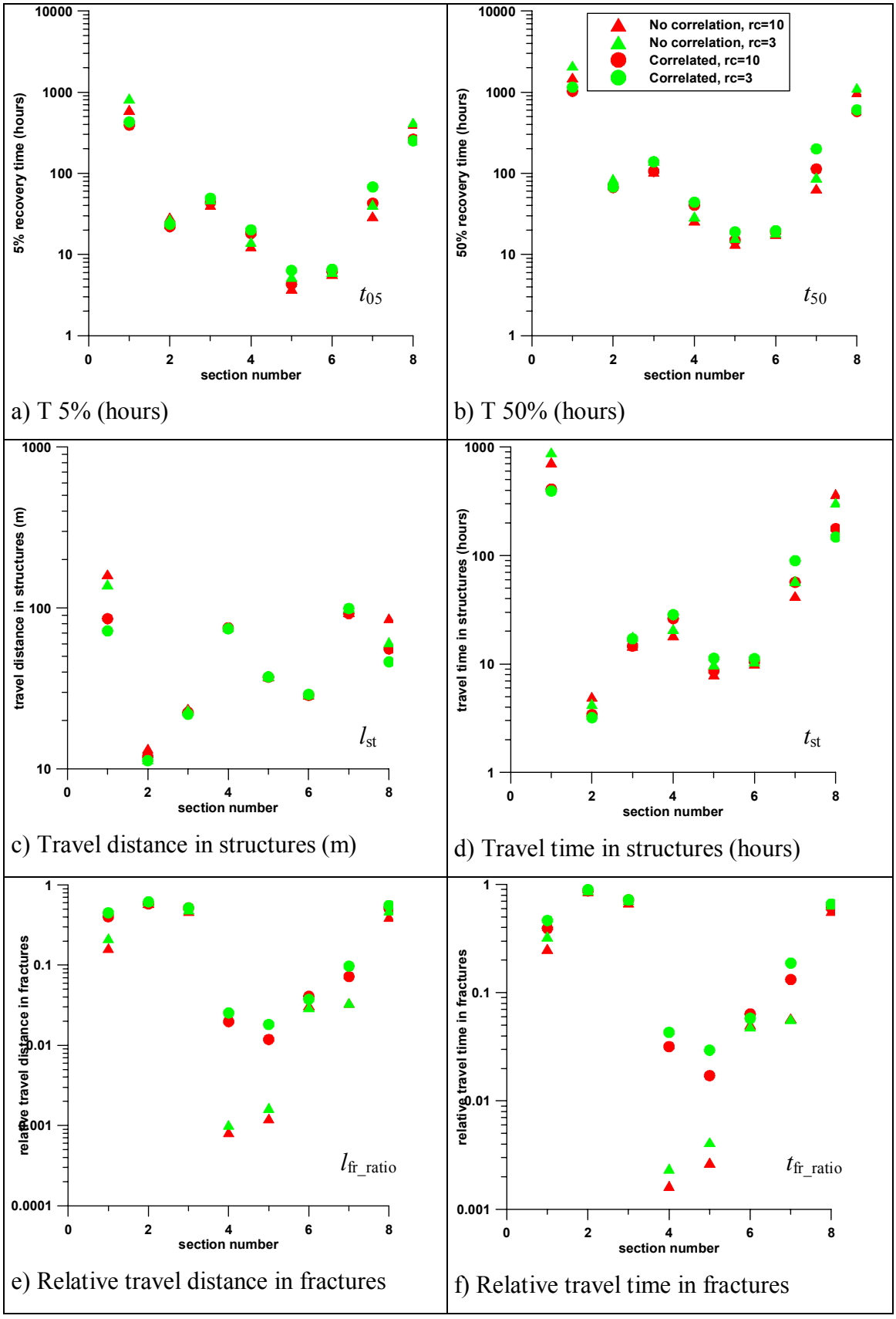

Figure 4-15: *Averaged results over Monte-Carlo simulations. Power law (a_{3d} = 3.6) radius distribution*

5 Discussion

Characteristic scales are used in essentially all models of the fracture system over the TRUE Block Scale rock volume and at Äspö in general. This is readily illustrated by the terms used to describe the fracture network: indeed, "Structures", for example, have an extension equivalent to the TRUE Block Scale Volume, while "Fractures" are more in the decametre range. These definitions have been adopted as a convenience, relative to the size of the volume studied, not specifically because of striking differences in nature between the two types (Note that differences may effectively exist in retention properties). This kind of description permits to model the specific site of concern. However it renders generalization difficult. The question arises whether it permits to relate scales or to assess the site properties from one scale to another. Note that this is not the main purpose of project BS2, which will be more focussed on an intermediate-size "Structure".

Different fracture sets exist at Äspö. They are identified by distinct orientations. However, from the tunnel wall scale of observation up to the kilometres-scale outcrop maps, no significant distinction could be identified between fracture length distributions and spatial patterns as a function of the fracture orientation set. This may be due to similar genetic histories of the fracture sets with different orientations. We therefore use a unique density/length distribution, regardless of orientation. This is specific to the site studied, and is by no means a restriction of the power-law model. In fact, in case several fracture sets having distinct length/spatial patterns can be distinguished at a site, several power-law models can be combined, as with any other size distribution function. A theoretical analysis using the power-law model then constitutes the basic element to predict the characteristic scales (and other properties) of the global fracture network. Note that the multiscale nature generally observed in a fracture network is rendered "naturally" by a power-law model, since such a model captures the scaling behaviour. This law therefore constitutes a thorough theoretical basis to model fracture systems, and to understand their properties even if characterization missed some of the scales of interest.

Results were presented in Sections 3.5.4 and 3.7. In summary, after assessing the relevance of a power-law model for fracture sizes, related to a Poissonian/fractal model for fracture positions, we used several techniques to obtain as robust as possible estimates of the corresponding parameters. We found that two pairs of parameters could explain the data at hand: either a power-law exponent a_{3d} of 3.8 combined with a fractal dimension D_{3d} of 2.8, or a power-law exponent a_{3d} of 4 combined with a fractal dimension D_{3d} of 3. The fact that "$a_{3d} = D_{3d} + 1$" indicates that the network is "self similar": the distribution of large and small fractures is the same at all the scales considered. This is in contrast to a lognormal distribution for fracture size, where some intermediate size dominates the behaviour. Note that in the self-similar case the connectivity is scale independent. At Äspö, the fracture system is above the percolation threshold, and all scales are connected. Note that this does not mean "all regions of the laboratory are connected to each other", but "connectivity exists at all scales, although some parts of the system may not be connected to each other, at any scale".

Many observers notice that an apparently unique fracture observed at a given resolution scale can appear as a cluster of smaller fractures at a lower scale. Could that introduce a bias in the present case? Here, since the model is dominated by the smallest fractures (a_{3d} close to 3.8 to 4), the surface density of fractures is also controlled by the smallest fractures, so that counting or not the mass of the largest ones is negligible.

One major point here is to assess the relevance of the power-law model at the metre – decametre scale. There is a lack of data here, indeed, the smallest scale of resolution during sampling should be decreased to confirm the validity of the power-law model below the 10m scale.

Our analysis of transport here is very much governed by the knowledge of the structures, in which (or close to which) the tracers tests will be performed. Nevertheless, the simulations described in Section 4.5 have shown more precisely how the behaviour of a background fracture network varies when considering a lognormal or a power law fracture radius distribution. In summary, using the parameters that were obtained in Chapter 3, the power law model results in more small fractures, more "large" fractures, and less "medium size" fractures. This affects the interplay of the structures and the background fractures. At small scale (i.e. one metre to maybe 10 metres), the power law model will produce less direct connections for the tracer injected in a background fracture to reach a structure and then a sink. However, at larger scale (tens of metres), the picture is reversed: whereas the lognormal model predicts few fractures of this scale, the power law one produces a "continuous" range of scales, up to the size of structures. Therefore, this model produces more pathways able to "short-circuit" structures. Also note that, as expected, the prediction variability increases with the proportion of tracer test forced to the stochastic fracture network.

For the BS2 program, the differences outlined above are not of great concern, for one main reason: we know well the main structures. Therefore, the number of 100 m "features" does not need to be assessed from other scales: these controlling features have been directly detected and characterized. In other words, we know enough here at the scales of interest, so that no "interpolation" is needed between scales. Such is likely not to be the case in most other set-ups, be it during site characterisation for a repository, or for performance assessment work at a larger-scale, not fully characterised site.

6 Conclusions and Perspectives

This study, in the context of preparations for the BS2 project, was aimed at helping assess the feasibility of tracer tests in the volume surrounding Structure 19. Such tests are feasible, provided injections in background fractures, if any, are operated close to the Structure 19, as in fact planned (injections in "Structure 25", a few metres from the structure).

In performing this task, we have strived at developing a view of the fracture system at Äspö that encompasses all scales in a unified conceptual framework. Such a view, because it takes into account data at several scales, is likely to provide a more robust description of the fracture network. It can help filling "voids" in scales, for sizes that are difficult to assess from field work, and may provide new insights in several directions, beyond the framework of the TRUE Block Scale Continuation project:

- Mapping at the "lower scale" (metres to tens of metres) is available, but often suffers from biases, as noted before. When looking at the natural geologic barrier close to canisters, properties of the smaller scale fractures become essential. Unbiased (i.e. systematic) mapping at this scale would then help confirm - or invalidate - the relevance of the power law model.
- More theoretical studies of the connectivity of such networks, using the fact that they show self-similarity, would yield estimates of the size of possible unconnected clusters within the network, on the conductive/non conductive proportion of the fracture system.
- Our use of transmissivity data in this work was conceptually quite simple. In fact, more theoretical work on the interplay of size/transmissivity/connectivity properties of fractures would improve the robustness of our models for varying hydraulic conditions.

The numerical model we have built from this theoretical framework has shown how the choice of a distribution function for fracture size can affect the advective response of the network, and how such assumptions influence the relative interplay of the structures and the background fractures. After this necessary first step, one can try to understand how reactive transport is affected. Specifically, stepping back to the tentative hypotheses which constitute the rationale for the BS2 project, we note that the possible differences in retention properties between smaller features (mostly background fractures) and larger ones (mostly structures) makes the understanding of the way they interact hydraulically all the more important.

7 References

Andersson P, Byegård J, Dershowitz W, Doe T,Hermanson J, Meier P, Tullborg E-L, Winberg A, 2002. TRUE Block Scale Project.Final report. 1.Characterisation and model development. Swedish Nuclear Fuel and Waste Management Company.SKB Technical Report TR-02-13.

Andersson P, Byegård J, Dershowitz W, Winberg A., 2002. TRUE Block Scale Project, Final report. 2.Tracer tests in the block scale. Swedish Nuclear Fuel and Waste Management Company.SKB Technical Report TR-02-14.

Berkowitz B, and Adler P, 1998. Stereological analysis of fracture network structure in geological formations, *J. Geophys. Res.*, *103*, 15339-15360.

Bonnet E, Bour O, Odling N, Main I, Berkowitz B, Davy P, and Cowie P, 2001. Scaling of fracture systems in geological media, Rev. Geophys., 39, 347-383, 2001.

Bossart P, Hermanson J and Mazurek M, 2001. Analysis of fracture networks based on the integration of structural and hydrogeological observations at different scales. Swedish Nuclear Fuel and Waste Management Company (SKB), Technical Report TR-01-21.

Bour O, and Davy P, 1997. Connectivity of random fault networks following a power law fault length distribution, *Water Resour. Res.*, *33*, 1567-1583, 1997.

Bour, O., and P. Davy, 1998. On the connectivity of three dimensional fault networks, *Water Resour. Res.*, *34*, 2611-2622.

Bour O, Davy P, Darcel C, and Odling N, 2002. A statistical scaling model for fracture network geometry, with validation on a multi-scale mapping of a joint network (Hornelen Basin Norway), *J. Geophys. Res.*, 107, 2113, doi: 2001JB000176.

Dershowitz B, Winberg A, Hermanson J, Byegård J, Tullborg E-L, Andersson P, Mazurek M, 2003. A semi-synthetic model of block scale conductive structures at the Äspö hard rock laboratory. Swedish Nuclear Fuel and Waste Management Company (SKB), IPR-03-13.

de Dreuzy JR, Darcel C, Davy P, Bour O, *in press*. Influence of fracture correlation on the permeability of two-dimensional fracture networks following a power-law length distribution, *Water Resour. Res*.

de Dreuzy JR, Davy P, and Bour O, 2000. Percolation parameter and percolation-threshold estimates for three-dimensional random ellipses with widely scattered distributions of eccentricity and size, *Phys. Rev. E*, *62*, 1-5.

Follin S and Hermanson J, 1996. A discrete fracture network model of the Äspö TBM tunnel rock mass. Swedish Nuclear Fuel and Waste Management Company (SKB), IPR-01-71.

Hermanson J, Follin S, Wei L, 1997. Input data for discrete feature network modelling of the TRUE BLOCK SCALE site, Swedish Nuclear Fuel and Waste Management Company (SKB), IPR-01-70.

LaPointe P, Wallmann P and Follin S, 1995. Estimation of effective block conductivities based on discrete network analyses using data from the Äspö site. Swedish Nuclear Fuel and Waste Management Company (SKB). Technical Report TR-95-15.

LaPointe P, Cladouhos T and Follin S, 1999. Calculation of Displacement of Fractures Intersecting Canisters Induced by Earthquakes. Aberg, Beberg, Ceberg, examples. Swedish Nuclear Fuel and Waste Management Co. Technical Report TR 99-03. SKB, Stockholm.

Mazurek M, Bossart P and Eliasson T, 1995. Classification and characterization of water-conducted features at Äspö: Results of phase I investigations. SKB Progress Report PR 25-95-03, Stockholm

Mazurek M, Bossart P and Eliasson T, 1996. Classification and characterization of water-conducting features at Äspö: Results of investigations on the outcrop scale. SKB ICR 97-01, ISSN 1104-3210.

Odling NE et al., 1999. Variations in fracture system geometry and their implications for fluid flow in fractured hydrocarbon reservoirs, *Pet. Geosci.I*, 5, 373-384.

Piggott A, 1997, Fractal relations for the diameter and trace length of disc-shaped fractures, *J. Geophys. Res.*, *B102*, 18121-128125.

Poteri A, Billaux D, Cvetkovic V, Dershowitz B, Gómez-Hernández J-J, Hautojärvi A, Holton D, Medina A and Winberg A, 2002. TRUE Block Scale Project. Final Report 3. Modelling of flow and transport. Swedish Nuclear Fuel and Waste Management Company. Technical Report TR 02-15.

Rachez X and Billaux D, 2002. Investigation of the effect of structural model updates on response to simulated tracer tests. Äspö Hard Rock Laboratory International Progress Report IPR-02-26.

Robinson PC, 1983. Connectivity of fractures systems - a percolation theory approach., *J. Phys. A*, *16*, 605-614.

Robinson PC, 1984. Numerical Calculations of critical densities for lines and planes., *J. Phys. A*, *17*, 2823-2830.

Stauffer D and A Aharony, 1992, *Introduction to percolation theory, second edition*, Taylor and Francis, Bristol.

Winberg A, Andersson P, Poteri P, Cvetkovic V, Dershowitz W, Hermanson J, Gomez-Hernandez J-J, Hautojärvi A, Billaux D, Tullborg H-L, Holton D, Meier P, Medina A, 2003. Final report of the TRUE Block Scale project, 4. Synthesis of flow, transport and retention in the block scale. Technical Report TR-02-16.

8 Appendix A: mean and standard deviations of tracer test simulations for the base case

This appendix is provided as a complement to Figure 4-7, by adding the error bars (standard deviation) to means resulting from Monte Carlo simulations for the base case (a_{3d}=3.8, see Table 4-4). Note that in contrast to Figure 4-7 the results are presented on linear axes.

The figure shows that the variability estimated from the Monte-Carlo simulations is positively correlated to the flow path length between injection and pumping points. Moreover, this effect is stronger for configurations including pathways within background fractures. The highest variability is obtained for test section 8 (injection in background fracture "far" from the pumping point in #19).

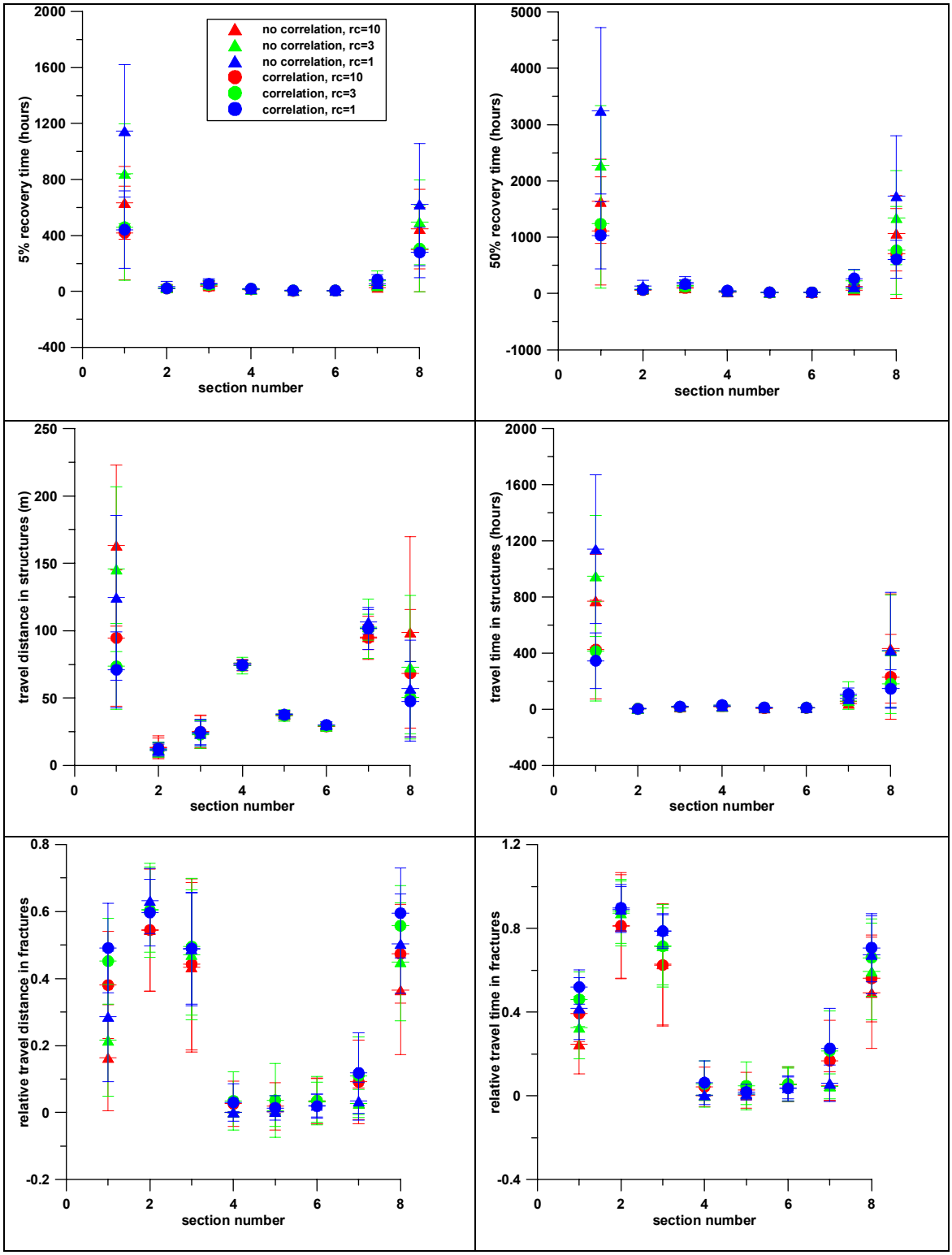

Figure 8-1: *(complement to Figure 4-7) average results over Monte Carlo simulations for the base case, representation with errors bars and linear ordinate axis.*

9 Appendix B: Verification / parameter assessment simulations

The simulations listed in *Table 4-5* are illustrated in this appendix.

Figure 9-1 is a check on the robustness of the channel representation of flow paths. We have doubled the density of the channel grid on background fractures, to a grid spacing of one metre, for the non-correlated case. Everything else is identical to the base case. One can verify that the results shown are almost identical to the ones shown in Figure 4-7.

Figure 9-2 shows the effect of doubling the density of (unconditioned) background fractures. The density of fractures does not have a striking effect on the behaviour of the structures/fractures network as tested by the planned tracer tests: the results are not identical, but in fact quite similar to the ones obtained in the base case (Figure 4-7). This stems from two opposite effects: the larger probability for any tracer travelling in a structure to enter the background fractures network, illustrated by larger relative distances travelled in fractures (plot e), and the slightly better transport efficiency of the background network.

Finally, Figure 9-3 illustrates a decupling of the average background fracture transmissivity. Here, the main effect is the increase in overall transport capacity of the background fracture network, so that travel times are significantly reduced for paths involving a significant length in fractures (mostly test sections 1, 2, 3 and 8, see plot e and f).

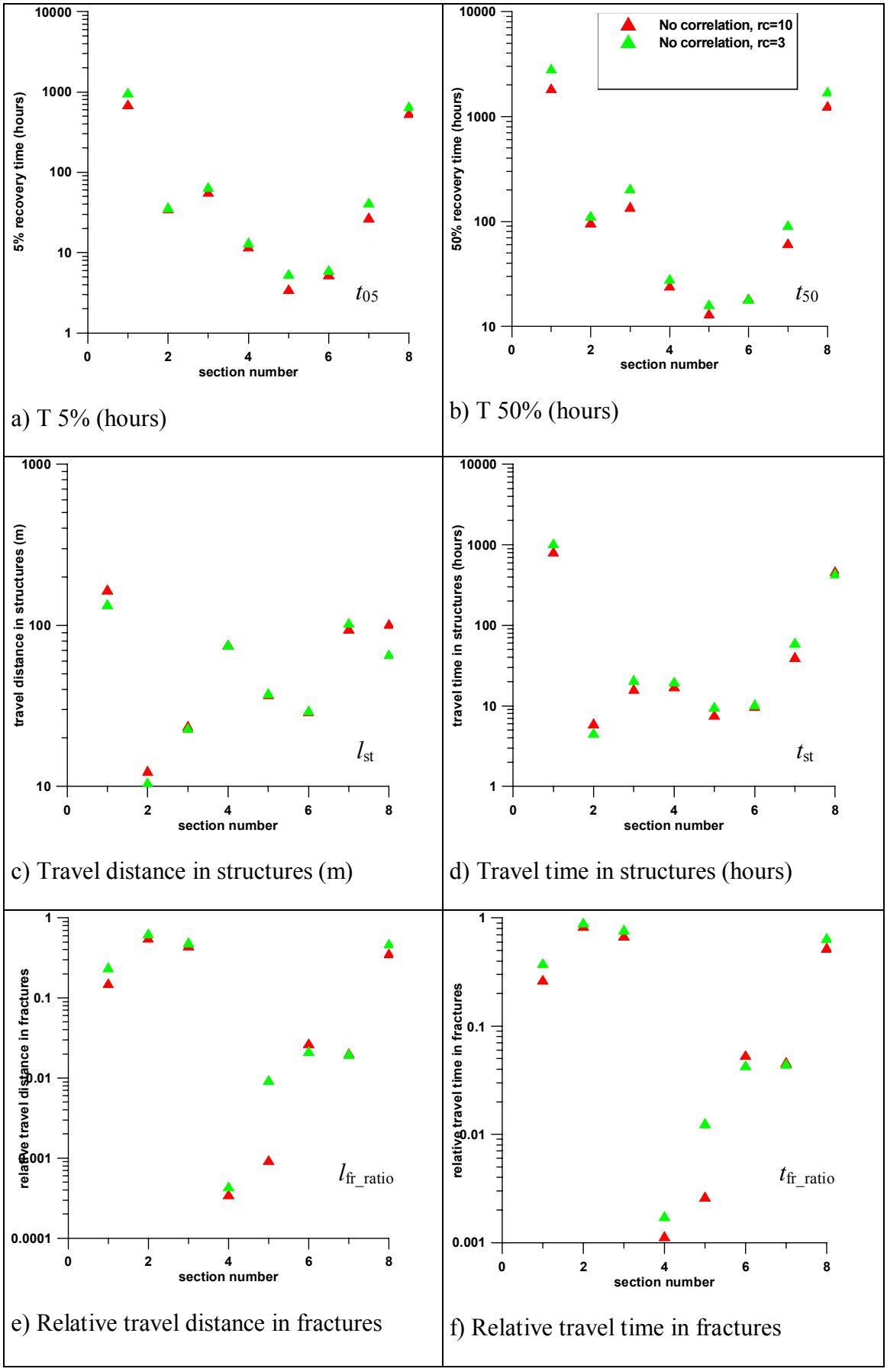

Figure 9-1: *Averaged results over Monte-Carlo simulations. Power law (a_{3d} = 3.8) radius distribution, double grid density*

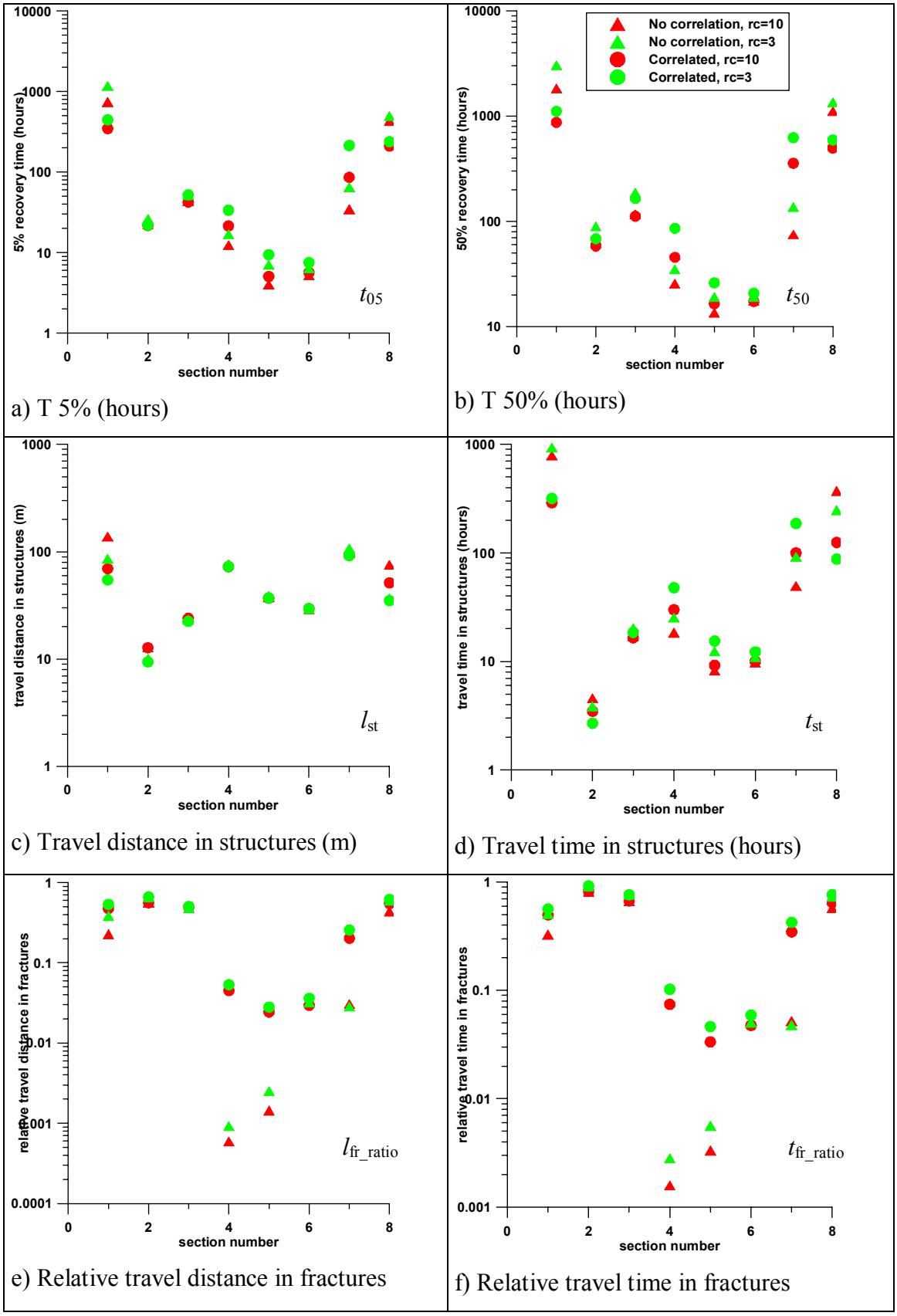

Figure 9-2: *Averaged results over Monte-Carlo simulations. Power law (a_{3d} = 3.8) radius distribution, double background fracture density*

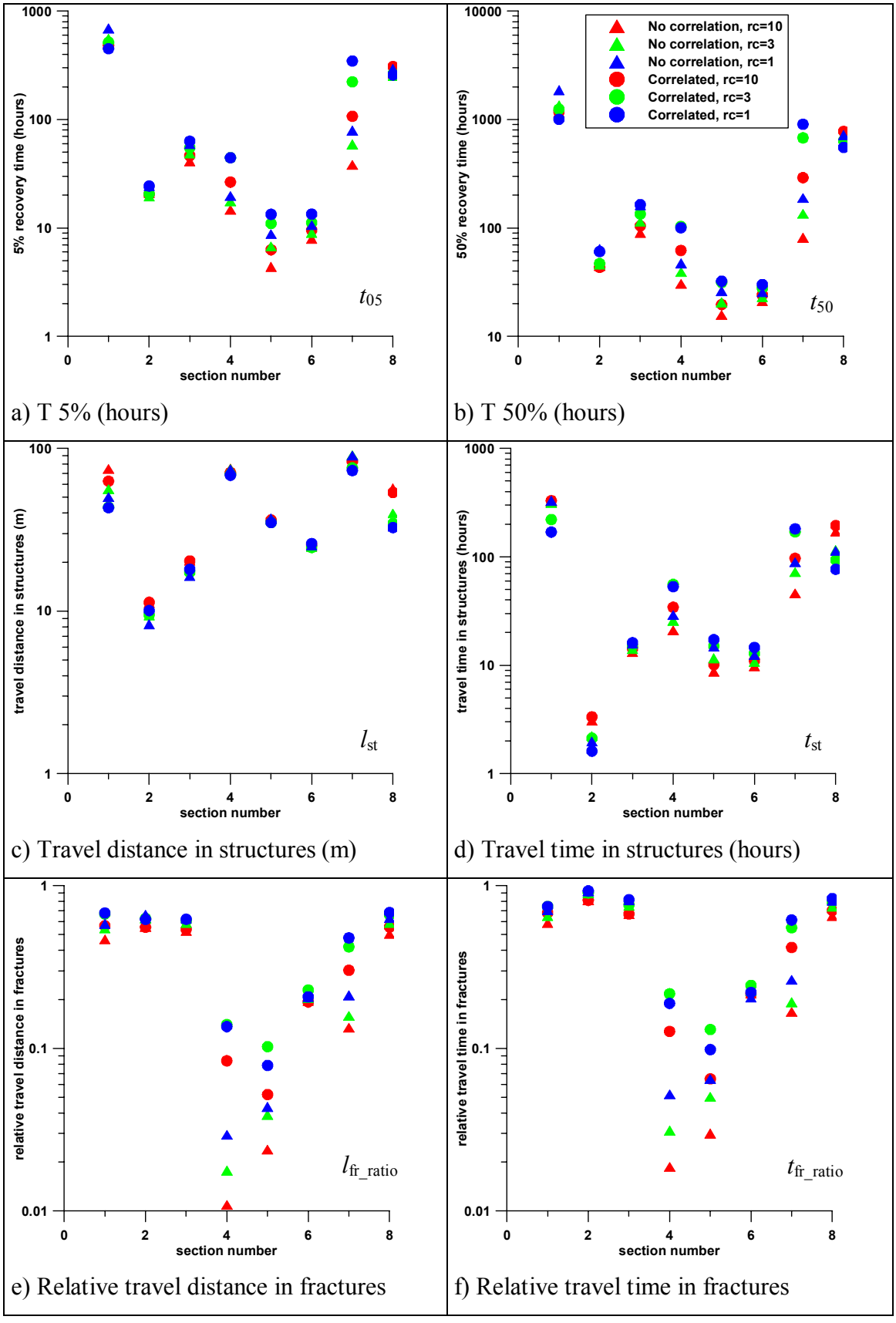

Figure 9-3: *Averaged results over Monte-Carlo simulations. Power law (a_{3d} = 3.8) radius distribution, decuple transmissivity in background*